Aus dem Institut für Prophylaxe und Epidemiologie der Kreislaufkrankheiten des Klinikums der Ludwig-Maximilians-Universität München

Direktor: Univ.-Prof. Dr. med. Christian Weber

The role of the co-stimulatory CD27/CD70 dyad in atherosclerosis

Dissertation
zum Erwerb des Doktorgrades der Naturwissenschaften
an der Medizinischen Fakultät
der Ludwig-Maximilians-Universität zu München

vorgelegt von

Holger Winkels

aus Geilenkirchen, Nordrhein Westfalen, Deutschland

2016

Mit Genehmigung der Medizinischen Fakultät
der Ludwig-Maximilians-Universität München

Erstgutachter:	Prof. Dr. rer. nat. Alexander Faussner
Zweitgutachter:	Prof. Dr. rer. nat. Ludger Klein
Dekan:	Prof. Dr. med. dent. Reinhard Hickel
Abgabe der Dissertation:	21.06.2016
Datum der Disputation:	10.01.2017

Eidesstaatliche Versicherung

Winkels, Holger

Name, Vorname

Ich erkläre hiermit an Eides statt, dass ich die vorliegende Dissertation mit dem Thema:

The role of the co-stimulatory CD27/CD70 dyad in atherosclerosis

selbständig verfasst, mich außer der angegebenen keiner weiteren Hilfsmittel bedient und alle Erkenntnisse, die aus dem Schrifttum ganz oder annähernd übernommen sind, als solche kenntlich gemacht und nach ihrer Herkunft unter Bezeichnung der Fundstelle einzeln nachgewiesen habe.

Ich erkläre des Weiteren, dass die hier vorgelegte Dissertation nicht in gleicher oder in ähnlicher Form bei einer anderen Stelle zur Erlangung eines akademischen Grades eingereicht wurde.

Ort, Datum

Unterschrift Doktorandin/Doktorand

THE RESULTS OF THIS WORK WILL BE PARTLY PUBLISHED IN:

Winkels H*, Meiler S*, Smeets E, Lievens D, Engel D, Spitz C, Buerger C, Beckers L, Dandl A, Reim S, Ahmadsei M, Hartwig H, Holdt LM, Hristov M, Megens RTA, Schmitt MM, Biessen EA, Borst J, Faussner A, Weber C, Lutgens E[#], Gerdes N[#]. CD27 co-stimulation increases frequency of regulatory T cells and reduces atherosclerosis in hyperlipidemic mice. *European Heart Journal*. In Revision

Winkels H*, Meiler S*, Smeets E*, Lievens D, Engel D, Spitz C, Buerger C, Rinne P, Beckers L, Dandl A, Reim S, Ahmadsei M, Van den Bossche J, Holdt LM, Megens RTA, Schmitt MM, de Winther M, Biessen EA, Borst J, Faussner A, Weber C, Lutgens E[#], Gerdes N[#]. CD70 limits atherosclerosis and promotes macrophage function. *Thrombosis and Haemostasis* 2017 117 1: 164-175

THE RESULTS OF THIS WORK WERE PRESENTED AT THE FOLLOWING CONFERENCES AS POSTER AND ORAL PRESENTATIONS:

Oral presentation

84th EAS Congress, Innsbruck, Austria, 29 May-1 June 2016
Title: 'CD27 co-stimulation fosters regulatory T cell survival and ameliorated progression of atherosclerosis'

Gordon Research Conference Atherosclerosis, Newry, Maine, USA, 21-26 June 2015
Title: 'Co-stimulation via CD27 increases frequency of regulatory T cells and ameliorates atherogenesis in hyperlipidemic mice'

Poster presentation

Cardiovascular Research Workshop @ Bayer, Heiligenhaus, Germany 14-16 April, 2016
Title: 'Deficiency of the co-stimulatory molecule CD27 impairs Treg survival and exacerbates atherosclerosis'

Annual Meeting of the German Atherosclerosis Society (DGAF), Rauischholzhausen, Germany, 7-9 April, 2016
Title: 'Deficiency of the co-stimulatory dyad CD27/CD70 exacerbates atherosclerosis'

Gordon Research Conference Atherosclerosis, Newry, Maine, USA, 21-26 June 2015
Title: 'Co-stimulation via CD27 increases frequency of regulatory T cells and ameliorates atherogenesis in hyperlipidemic mice'

17th International Symposium on Atherosclerosis, Amsterdam, The Netherlands, 23-26 May 2015
Title: 'Deficiency of the co-stimulatory molecule CD27 impairs Treg survival and exacerbates atherosclerosis'

ATVB/PVD Arteriosclerosis, Thrombosis and Vascular Biology/Peripheral Vascular Disease, San Francisco, California, USA, 7-9 May 2015
Title: 'Deficiency of the co-stimulatory molecule CD27 impairs Treg development and exacerbates atherosclerosis'
Gordon Research Conference Atherosclerosis, Stowe, Vermont, USA, 16-21 June 2013
Title: 'Pharmacological inhibition of CD70 hampers progression of atherosclerosis'

World Immune Regulation Meeting (WIRM) VI, Davos, Switzerland, 18-21 March 2012
Title: ‘T cell homeostasis in atherosclerosis‘

TABLE OF CONTENTS

LIST OF ABBREVIATIONS

^{3}H	Tritium
ABCA1	ATP-Binding Cassette, Sub-Family A, Member 1
ABCG1	ATP-Binding Cassette, Sub-Family G, Member 1
ACAT1	Acetyl-coenzyme A:cholesterol Acetyltransferase 1
AIRE	Autoimmune Regulator
Anti-dsDNA	Anti-double Stranded Deoxyribonucleic Acid
APC	Antigen Presenting Cell
ApoA1	Apolipoprotein A1
ApoB	Apolipoprotein B
ApoE	Apolipoprotein E
ATP	Adenosine Triphosphate
Bcl-xL	B-cell lymphoma-extra large
BMDM	Bone Marrow-Derived Macrophages
bp	Base Pair
BSA	Bovine Serum Albumin
CCL5	Chemokine (C-C motif) Ligand 5
CCR5	Chemokine (C-C motif) Receptor 5
CD206	Mannose Receptor 1
CD25	IL-2 receptor a chain
CD3	Cluster of Differentiation 3
cDNA	Complimentary DNA
CEA	Carotid Endarterectomy
CFSE	Carboxyfluorescein Succinimidyl Ester
CO_2	Carbon Dioxide
CTLA-4	Cytotoxic T-lymphocyte-associated protein 4
CVD	Cardiovascular Disease
CX3CL1	Chemokine (C-X3-C motif) ligand 1, also known as Fractalkine
CXCL1	Chemokine (C-X-C motif) Ligand 1
CXCL10	C-X-C motif chemokine 10
Cy	Cyanine
DAMP	Danger-associated Molecular Pattern
DAPI	4',6-diamidino-2-phenylindole
DC	Dendritic Cell
DMEM	Dulbecco’s Modified Eagle Medium
DMSO	Dimethylsulfoxid

DNA	Deoxyribonucleic acid
DNase	Deoxyribonuclease
dNTP	Deoxynucleotide Triphosphate
Dnmt	DNA methyltransferase
ECAR	Extracellular Acidification Rate
EAE	Experimental Autoimmune Encephalitis
EBV	Epstein-Barr Virus
EC	Endothelial Cell
EDTA	Ethylenediaminetetraacetic Acid
ELISA	Enzyme-linked Immunosorbent Assay
ER	Endoplasmatic Reticulum
EVG	Elastic Von Gieson Stain
FACS	Fluorescence-activated Cell Sorting
FCA	Fibrous Cap Atheroma
FCCP	Carbonyl cyanide-p-trifluoromethoxyphenylhydrazone
FBS	Fetal Bovine Serum
FcγR	Fragment Crystallizable Gamma Receptor
FITC	Fluorescein Isothiocyanate
Fizz1	Resistin-like Beta
Foxp3	Forkhead Box P3
GAPDH	Glyceraldehyde 3-phosphate Dehydrogenase
Gata3	GATA binding protein-3
GM-CSF	Granulocyte-macrophage Colony-stimulating Factor
H&E	Hematoxylin and Eosin
HCl	Hydrochloric Acid
HDAC1	Histone Deacetylase 1
HDL	High-density Lipoprotein
HEPES	4-(2-hydroxyethyl)-1-piperazineethanesulfonic Acid
WD	High Fat, Cholesterol-enriched, Western Type Diet
HRP	Horseradish Peroxidase
HSP	Heat Shock Protein
ICAM-1	Intercellular Adhesion Molecule 1
IFNγ	Interferon gamma
IgG	Immunoglobulin G
IL-6	Interleukin 6
iNOS	Inducible Nitric Oxide Synthase
IRA B cells	Innate Response Activator B cells

IRF4	Interferon Regulatory Factor 4
IX	Intimal Xanthoma
JNK	C-Jun-N-terminal Kinase
$KHCO_3$	Potassium Bicarbonate
LCMV	Lymphocytic Choriomeningitis Virus
LDL(R)	Low-density Lipoprotein (Receptor)
LFA-1	Lymphocyte Function-associated Antigen 1
LOX1	Lectin-type oxLDLR1
LPS	Lipopolysaccharides
LXR	Liver X Receptor
MCP1	Monocyte Chemotactic Protein 1
M-CSF	Macrophage Colony-stimulating Factor
MDA-LDL	Malondialdehyde-LDL
MEK	Mitogen-activated Protein Kinase Kinase
MFI	Mean Fluorescence Intensity
$MgCl_2$	Magnesium Chloride
MHC	Major Histocompatibility Complex
MMP	Matrix Metalloproteinases
MOG	Myelin Oligodendrocyte Glycoprotein
mTEC	Medullary Thymic Epithelial Cells
NaN_3	Sodium Azide
NaOH	Sodium Hydroxide
NFκB	Nuclear Factor Kappa-light-chain-enhancer of Activated B Cells
NH_4Cl	Ammonium Chloride
NK cells	Natural Killer Cells
NLRP3	NACHT, LRR and PYD domains-containing protein 3
NO	Nitric Oxide
OCR	Oxygen Consumption Rate
OM	Oligomycin
oxLDL	Oxidized LDL
OXPHOS	Oxidative Phosphorylation
PAMP	Pathogen-associated Molecular Pattern
PBS	Phosphate-buffered Saline
PBS-T	PBS-Tween
PCR	Polymerase Chain Reaction
PE	Phycoerythrin
PerCP	Peridinin Chlorophyll

PFA	Paraformaldehyde
PI	Propidium Iodide
PI3K	Phosphatidylinositol-4,5-bisphosphate 3-kinase
PIT	Pathological Intimal Thickening
PRR	Pattern Recognition Receptor
RA	Rheumatoid Arthritis
RAG2	Recombinase Activating Gene 2
RIPA	Radioimmunoprecipitation Assay
RNA	Ribonucleic Acid
RNase	Ribonuclease
Rorγt	RAR-related Orphan Receptor Gamma t
ROS	Reactive Oxygen Species
RPMI 1640	Roswell Park Memorial Institute 1640
SD	Standard Deviation
SDS	Sodium Dodecyl Sulfate
SEM	Standard Error of the Mean
Siva1	Apoptosis Inducing Factor 1
SLE	Systemic Lupus Erythematosus
SLEDAI	SLE Disease Activity Index
SMC	Smooth Muscle Cell
SR-A1	Scavenger Receptor A1
SR-B1	Scavenger Receptor B1
STAT6	Signal Transducer and Activator of Transcription 6
TBX21	T-box 21, known as T-Bet
TBS	Tris-buffered Saline
TCR	T Cell Receptor
TGFβ	Transforming Growth Factor beta
TLR2	Toll-like Receptor 2
TMB	3,3’,5,5’-Tetramethylbenzidine
TNF(R)	Tumor Necrosis Factor (Receptor)
Tr1	IL-10-producing Tregs
TRAF2	TNFR-associated Factor 2
Treg	Regulatory T cells
TRIS	Tris(hydroymethyl)aminoethamine
VCAM-1	Vascular Adhesion Molecule-1
VLDL	Very-low-density lipoprotein
ASMA/α-SMA	Alpha Smooth Muscle Actin

1 INTRODUCTION

1.1 Atherosclerosis – a chronic inflammatory disease

Atherosclerosis, previously considered merely a lipid deposit-driven narrowing of the vessel lumen, is nowadays appreciated as a chronic inflammatory disease of the arterial wall. The main clinical manifestations of atherosclerosis include coronary artery disease, stroke, and peripheral arterial disease which still represent the leading cause of death in Europe and North America.[1]

During the development of atherosclerosis, plaque progression and vascular dysfunction are influenced and promoted by the immune system.[2] Atherosclerotic lesions preferentially develop at sites of disturbed blood flow where the endothelium is locally activated. As lipoproteins and lipids in the vessel wall accumulate to a degree exceeding the capacity of clearance they are retained in the extracellular matrix of the vessel thereby activating endothelial cells (EC) (Figure 1 A).[3] Upon activation EC express leukocyte adhesion molecules such as intercellular adhesion molecule-1 (ICAM-1) and vascular cell adhesion molecule-1 (VCAM-1) which will lead to the adherence of circulating leukocytes.[4] Subsequently, the adherent leukocytes respond to attractant stimuli, such as chemokines produced by the inflamed intima, and transmigrate across the endothelium along a chemokine gradient into the sub-endothelial space further perpetuating lesional inflammation (Figure 1 B). Among those leukocytes are neutrophils, T cells, B cells, monocytes, and natural killer (NK) cells. Chronic hyperlipidemia and local inflammation contribute to enhanced endothelial dysfunction resulting in the infiltration and retention of lipoprotein particles in the nascent plaque.[5] Retained lipoprotein particles such as low-density lipoprotein (LDL) might undergo chemical modification. Presumably, LDL particles are oxidized by anti-microbial products of macrophages, such as reactive oxygen species (ROS), released into the developing atherosclerotic plaque. Excessive uptake of modified and natural lipid particles by macrophages leads to their cytosolic accumulation as droplets transforming the macrophage into foam cells, termed according to their morphologic appearance. Foam cells will undergo apoptosis, necroptosis, and necrosis due to the massive cholesterol scavenging forming the necrotic core of the plaque. The necrotic core and the uncontrolled release of inflammatory mediators from dying macrophages will attract further immune cells, thus perpetuating inflammation (Figure 1 C). Lesional macrophages derive from circulating monocytes and represent an elaborate source of pro-inflammatory mediators such as cytokines. This inflammatory response is further fueled by cell death of chronically overwhelmed macrophages further recruiting more

immune cells including monocytes and lymphocytes to the plaque.[6, 7] Immune cells within the atherosclerotic lesion will release further cytokines which reduce smooth muscle cell (SMC) survival and proliferation.[8]

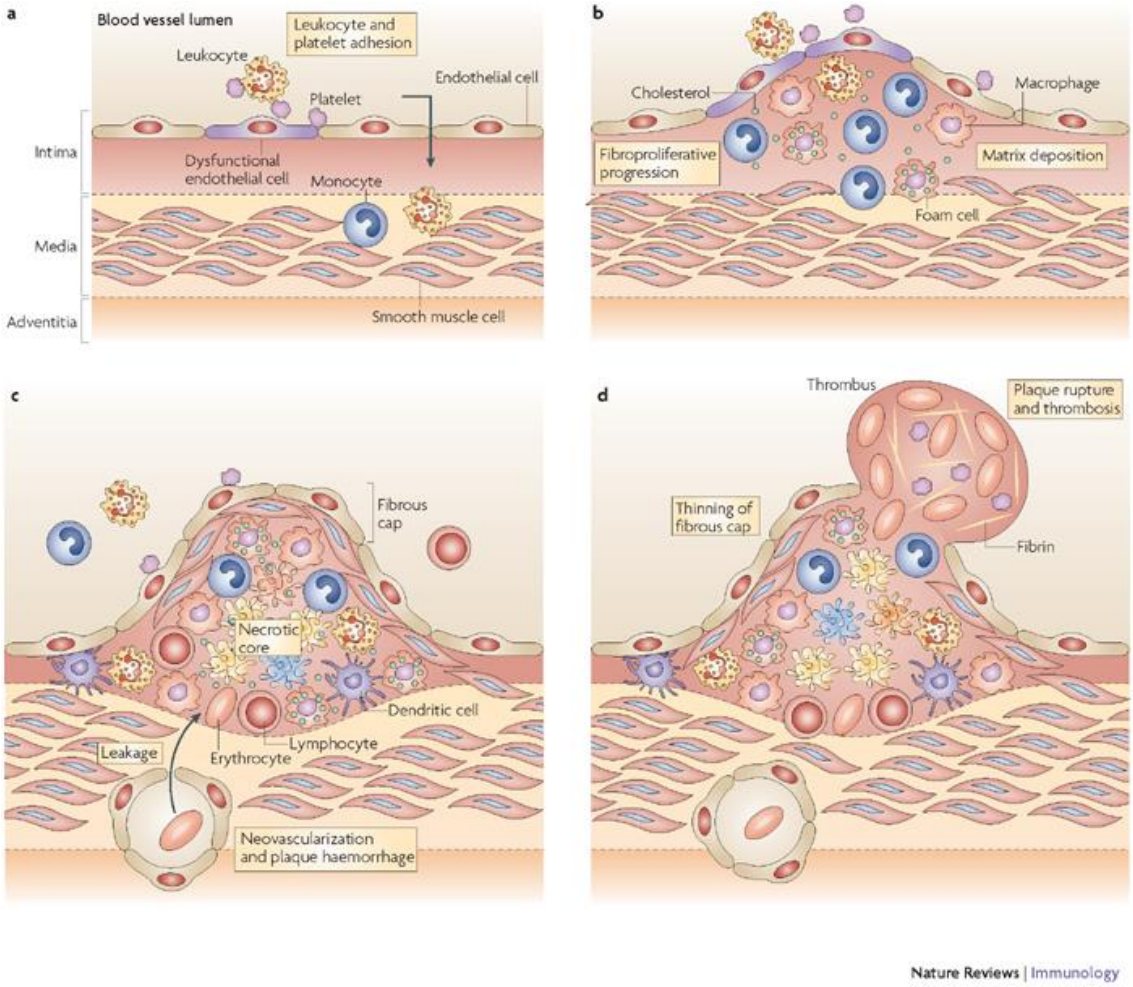

Figure1. Evolution of atherosclerosis.
(**A**) EC dysfunction and activation under pro-inflammatory conditions of hyperlipidemia leads to early platelet and leukocyte adhesion and increased permeability of the endothelium. (**B**) Monocytes that are recruited to the intima and subintima accumulate lipids and transform into macrophages or foam cells, which form fatty streaks. Continued mononuclear-cell influx, deposition of matrix components and recruitment of SMC give rise to the fibroproliferative progression of the plaques. (**C**) Apoptosis of macrophages and other plaque cells creates a necrotic core covered by a fibrous cap consisting of matrix and a SMC layer. Neovascularization can occur within the plaque and from the adventitia, and leakage of fragile vessels can lead to plaque hemorrhage. (**D**) Thinning and erosion of the fibrous cap in unstable plaques, for example, owing to matrix degradation by proteases, may ultimately result in plaque rupture, with release of debris, activation of the coagulation system and plaque thrombosis of the artery. This leads to arterial occlusion and myocardial infarction or stroke. Modified from: Weber, C., Zernecke A., and Libby P.[9]

Thus, the abundance of SMCs and their capacity to produce collagen will be reduced in this pro-inflammatory environment. Furthermore, the release of proteases degrades matrix proteins such as collagen fibers contributing to the thinning of the fibrous cap. The fibrous cap is a layer of fibrous connective tissue and containing collagen, elastin, SMC, EC, and immune cells which protects contact of circulating platelets with plaque-resident, pro-thrombotic material. During advanced atherosclerosis neovascularization

might occur promoting plaque hemorrhage by the leakage of fragile vessels thus contributing to the destabilization of the atherosclerotic lesion. Ultimately, the rupture of the destabilized plaque will be provoked leading to a release of highly-coagulant substances into the blood stream causing rapid thrombus formation and its life-threatening clinical manifestations, namely myocardial infarction and stroke (Figure 1 D).[10]

1.2 The role of T cells in atherosclerosis

Although monocytes/macrophages are the most abundant immune cells in the plaque, several studies have proven a pivotal role for T cells in the pathogenesis of atherosclerosis.[11] Mice deficient for the recombinase activating gene 2 (RAG-2) do not harbor any T- and B cells as the gene re-arrangement of immunoglobuline (Ig)- and T cell receptor (TCR) depends on RAG-2. Atherosclerosis prone *Rag2*$^{-/-}$ mice display reduced atherosclerosis only under mildly elevated hypercholesterolemia.[12, 13] If hypercholesterolemia is exaggerated by administration of a cholesterol-enriched, western-type diet, the innate immune system overrides effects caused by adaptive immune cells.

Cluster of differentiation (CD) 4^{+} T cells are the predominant T cell subset in atherosclerotic lesions of Apolipoprotein E-deficient (*Apoe*$^{-/-}$) mice and accelerate atherosclerosis as demonstrated by reconstitution of lymphocyte-deficient *scid* mice with CD4^{+} T cells.[14, 15] However, subsets of CD4^{+} T cells contribute differently to atherosclerosis which will be discussed in detail below.

CD8^{+} T cells have a controversial role in atherogenesis. In comparison to *Apoe*$^{-/-}$ mice, *Apoe*$^{-/-}$*Cd8*$^{-/-}$ mice exhibit no alteration in lesion formation.[16] However, antibody-mediated depletion of CD8^{+} T cells in LDL receptor-deficient (*Ldlr*$^{-/-}$) mice ameliorated atherosclerosis by the reduction of circulating Ly6C^{hi} monocytes, which are considered to be main driving forces of atherogenesis.[17] Furthermore, CD8^{+} T cells seem to contribute to vulnerable plaque formation by inducing apoptosis of lesional macrophages, SMC, and EC via their cytotoxic products, perforin and granzyme B when adoptively transferred into lymphopenic *Apoe*$^{-/-}$ mice.[18] However, adoptive transfer of CD8^{+}CD25^{+} T cells, a CD8^{+} subset that is considered anti-inflammatory and exerting suppressive effects, decreased atherosclerotic burden in *Apoe*$^{-/-}$ mice.[19] In general, CD8^{+} T cells are considered pro-atherogenic, but their contribution to atherogenesis seems to depend on timing and the subset.

Although T cell activation accelerates early progression of atherosclerosis, it is not required for its initiation, as shown using conditional ablation of dividing T cells in *Apoe*$^{-/-}$ mice.[20] Expression analysis of TCR from atherosclerotic lesions and spectratyping of

fragment lengths revealed a restricted heterogeneity of TCR variation in the atherosclerotic plaque suggesting an accumulation of oligo-clonal T cells.[21] This strongly indicates the recognition of antigen via specific TCR. Antigen-presenting cells (APC) including B cells, dendritic cells (DC) and macrophages express major histocompatibility complex (MHC) II on their surface displaying antigen to $CD4^+$ T cells, typically in secondary lymphoid organs. Recognition of cognate antigen by $CD4^+$ T cells results in their activation und subsequent mode of action. Of note, in human atherosclerotic lesions APCs were shown to express MHCII-complexes, especially the variant HLA-DR, indicating a constant activation of T cells in atherosclerotic lesions.[22]
However, atherosclerosis relevant antigens are largely unknown although current research aims to identify such antigens. Recent evidence suggests peptide moieties of apolipoprotein B (ApoB)-100 as major atherosclerosis-specific antigens.[23] Additional candidate antigens contributing to an adaptive atherosclerosis-specific immune response are heat shock protein (HSP) 60 and HSP65.[24]
As discussed above, $CD4^+$ T cells come in different flavors and each subset contributes differently to atherosclerosis. Naïve $CD4^+$ T cells are undergoing differentiation during their activation and each subset classically bears a hallmark transcription marker specific for their lineage. However, there is increasing evidence, also in atherosclerosis, that committed and lineage-restricted $CD4^+$ subsets display a certain degree of plasticity. For instance, anti-inflammatory regulatory T cells (Treg) represented by Forkhead Box P3 (Foxp3) expression gain expression of the pro-inflammatory and Treg-atypical cytokine interferon gamma (IFNγ) in the inflammatory milieu of the atherosclerotic lesion.[25, 26]
T helper (Th) 1 cells are considered to be the prototypical pro-inflammatory and –atherogenic T cells. They are characterized by IFNγ–secretion and the expression of the T-box transcription factor (T-bet), which fosters Th1 differentiation whilst suppressing Th2 differentiation.[27] Deficiency of T-bet decreases atherosclerotic burden in mice accompanied by reduced IFNγ levels and an enhanced, atheroprotective Th2-mediated antibody response.[28] Further studies identified significant IFNγ-expression in atherosclerotic lesions indicating Th1 cells as the most abundant $CD4^+$ T cell subset. Deficiency of IFNγ or its receptor led to diminished atheroma development.[29, 30] However, atheroprotection based on IFNγ-deficiency was gender-biased and only conferred protection to male mice. IFNγ enhances recruitment of T cells and macrophages to the plaque, inhibits SMC infiltration and proliferation, reduces collagen production and increases the synthesis of extracellular matrix-degrading proteins thereby promoting a rather unstable plaque phenotype which is prone to rupture.[31]
Additional cytokines associated with Th1 cells are interleukin (IL)-12 and IL-18. IL-12 is

typically produced by DC, macrophages, neutrophils and a subset of T cells. IL-12 stabilizes the Th1 subset whilst reducing IL-4 production, a cytokine typically expressed by Th2 cells that in turn suppresses IFNγ production. Furthermore, IL-12 increases expression of MHCII, CD80, and CD86 on APCs thereby enabling an efficient immune response.[32] Conversely, IL-12-deficiency impairs a Th1-mediated immune response and is atheroprotective.[33] IL-18 acts synergistically with IL-12 by inducing Th1 differentiation and IFNγ production in NK cells, T cells, macrophages, and in SMCs.[34, 35] In addition, IL-18 increases the expression of matrix metalloproteinases (MMP) which degrade extracellular matrix thereby rendering the atherosclerotic plaque vulnerable.[36]

The role of Th2 cells in atherosclerosis is still controversial. The Th2 lineage transcription factor is trans-acting T cell-specific transcription factor (GATA-3) and Th2 associated hallmark cytokines are IL-4, -5, and -13.[37-39] IL-4 is repressing differentiation of pro-inflammatory Th1 cells and lack of IL-4 leads to increased atheroprogression.[33] However, this phenotype was very mild in *Apoe*$^{-/-}$ mice whereas *Ldlr*$^{-/-}$ mice deficient for IL-4 demonstrated reduced atherosclerotic plaque formation.[37] Next to T cells a variety of plaque-resident cells are affected by IL-4 leading to increased lipid oxidation in the nascent lesions, recruitment of leukocytes by enhanced endothelial activation and cytokine secretion, increased macrophage activation to scavenge lipoproteins deposited in the arterial wall and concomitantly foam cell formation.[40, 41] Furthermore, IL-4 induces atheroprotective M2-like macrophages via map kinase signaling pathways.[42] Surprisingly, hypercholesterolemic *Apoe*$^{-/-}$ mice demonstrate pronounced Th2 responses as defined by enhanced IL-4 production in atherosclerotic lesions without positively influencing atheroprogression.[43]

The cytokine IL-5 is considered anti-atherogenic and is pivotal for development of B1 cells. This subclass of B cells is anti-atherogenic by their potent secretion of oxidized (ox)LDL-directed natural IgM antibodies. These antibodies support the clearance of oxLDL particles thus contributing to reduced foam cell formation.[38]

IL-13 is also atheroprotective. Transplantation of *Il13*$^{-/-}$ bone marrow exacerbated atherosclerosis whereas injection of recombinant IL-13 limited plaque progression by reduced lesional macrophage content and a M2 macrophage skewed phenotype.[39]

Overall, the influence of the Th2 lineage on atherosclerosis requires careful interpretation. The most frequently applied mouse models in atherosclerosis-related research, *Apoe*$^{-/-}$ and *Ldlr*$^{-/-}$ mice, were derived from the C57Bl/6 strain that intrinsically favors a Th1 driven immune response.[44]

Recently, the Th17 subset of CD4^{+} T cells was discovered and categorized different from the Th1 and Th2 lineages.[45, 46] IL-17 is the characteristic Th17 cytokine by which chronic inflammation and autoimmune diseases, such as arthritis and colitis, are

promoted.[47, 48] Furthermore, murine Th17 cells are defined by expression of the lineage marker of retinoic acid receptor-related orphan receptor (ROR)-γt. Th17 cells derive from naïve T cells in the presence of antigen and the cytokines TGFβ and IL-6.[49] Th17 cells are potent sources of IL17A, IL-17F, IL-21, IL-22, and IL-23.[50] Although the presence of IL-17- and IFNγ-producing T cells in atherosclerosis was observed, their contribution to atherosclerosis is under debate.[51] As Th17 cells are potent sources of the aforementioned cytokines they fuel the inflammatory component in atherosclerosis.[52, 53] However, other reports detected anti-atherogenic features of the hallmark cytokine IL17.[54, 55]

1.3 Tregs in atherosclerosis

Tregs are important to sustain self-tolerance and play a pivotal role in the prevention of autoimmunity controlling the balance of an immune response, particularly those driven by T cells. They are generally defined as CD4+ T cells expressing high-levels of CD25, and Foxp3.[56] Natural (n)Tregs derive from the thymus where they undergo selection against self-antigens expressed in the context of MHCII by medullary thymic epithelial cells (mTEC) and DC under the transcription factor autoimmune regulator (AIRE). During this process, called negative selection, the developing Treg needs to receive low to intermediate signals provided by the TCR and proper costimulatory signals.[57, 58] A strong TCR signal would lead to the deletion of the developing thymocytes since it represents a potential threat to the host immune system. Induced (i)Treg originate from peripheral naïve T cells during an ongoing immune reaction. In mice, nTregs are characterized by the expression of Neuropilin-1 and Helios.[59] Nonetheless, this concept might need further careful evaluation. Neuropilin-1 may be a more reliable marker for nTreg as Helios expression was recently also reported by murine iTregs, however, Neuropilin-1 is not expressed by human Tregs.[60, 61]

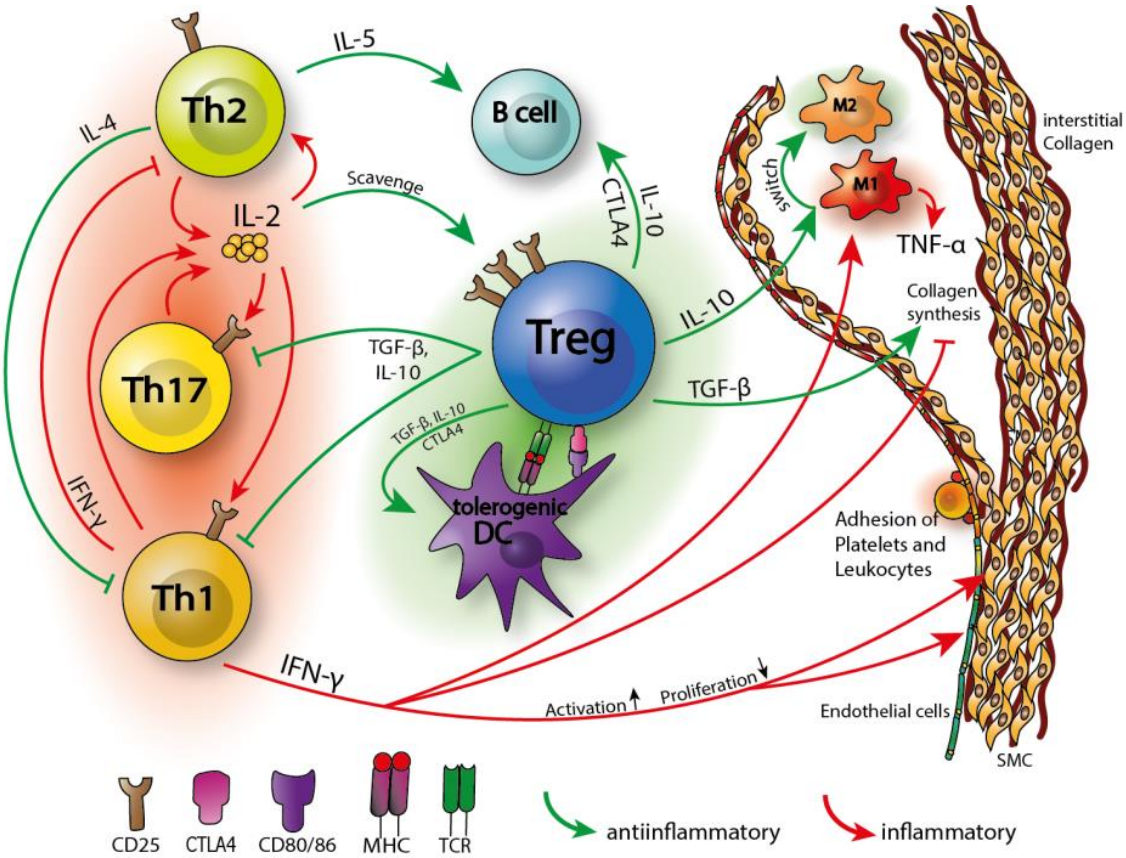

Figure 2. Tregs employ several modes to act on other immune cells in atherosclerosis.
By releasing IL-10 and transforming growth factor β (TGFβ) Tregs suppress Th1 and Th17 activation and proliferation. Accordingly, release of pro-inflammatory IFNγ is limited leading to reduced M1 macrophage polarization, SMC-, and EC activation. Activated endothelium fosters adhesion of platelets and leukocytes promoting progression of atherosclerosis. IFNγ inhibits Th2 differentiation and collagen synthesis enhancing inflammation and destabilizing the plaque. Treg-derived TGFβ can antagonize these IFNγ-mediated effects and stabilizes the plaque. Furthermore, secretion of IL-10 can induce a switch of pro-inflammatory M1 macrophages to a more anti-atherogenic M2 phenotype. Tregs support development of tolerogenic DC by secretion of TGFβ and IL-10 or interaction of cytotoxic-T-lymphocyte-associated protein 4 (CTLA-4) with CD80/86. Amongst other pathways, Tregs can inhibit B cell activation via CTLA-4- or IL-10-mediated mechanisms. Activated T effector (Teff) cells release IL-2 which they require as an autocrine survival factor for further activity. High expression of CD25, the IL-2 receptor a chain, on Tregs scavenges IL-2, thus depriving the microenvironment of this growth factor and ultimately dampening the pro-inflammatory T cell responses. Red-shaded cells and red arrows are considered mainly pro-inflammatory and contribute to athero-progression. Conversely green-shaded cells and green arrows diminish inflammatory response and mitigate the course of the disease. Modified from Spitz, Winkels et al.[62]

Tregs harbor a powerful anti-inflammatory arsenal and are versatile in the modes of action by which they prevent autoimmunity or tissue damage by host-derived immune cells. Conventional $CD4^+$ T cells need to receive co-stimulatory signals via CD28 which binds to co-stimulatory molecules CD80/CD86 provided by APCs. Tregs constantly express CTLA-4, which is a co-inhibitory molecule also binding to CD80/CD86. Thus, Tregs prevent physically the activation of conventional T cells (Figure 2).[63] Furthermore, engagement of CTLA-4 with CD80/CD86 leads to their internalization further reducing their surface abundance and rendering the APC tolerogenic.[64] The high expression of CD25 enables Tregs to deprive the micromilieu from the T cell autocrine growth factor IL-2 limiting growth and survival of effector T cells.

Furthermore, Tregs are potent sources of the anti-inflammatory cytokines IL-10, IL-35, and TGFβ which modulate and reduce the activation of APCs. Additionally, similar to $CD8^+$ T cells, Tregs are equipped with the molecular machinery to produce and release granzyme B and perforin, which can negatively modulate function and survival of conventional T cells, B cells, and NK cells.[65, 66]

Given the aforementioned anti-inflammatory features of Tregs they were also ascribed anti-atherogenic functions. A landmark paper by Ait-Oufella demonstrated that Tregs conferred atheroprotection. The authors observed decreased Treg development and abundance in hyperlipidemic *Ldlr*$^{-/-}$ reconstituted with CD80/CD86- or CD28-deficient bone marrow accompanied by increased atherosclerotic burden.[67] However, CD28 and CD80/CD86 interactions pertain not only to Treg function and development as IFNγ-producing T cells display markedly reduced activation in absence of either molecule. In hyperlipidemic mice, this can lead to complex, vulnerable atherosclerotic lesions.[68]

Injection of an anti-CD25 antibody in hyperlipidemic mice reduced abundance of Tregs and concomitantly increased lesion size and infiltration of macrophages and conventional T cells.[67] However, besides Tregs, also activated conventional T cells, NK cells, B cells, and DC express CD25, thus, pharmacological depletion of Tregs might also affect other immune cell subsets.[69] Vice versa, the adoptive Tregs was atheroprotective in mice.[70] However, Tregs were isolated by fluorescence activated cell sorting (FACS) and defined as $CD4^+CD25^{hi}$ leaving this population contaminated by activated conventional T cells and only enriched for natural Tregs.

A recent study provided by Klingenberg *et al.* indirectly confirmed the anti-atherogenic propensities of Treg. Hyperlipidemic *Ldlr*$^{-/-}$ mice were transplanted with bone marrow from transgenic mice expressing the diphtheria toxin receptor under control of the Foxp3 promotor. Treatment of the resulting bone marrow chimeric mice with diphtheria toxin induced cell death of all $Foxp3^+$ Tregs resulting in their systemic ablation.[71]

Tregs represent potent sources of the anti-inflammatory cytokine TGFβ. Nevertheless, TGFβ is also expressed by other circulating and plaque-resident cells, such as platelets and macrophages. Presence of TGFβ stabilizes the atherosclerotic lesion by increasing SMC survival and enhancing their capacity to synthetize collagen. Concomitantly, macrophages become foam cells to a lower extent (Figure 2).[72, 73] Conversely, desensitizing T cells or DCs for TGFβ-mediated signals by overexpression of a dominant-negative TGFβ receptor induced increased atherosclerotic burden and pronounced T cell responses in atherosclerosis-prone mice.[74, 75] As demonstrated for defective TGFβ signaling, deficiency of IL-10 increased atherosclerotic burden accompanied by increased macrophage and T cell infiltration.[76, 77] In contrast, IL-10 overexpression was atheroprotective, prevented a Th1-mediated immune response in

the atherosclerotic lesion and fostered the generation of IL-10-producing iTregs, called Tr1 cells.[78]

Interestingly, the development of both Th17 and Tregs depends on the presence of TGFβ suggesting linkage between both cell types. During the progression of atherosclerosis Th17 cells dominate over Tregs further contributing to the pro-inflammatory component of the chronic disorder.[79] In notion of this phenomenon, a recent study demonstrated the vanishing of Tregs from atherosclerotic lesions in hyperlipidemic *Ldlr*$^{-/-}$ mice at later stages of atherosclerosis.[80] However, further research will have to demonstrate whether Tregs emigrate from the atherosclerotic lesion, lose expression of their hallmark transcription factor Foxp3, or whether they undergo cell death.

Although Tregs are anti-inflammatory and a plethora of data ascribes Tregs anti-atherogenic propensities, there is only indirect evidence linking Treg numbers to atheroprogression and further research is required to formally demonstrate the role of Tregs in atherosclerosis.[62]

1.4 Macrophages in atherosclerosis

Macrophages are cellular key players in atherosclerosis and they are involved in plaque initiation, progression, but also in regression.[81] Most macrophages derive from circulating monocytes which roll along the endothelium. Monocytes express chemokine (C-C motif) receptors (CCR)5 and CCR1 which enable them to sense chemokine (C-C motif) ligand (CCL)5 (aka RANTES) and CXCL1 deposited on the activated endothelium fostering their local arrest. Subsequently, VCAM-1 and ICAM-1 expressed on the endothelium interacting with lymphocyte function-associated antigen 1 (LFA-1) and very late antigen-4 (VLA-4) expressed by monocytes leads to firm adhesion. The chemokines CCL2, CX3CL1 (also known as fractalkine), and CCL5 secreted by activated EC, macrophages, and SMCs mediate transmigration of macrophages into the nascent atherosclerotic lesion via CCR2, CCR5, and CX3CR1, respectively.[82] However, lesional macrophage content is not only dependent on monocyte recruitment but there is substantial contribution by proliferation of plaque-resident macrophages.[83, 84] Once recruited to the intima, the macrophages will scavenge deposited lipoprotein particles and turn into foam cells. Macrophages express LDLR, however, increased cellular cholesterol content decreases LDLR expression, diminishing their capacity to scavenge ApoB-containing lipoproteins.[85] Furthermore, macrophages express substantial amounts of scavenger receptors. These receptors are pattern recognition receptors (PRR) and a variety has been described to promote foam cell formation including scavenger receptor (SR)-A1, SR-B1, lectin-type oxLDLR 1 (LOX1), and

CD36.[86] Deficiency for CD36 and SR-A1 reduced foam cell formation in hyperlipidemic *Apoe*$^{-/-}$ mice, but did not completely prevent it, suggesting other pathways being involved in foam cell formation.[87] Indeed, macrophages exert pinocytosis in the intima to take up native and modified LDL particles in a receptor-independent fashion. The internalized lipoproteins are degraded in the late endosomal compartment where the cholesteryl esters are hydrolyzed to free cholesterol and free fatty acids. The free cholesterol will be transported to the endoplasmatic reticulum (ER) where the enzyme acetyl-coenzyme A:cholesterol acetyltransferase 1 (ACAT1) catalyzes esterification of free-cholesterol to cholesteryl fatty acid esters that will occur as lipid droplets in foam cells as defined by their microscopic appearance.[88]

The oxidative and enzyme rich milieu of the nascent atherosclerotic lesion results in the generation of modified lipoproteins, particularly oxLDL. Macrophages scavenge significant amounts of oxLDL *in vitro* and demonstrate PRR expression, especially toll-like receptor (TLR)2 and TLR4 which are both exerting pro-atherogenic functions.[89-91] PRR sense pathogen-associated molecular patterns (PAMP) exposed by infectious threats to activate the innate immune system. Furthermore, they can recognize danger-associated molecular patterns (DAMP) provided by endogenous agents which display molecular similarities to PAMPs. Reactivity to agents of both families is pivotal by maintaining physiological homeostasis. Reactivity to PAMPs helps to clear the body from pathogens whereas DAMPs induce a sterile inflammatory response towards tissue damage involving the recruitment of phagocytes. In atherosclerosis, among others, cholesterol crystals and oxLDL represent such DAMPs triggering activation of innate PRR.[24]

Besides passive diffusion of cholesterol from the cell membrane, macrophages increase expression of cholesterol efflux transporters such as ATP-binding cassette subfamily A member 1 (ABCA1) and ABCG1.[92] Increased cholesterol levels activate the liver X receptor (LXR) which drives expression of the genes encoding for ABCA-1 and ABCG-1. ABCA-1 mediates cholesterol efflux to Apolipoprotein A1 (ApoA1) whereas ABCG-1 mediates high-density lipoprotein (HDL)-directed efflux. Esterified cholesterol in macrophages is non-reactive, however, free cholesterol is toxic to cells. The increased accumulation of free cholesterol changes membrane fluidity and enhances inflammatory signaling in lipid rafts via TLR and subsequent nuclear factor kappa-light-chain-enhancer of activated B cells (NFκB) activation, but also inhibits further esterification of free cholesterol by ACAT1.[93, 94] The increased accumulation of free-cholesterol and a misbalanced lipid metabolism of macrophages promote sustained ER stress which induces apoptosis.[95] Furthermore, lipid-laden macrophages are less competent in uptake, or so called efferocytosis, of apoptotic cells and particles

from the local environment, leading to secondary necrosis. Due to membrane instability cellular components and lipids are released and further contribute to advanced atherosclerotic lesion development by necrotic core formation.[96] Lesional macrophages phagocytosing cholesterol crystals demonstrate NACHT, LRR and PYD domains-containing protein 3 (NLRP3) inflammasome activation resulting in the enhanced secretion of activated IL-1β.[97] IL-1β is a driving force in atherosclerosis and mice without IL-1β are protected from atherosclerosis.[98]

1.5 Macrophage polarization in atherosclerosis

Macrophages exist in different phenotypes and are classified according their distinct features based on *in vitro* generation. However, the paradigm of M1 and M2 macrophages is nowadays under discussion as the phenotype of macrophages induced by immune-related ligands *in vitro* is not linkable to *in vivo* existing macrophage phenotypes in pathological conditions.[99] However, for reasons of simplicity, I will continue to refer to the classical M1/M2 nomenclature in the following.

M1 macrophages are classically activated *in vitro* by TLR4 agonists such as lipopolysaccharide (LPS) or by IFNγ and their presence was demonstrated in murine and human atherosclerotic lesions.[100, 101] M1 macrophages are rich sources of inducible nitric oxide synthase (iNOS), CCL2, tumor necrosis factor (TNF)α, IL-1β, IL-6, and IL-12. All these pro-inflammatory mediators recruit additional macrophages and T cells and activate the latter mentioned immune cells, EC, and SMC, respectively, thus further perpetuating inflammation.[101] M1 macrophages contribute to plaque destabilization as they secrete significant amounts of matrix-degrading enzymes such as MMP2 and MMP9. Additionally, *in vitro* polarized M1 macrophages display significant reduction in ABCA-1 expression accompanied by decreased cholesterol efflux capacity.[102] However, this *in vitro* generated data is not directly confirmable *in vivo*. Thus, these findings have to be interpreted carefully and *in vitro* generated data cannot necessarily be extrapolated to the actual disease progression.[81]

M2 polarized macrophages are induced by Th2-related cytokines IL-4, IL-13, and IL-10, the latter also produced by Tregs (as discussed above).[100, 103] Phenotypically, M2 macrophages demonstrate expression of CD163, CD206 (also known as mannose receptor 1), resistin-like beta (Fizz1), and arginase 1.[81] This subtype of macrophages harbors anti-inflammatory propensities by the production of TGFβ, IL-10, and IL-1 receptor agonists. In addition, TGFβ can promote M2 macrophage differentiation representing an autocrine feed-forward loop.[104] Furthermore, M2 macrophages produce collagen contributing to plaque stability. Accordingly, these macrophages are predominantly found in regressing plaques.[105]

The presence of both, M1 and M2 macrophages is increased during the progression of atherosclerosis in patients. However, the localization of M1 and M2 macrophages differed in human atherosclerotic plaques where M1 macrophages predominantly locate to rupture-prone shoulder regions whereas M2 macrophages are mostly abundant in the adventitia and in stable regions of the plaque.[106] In mice, atherosclerotic lesions are initially dominated by M2 macrophages whereas the M1 macrophage subset dominates during atheroprogression.[107]

1.6 B cells and Immunoglobulins in atherosclerosis

B cells are predominantly found in the adventitia and contribute to and regulate lesional inflammation.[108, 109] Antibodies specific for plaque-restricted antigens such as oxLDL were detected in human atherosclerotic plaques.[110] Further antigens that can be detected by antibodies in atherosclerosis are HSP60, HSP65, and in general antigenic motifs derived from lipid peroxidation motifs as found on the surface of oxLDL and also on apoptotic cells.[24] The accumulation of oxLDL and apoptotic cells in atherosclerotic lesions represents potent innate immunity activators.

The spleen is a large reservoir for B cells. Splenectomy of *Apoe*$^{-/-}$ mice induced pronounced atherosclerosis compared to sham-operated mice.[111] Furthermore, transplantation of *μMT*$^{-/-}$ bone marrow which is B cell-deficient into *Ldlr*$^{-/-}$ mice aggravated atherosclerosis.[112] However, pharmacological depletion of B cells with anti-CD20-antibodies was atheroprotective in *Apoe*$^{-/-}$ and *Ldlr*$^{-/-}$ mice.[113, 114]

This data suggests that B cell subsets contribute differently to atherosclerosis. In mice, there are two major subsets of B cells, B2 and B1 cells. Whereas (marginal and follicular) B2 cells are bone marrow-derived, B1 cells are most apparent in peritoneal and pleural cavities and seem to be of a different developmental origin.[115, 116] Markers for B1a cells are $CD19^{+}B220^{low}IgM^{hi}CD5^{+}CD43^{+}CD23^{-}$ whereas B1b cells are CD5 negative.[117] IL-10-producing regulatory B cells (Bregs) represent another subset of B cells mediating an immune-modulatory function, however, their contribution to atherosclerosis by IL-10 seems negligible.[118] Innate response activator (IRA) B cells express granulocyte-macrophage colony-stimulating factor (GM-CSF) by which they seem to foster expansion of mature DCs which in turn stimulate differentiation of naïve T cells into IFNγ-producing Th1 cells accompanied by a switch from IgG1 to IgG2c oxLDL-specific antibodies ultimately leading to pronounced atherosclerosis.[119] Interestingly, patients with symptomatic cardiovascular disease (CVD) have elevated numbers of splenic IRA B cells.[119]

Although the role of B2 cells in atherosclerosis is controversial, the picture for B1 cells, particularly B1a cells, seems clearer. The exact contribution of B1b cells to

atherosclerosis however, needs to be defined. As outlined above (1.2), IL-5, a Th2-associated cytokine, is necessary for B1a cell development and maintenance. Conversely, lack of IL-5 leads to pronounced atherosclerosis in hyperlipidemic mice.[38]

Levels of circulating IgM antibodies recognizing oxLDL or malondialdehyde (MDA)-modified LDL, another naturally-occurring oxidized form of LDL, are inversely correlated with the carotid intima–media thickness or the risk of developing a >50% diameter stenosis in the coronary arteries.[120, 121] Natural IgM antibodies are germline-encoded and mainly produced by B1 cells. The generation of natural IgM is independent of exogenous antigen presentation.[122]

Transplantation of B1a cells isolated from *sIgM*$^{-/-}$ donor mice, which express but do not secrete IgM did not protect from pronounced atherogenesis suggesting B1a cell-derived IgM responsible for the anti-atherogenic effects of B1a cells.[123] Indeed, anti-oxLDL-specific IgM antibodies, in particularly clone E06, prevent the binding of oxLDL to CD36 and SR-B1 on macrophages *in vitro* subsequently reducing oxLDL uptake and foam cell formation.[124]

B2 cells express different subclasses of IgG which are IgG1, IgG2, IgG3, and IgG4 in humans and IgG1, IgG2a/c, IgG2b, and IgG3 in mice.[117] Each of the IgG subtypes exhibits different fragment crystallizable gamma receptor (FcγR) affinity and harbors different capacities to activate the complement system.[125, 126] OxLDL-specific IgG antibodies were detected in atherosclerotic lesions, however, the correlation between circulating oxLDL-antibody titers and CVD risk remains controversial.[110, 127] As mentioned before, the depletion of B cells lowered atherosclerotic burden and concomitantly titers of oxLDL-specific IgG antibodies and to a lesser extent those of IgM antibodies.[113, 114] However, most information about IgG antibodies in atherosclerosis was derived from immunization approaches with HSP65 or oxLDL. *Ldlr*$^{-/-}$ mice administered a regular chow diet and immunized with HSP65 mounted high anti-Hsp65 IgG antibody titers and displayed aggravated atherosclerosis.[128] Most likely, this effect was caused by damage of EC expressing the HSP65 homologue HSP60.[129] On the contrary, immunization with MDA-LDL induced increased amounts of specific antibodies and was atheroprotective in hyperlipidemic mouse models.[130, 131] Contrasting results were obtained *in vitro*, where plasma from mice with high IgG titers to MDA-LDL inhibited oxLDL uptake by macrophages whereas recombinant human MDA-LDL–specific IgG1, which is atheroprotective, promoted uptake of oxLDL by macrophages.[132, 133] Whether these effects are actually representative of the processes occurring *in vivo* remains to be determined.

The role of the allergy-mediating IgE was only indirectly tested in atherosclerosis. *Apoe*$^{-/-}$ mice deficient for the high-affinity FcεRI receptors contained smaller

atherosclerotic lesions accompanied by reduced macrophage and apoptotic cell content. Mechanistically, the binding of IgE induced activation of FcεRI which cooperates with TLR4 on macrophages inducing cytokine secretion and cell death.[134]
Another Ig subclass is represented by IgA which confers mucosal protection against pathogens, however, substantial amounts are found in the circulation of humans. The mechanistic contribution of IgA to atherosclerosis is not resolved yet. However, epidemiologic studies correlate circulating IgA titers with myocardial infarction, CVD, and cardiac death in hyperlipidemic humans.[135, 136]

1.7 An introduction to the CD27/CD70 dyad

A functional T cell response requires not only ligation of the antigen-specific TCR by its cognate MHC:antigen complex but also proper signaling provided by costimulatory molecules. These signals are important during different stages of a T cell response, such as clonal expansion and during the function and survival of T cells in primary and secondary immune responses. Many studies revealed the effects of costimulatory molecules belonging to the Ig-like CD28 family or TNF receptor (TNFR) family. Activation of CD28 by its ligands CD80 and CD86 leads to T cell division and survival. The costimulatory axis CD40/CD154 exerts many different effects beyond its critical involvement in B cell help and subsequent switch of the antibody isotype. Most notable these interactions also contribute to cell activation and promote cytokine release.
CD27 and CD70 are members of the TNFR family. The homology between murine und human CD27 and CD70, respectively, is 60-65% and their respective expression patterns between species are comparable.[137-139]
CD27 is expressed on naïve T cells at steady state. In addition, CD27 is expressed on NK cells, activated B cells, and hematopoietic stem cells.[139, 140] CD70 - the ligand of CD27 - is transiently expressed on T cells, B cells, and DCs upon activation thus reflecting recent antigenic priming.[141] However, APC in the thymus including mTEC[141] and in the lamina propria[142] express CD70 constitutively. Furthermore, NK cells were reported to express CD70.[143] Expression of CD70 is induced by signaling via TLR, CD40-CD40L interactions, and signaling via antigen receptors.[141, 144]
The exclusive expression pattern of CD27 and CD70 suggests important impacts of these molecules during the initiation of a T cell and B cell response not only at the priming site but also in the periphery where the T cell receives signals via CD27 ligating to CD70 on activated B cells, DCs, or through the interaction with other T cells.[145]
CD27 forms stable dimers via disulfide-bonds which upon activation trimerize thus enabling interaction with the homotrimeric type II membrane bound CD70. The interaction of CD27 with CD70 leads to the cleavage of CD27 from activated T cells by

surface expressed metalloproteases displaying a first step of negative regulation.[146, 147] CD27 and CD70 are exclusive interaction partners and so far no other potential binding partner has been found. The ligation of both molecules elicits bidirectional signaling. CD27, like other members of the TNFR family, has an intracellular domain to which the TNFR-associated factor 2 (TRAF2) and TRAF5 bind relaying further signals to activate NFκB pathways.[148] Indeed, TRAF5 deficiency blocks CD27-mediated signaling.[149] Furthermore, coupling of TRAF2 to CD27 activates the c-Jun-N-terminal kinase (JNK)-signaling cascade further contributing to inflammatory processes and potentially exerting anti-apoptotic effects.[150] Moreover, CD27 can bind to apoptosis-inducing factor (Siva1) which is an intracellular mediator of apoptosis and, indeed, these interactions induce cell death.[151, 152] However, as discussed below, CD27 costimulation contributes to cellular activation and survival, thus the exact function of this interaction remains undefined.

Furthermore, CD70 also bears signaling activity. Suboptimally-activated B cells triggered with an agonistic CD70 antibody elicited phosphatidylinositol-4,5-bisphosphate 3-kinase (PI3K) and mitogen-activated protein kinase (MEK) pathways resulting in enhanced proliferation and IgM production *in vitro*.[153] Further studies substantiated signaling via CD70. Ligation of soluble CD27 to CD70 increased surface expression of other immune-regulatory molecules such as CD40L on $CD4^+$ T cells whereas $CD8^+$ T cells displayed enhanced CD25, CD70, and 4-1BB expression, which is also a costimulatory molecule of the TNFR family.[154]

1.8 The CD27/CD70 dyad in T cell responses

CD27 signaling plays an important role in Treg development as well as for antigen-specific $CD4^+$ and $CD8^+$ T cell memory formation, which is reduced in virus-infected *Cd27*$^{-/-}$ mice rendering them more susceptible for a second infection.[155, 156] However, CD27 is not a classical costimulatory molecule per definition such as CD28 since it does not influence the rate of cell division of antigen-primed T cells but seems to prolong T cell survival. Indeed, B-cell lymphoma-extra large (Bcl-x_L), an anti-apoptotic molecule, is upregulated in T cells triggered *in vitro* by CD27 signaling.[157] Additional *in vitro* experiments demonstrated enhanced T cell proliferation and cytokine production upon treatment with an agonistic anti-CD27-antibody and administration of growth factors such as phytohaemagglutinin or IL-2.[158, 159] Furthermore, CD27 signaling was pivotal for the IL-2 production of antigen-primed CD8 T cells at the site of infection in non-lymphoid tissue regulating their survival and proliferation.[160] Moreover, CD27 costimulation promoted expression of the chemokine CXCL10 by primed $CD8^+$ T cells further attracting T cells to the site of infection.[161] In addition, CD27/CD70-driven

costimulation seems to influence T cell polarization. Human $CD4^+$ T cells stimulated via CD27 displayed increased survival and enhanced expression of T-bet and the cytokine receptor IL-12 receptor β2 chain (typical for Th1 cells).[157] Furthermore, the constitutive expression of CD70 induced conversion of naïve T cells into IFNγ-producing effector T cells which induced a patho-inflammatory condition increasing mortality of these transgenic mice.[162, 163]

1.9 The CD27/CD70 dyad in B cell responses

The CD27/CD70 dyad exerts important effects on the B cell compartment as well. CD70 surface expression is increased on activated human and murine B cells.[164, 165] However, in humans, CD27 is upregulated during T cell help in the germinal center reaction and is still highly expressed on memory B cells whereas in mice only splenic marginal zone B cells and a subset of B1 cells express CD27.[164, 165] Hence, murine B cells express CD27 temporarily and spatially restricted suggesting involvement in the germinal center response. Proper CD27/CD70 signaling is needed for B cell proliferation and plays an important role during the process of Ig synthesis.[166] Insufficient CD70 triggering on B cells leads to an impaired germinal center formation thereby affecting the humoral immune response.[167] However, B cells from *Cd27*$^{-/-}$ mice still undergo class switching and Ig maturation in aged mice, thus, other factors contribute and compensate for CD27 defects which are only present during early phases. In contrast, human $CD27^+$ B cells produced a higher amount of Ig, IL-10, and displayed enhanced survival.[168-170] In accordance, humans carrying mutations in the CD27 gene suffer from a severe immunodeficiency characterized by hypogammaglobulinemia, dysregulated lymphoproliferation and increased susceptibility for infections with Epstein-Barr virus (EBV).[171-173] Costimulation of CD70 via CD27 induced B cell proliferation but impaired terminal differentiation and Ig secretion of human and murine B cells although stimulation of CD70 via soluble CD27 resulted in increased Ig secretion.[153, 166, 174] Thus, soluble and membrane bound CD27 interacting with CD70 exerts species-specific effects and seems to contribute to a germinal center reaction in mice whereas in humans, CD27 promotes terminal B cell differentiation and CD70 might downregulate humoral immunity. Interestingly, blocking CD27/CD70 interactions in lymphocytic choriomeningitis virus (LCMV) infections enhanced the clearance of pathogens from the area of infection by enhanced production of neutralizing antibodies by B cells.[175]

1.10 Implications of the CD27/CD70 dyad in autoimmune disorders

The co-stimulatory dyad CD27/CD70 plays important roles in several autoimmune disorders.

Patients suffering from systemic lupus erythematosus (SLE) had higher numbers of circulating $CD27^{high}$ plasma cells which correlated with SLE disease activity index (SLEDAI) and titers of anti-double stranded deoxyribonucleic acid (anti-dsDNA) autoantibodies.[176] Additionally, levels of serum sCD27 positively correlated with SLEDAI.[177] Furthermore, SLE patients demonstrated enrichment of $CD70^+$ $CD4^+$ T cells among memory T cells. This population remained stable over time possibly involving these cells in SLE progression and susceptibility, however, excluding them as a biomarker for SLE prognosis.[178] Interestingly, $CD4^+$ T cells isolated from SLE patients and healthy controls substantially increased CD70 expression when incubated with DNA methylation inhibitors. These treated $CD4^+$ T cells enhanced IgG production by B cells in *in vitro* co-cultures in a CD70-specific fashion.[179] Downregulation of the transcription factor RFX1 increased CD70 overexpression by failed recruitment of transcriptional co-repressors to the CD70 promotor and decreased interactions with DNA methyltransferase 1 (Dnmt1) and histone deacetylase 1 (HDAC1) resulting in an active, hypomethylated CD70 promotor.[180, 181] Similar observations were made in MRL/lpr mice with established lupus-like disease harboring splenic $CD4^+$ T cells with enhanced CD70 expression which was again associated by decreased Dnmt1 expression and a hypomethylated CD70 locus.[182]

Similarly to SLE patients, $CD4^+$ T cells from patients with rheumatoid arthritis (RA) display increased CD70 expression which concomitantly had elevated IFNγ and IL-17 production.[183] However, CD70 expression on $CD4^+$ T cells did not correlate with disease severity, again, excluding its function as a biomarker. Nonetheless, CD70 expression could contribute to lowering of the activation threshold of bystander naïve $CD4^+$ T cells.[181, 184] Moreover, pharmacological inhibition of CD70 with antibodies reduced disease burden and titers of anti-collagen autoantibodies in mice with collagen-induced arthritis, potentially demonstrating a new therapeutical strategy in RA.[185]

As mentioned above, CD70 is constitutively expressed on APCs in the lamina propria of the intestine. This unique APC subset is involved in Th17 differentiation when stimulated with ATP in a germ-free environment via IL-6 and IL-23 production and controls the T cell response towards a listeria infection in the intestinal mucosa.[142, 186] These observations raised the possibility of CD27/CD70 involvement in intestinal associated pathologies, which are also influenced by the microbiome. Indeed, transfer

of naïve *Cd27*$^{-/-}$ CD4^{+} T cells into *Rag*$^{-/-}$ mice induced a less pronounced colitis, which is the murine model of inflammatory bowel disease. In addition, pharmacological CD70 inhibition with antibodies not only protected against colitis when naïve wild-type CD4^{+} T cells were transferred, but also rescued mice from established colitis.[187]

Besides the aforementioned pathologies, the CD27/CD70 axis plays a pivotal role in neuro-immunological disorders. Although patients suffering from multiple sclerosis display increased sCD27 levels in cerebrospinal fluid, the exact involvement of the CD27/CD70 dyad has to be elucidated.[188] Murine models of multiple sclerosis, experimental autoimmune encephalomyelitis (EAE), were used to assess CD27/CD70 implications. Immunization of myelin oligodendrocyte glycoprotein (MOG)-specific TCR transgenic mice with MOG peptide induced profound EAE accompanied by reduced Treg abundance when CD70 was constitutively expressed by B cells.[189] Moreover, MOG-TCR transgenic mice immunized with MOG displayed exacerbated EAE when deficient for CD27 or CD70 based on a pronounced Th17 response which is considered a driving pathogenic force in EAE progression.[190] These facts argue for a tempo-spatial context of CD27 and CD70 expression on the outcome of EAE in the investigated murine models.

1.11 The role of CD27/CD70 interactions in tumor immunology

Hematologic malignancies and solid tumors feature high CD70 expression.[191-195] Constitutive expression of CD70 might cause immune-evasive effects and thus positively propagate tumor growth. Indeed, as pointed already out in aforementioned sections, CD27/CD70 interactions drive the development of Tregs. Furthermore, recent work demonstrated abrogated expansion and differentiation of intratumoral iTregs in *Cd27*$^{-/-}$ mice resulting in decreased tumor growth and an effective anti-tumor immune response.[196] Conversely, constant CD27/CD70 interactions promote IL-2 production and conventional CD4^{+} and CD8^{+} T cell survival which further nourishes Tregs resulting again in an immune-evasive and anti-inflammatory tumor micromilieu.[196] Indeed, increased abundance of intratumoral Tregs is linked to a poor prognosis for cancer patients.[197-199] Secondly, the constitutive expression of CD70 in combination with persistent antigen exposure causes exhaustion of effector T cells which was demonstrated in patients suffering from B cell non-Hodgkin's lymphoma.[200] Exhausted T cells are less active and cytotoxic and thus do not mount a resounding attack on the tumor. Furthermore, antibodies targeting CD70 could induce antibody-dependent cellular cytotoxicity and phagocytosis enabling the destruction of tumor cells by immune cells ultimately leading to tumor regression. Thus, blocking-CD70 antibodies

provide a promising therapeutical strategy in the treatment of aforementioned malignancies and several antibodies are currently clinically evaluated.[201, 202]

Another therapeutical intervention represents the agonistic modulation of CD27 which could complement and amplify current anti-tumor strategies. Moreover, agonistic modulation of CD27 also represents a promising therapeutical strategy. As highlighted above, T cells demonstrate exhaustion in a variety of malignancies leading to a reduced cytotoxic activity and propagated tumor growth. The re-activation of T cells facilitates recognition of tumor cells by T cells and their destruction. To test this hypothesis, mice with a transgenic human CD27 locus were challenged with colon carcinoma and T cell lymphoma.[203] The administration of a humanized CD27-agonistic antibody successfully reduced tumor burden and induced resistance of those mice towards future tumor challenges. Causative for tumor regression was a highly effective anti-tumor cytotoxic $CD8^+$ T cell response which was supported by a $CD4^+$ T cell response.[203] This particular agonistic CD27 antibody, CDX-1127 (varlilumab), is now investigated in clinical trials therapeutically targeting B-cell malignancies, melanoma, and renal cell carcinoma.[199, 204] Of note, the antibody transiently influenced abundance of circulating $CD27^+$ immune cells in cynomolgus monkeys and rhesus macaques. $CD8^+$ T cells, Treg, and NK cells were transiently reduced in circulation whereas CD4 T cells were increased.[203, 205] However, the successful regression in tumor burden outweighs potential off-target effects caused by a reduction in circulating immune cells.

The CD27/CD70 dyad plays an important and complex role in tumor immunology. Targeting CD27/CD70 interactions in advanced cancer malignancies represents a promising therapeutical approach. Patients with advanced malignancies displaying high CD70 expression on tumor cells would benefit from a CD70 blocking antibody whereas the therapeutical, agonistic stimulation of CD27 reconstitutes the activity of exhausted cytotoxic $CD8^+$ T cells. Subsequently, these cells can mount a cytotoxic anti-tumor immune response leading ultimately to the regression of tumor burden. Both therapeutical strategies modulate the patients' immune system to respond to the tumor without the need for treatment with chemotherapeutic agents that can have severe side effects. These novel approaches, however, aim to complement and amplify existing anti-tumor strategies.

1.12 The role of CD27/CD70 costimulation in atherosclerosis

The role of T cells and B cells in atherosclerosis and the imminent role of interactions between CD27 and CD70 on these and other cell types strongly suggest the detailed investigation of this costimulatory dyad in the field of atherosclerosis. Little is known about CD27 and CD70 function in atherosclerosis. A recent study demonstrated

chronic CD70 overexpression in B cells to be atheroprotective.[206] This group engineered mice harboring B cells to overexpress CD70 backcrossed to ApoE*3-Leiden mice and administered a high cholesterol/fat diet. The continuous triggering CD27 on T cells led to an increase in the presumably pro-atherogenic Th1 subset. Surprisingly, this transgenic CD70 overexpression exerts rather atheroprotective effects which are probably due to an increased rate of apoptosis among the pro-atherogenic Ly6C^{+} monocytes. As atherosclerosis is largely monocyte-driven it is likely that loss in monocytes ameliorates atherosclerosis. However, the mouse model used in this study suffers additional side effects. Constitutive overexpression of CD70 in B cells results in exhaustion of the T cell pool, due to excessive and continuous activation and thus does not provide conclusive evidence regarding the precise roles of CD27 and CD70 in atherosclerosis.

1.13 Rationale

CD27 and CD70 interactions play important roles in various auto-immune disorders and advanced malignancies. In respect of the limited knowledge of the involvement of CD27 and CD70 interactions in atheroprogression, the here proposed studies aim to specify the influence of costimulation via CD27/CD70 on atherosclerosis at early and late timepoints of atherogenesis. Particularly, athero-prone *Apoe*$^{-/-}$ mice will be crossed to either *Cd27*$^{-/-}$ or *Cd70*$^{-/-}$ mice to investigate the impact of a global deficiency in one of these costimulatory molecules on the generation of atherosclerosis. Furthermore, transplantations of bone marrow derived from CD27- or CD70-Apoe compound mutant mice will help to understand the contribution of each molecule by the hematopoietic component. In addition to atherosclerosis-specific parameters such as plaque size and plaque phenotype other organs and tissues will be analyzed to examine whether and how the different T cell subsets and memory types are influenced by a deficiency in one of the costimulatory molecules. Furthermore, *in vitro* based assays will be performed to elucidate the function of immune cells isolated and generated from CD27- or CD70-compound mutant mice and their potential contribution to atherosclerosis.

The research presented here will provide novel insights in the complex field of adaptive T cell immunity and in particular the effects exerted by CD27 and CD70 in atherogenesis. The most promising approaches to treat atherosclerosis employ different vaccination regimen thereby very specifically influencing the adaptive immune system and long-term T cell homeostasis. As the CD27/CD70 dyad plays an imminent role in the interaction of T cells and B cells, it is important to understand pathways elicited by CD27 and CD70 in immune responses and also upon immunization to

modulate and improve potential vaccination therapies. Furthermore, CD27/CD70 interactions and modulation of both molecules needs to be understood in cancer therapy to gauge potential vascular harmful offside effects.

2 MATERIALS AND METHODS

2.1 General equipment

2.1.1 Table 1: General equipment used for this thesis

Equipment	Modell	Source
Autoclave	VX150	Systex, Linden, Germany
Balance	BP2100S R160P	Sartorius, Goettingen, Germany
Centrifuges	5415R 5810	Eppendorf, Hamburg, Germany
	Multifuge 3S-R Heraeus Multifuge 40R Heraeus	Thermo Scientific, Waltham, MA, USA
	Galaxy Mini Star	VWR, Radnor, PA, USA
Cryotome	CM3050S	Leica, Wetzlar, Germany
Flow cytometer	FACS Canto II FACS Aria III	BD Biosciences, San Jose, CA, USA
Heating block	SBH130DC	Stuart, Staffordshire, United Kingdom
Incubator	Binder CB150	Binder, Tuttlingen, Germany
Laminar Flow Hood	Bdk UVF 6.18 S	Weisstechnik, Sonnenbuehl, Germany
	Herasafe (Heraeus)	Thermo Scientific
Luminex xMAP instrument	MAGPIX	Luminex, Austin, TX, USA
Microplate reader	Tecan GENios	Tecan Group, Maennedorf, Switzerland
Microscopes	DMLB DM6000 SP8 3X	Leica
Microtome	RM2155	Leica
pH-meter	HI2211 pH/ORP meter	Hanna Instruments, Voehringen, Germany
Plate shaker	Titramax 101	Heidolph, Schwabach, Germany
qPCR system	7900 HT Fast Real-Time PCR System ViiA 7 Real-Time PCR System	Thermo Scientific
Spectrometer	ND1000 Nanodrop Peqlab	VWR, Radnor, PA, USA
Thermal cyclers	MyCycler Bio-Rad T100	Bio-Rad, Hercules, CA, USA

Tube Rotator	MACS Mix Tube Rotator	Miltenyi, Bergisch-Gladbach, Germany
Vortex	REAX top	Heidolph
Water purification system	Milli Q Direct Q 16	Merck Millipore, Billerica, MA, USA

All solutions were prepared with Millipore water (Milli Q Direct Q 16, Merck Millipore, Billerica, MA, USA), if not stated otherwise.

2.2 Human specimen

2.2.1 Gene expression of CD27 and CD70 in human plaques

CD27 and *CD70* gene expression data was taken from an existing database and analyzed as described previously.[106, 207] In short, human carotid endarterectomy (cea) specimens were obtained from the Maastricht Pathology Tissue Collection. Atherosclerotic lesions were classified according to the Virmani criteria.[208] Segments considered as stable harbored fibrous cap atheromata or a pathological intimal thickening whereas segments designated ruptured displayed intra-plaque hemorrhage and/or a thrombus encroaching the lumen. Sections were considered stable or ruptured if they were flanked at both sides by a similar plaque type within the same endarterectomy specimen. Only endarterectomy specimen containing stable and ruptured plaque segments (n = 20, respectively) within the same specimen were applied for a microarray analysis to determine mRNA expression by Illumina Human Sentrix-8 V2.0 BeadChip technology (Illumina, Inc., San Diego, USA). All use of tissue and patient data was in agreement with the “Code for Proper Secondary Use of Human Tissue in the Netherlands”. Patients suffering from acute inflammatory disorders (sepsis etc.) were excluded. The patient cohort was 72.55±6.36 and 72.38±7.89 (stable vs. ruptured) years old and 100% vs 95.8% male (stable vs. ruptured).

2.2.2 Human carotid endarterectomy specimens and tissue processing

For (immune-) histological analysis, CEA specimens were obtained from the vascular surgery department of the Academic Medical Center in Amsterdam and immediately fixed in 10% formalin and processed for paraffin embedding. All use of tissue was in agreement with the “Code for Proper Secondary Use of Human Tissue in the Netherlands”.

2.2.3 Histological staining of CEA sections

To determine the plaque phenotype, consecutive sections (4µm) were stained with standard hematoxylin and eosin (H&E) and elastin von Gieson (EVG).
For CD27-positive T cell visualization, sections were boiled in 1 M solution of Tris(hydroxymethyl)aminoethamine (Tris) with a 0.1 M ethylenediaminetetraacetic acid (EDTA) (pH 8.0, Lab Vision, Fremont, USA) and blocked with Lab VisionTM Ultra V-Block (Thermo Scientific). Next, specimens were incubated with monoclonal rabbit anti-human CD3 (dilution: 1:1000; Immunologic BV, Duiven, The Netherlands) antibody. BrightVision poly-horseradish peroxidase-anti-rabbit IgG (Immunologic BV) was used as secondary antibody and visualized by ImmPACTTM AMEC Red Substrate (Vector Laboratories, Burlingame, USA). Furthermore, staining for CD27-positive cells was performed using monoclonal mouse anti-human CD27 (LifeSpan BioSciences, Inc., Seattle, USA) antibody. BrightVision poly-alkaline phosphatase-anti-mouse IgG (Immunologic BV) was used as secondary antibody and visualized by Vector® Blue Substrate (Vector Laboratories, Burlingame, USA). Sections stained solely for CD3 were counterstained with hematoxylin or with nuclear red for CD27, respectively.

2.3 Mice

Cd27$^{-/-}$ mice[155] and *Cd70*$^{Cre/Cre}$ mice[190] were crossed with *Apoe*$^{-/-}$ mice (stock No. 002052, The Jackson Laboratory, Bar Harbor, Maine, USA) mice to generate *Cd27*$^{+/-}$ *Apoe*$^{-/-}$ mice or *Cd70*$^{+/Cre}$*Apoe*$^{-/-}$ mice, respectively. *Cd70*$^{Cre/Cre}$ mice are CD70-deficient as exon 1 of the CD70 locus was replaced by a DNA sequence coding for the Cre recombinase.[156] To simplify matters, *Cd70*$^{Cre/Cre}$ mice will be referred to as *Cd70*$^{-/-}$ mice throughout this thesis. Heterozygous mice were intercrossed and *Cd27*$^{+/+}$*Apoe*$^{-/-}$ and *Cd27*$^{-/-}$*Apoe*$^{-/-}$ or *Cd70*$^{+/+}$*Apoe*$^{-/-}$ and *Cd70*$^{-/-}$*Apoe*$^{-/-}$ littermates, respectively, were used. Housing and breeding of mice followed institutional guidelines. All animal experiments were approved by the local ethical committee for animal experimentation.

2.3.1 Genotyping

Newly weened mice were marked by individual ear notches and holes produced by an ear punch device. A tail biopsy of 1-2 mm length was taken for genotypic analysis of mice.
The tail biopsy was incubated overnight at 56°C in 250 µl tissue lysis buffer (see 2.8) supplemented 1:100 with proteinase k solution (Qiagen, Hilden, Germany). Subsequently, automatic DNA isolation was performed with the QIAxtractor (Qiagen)

according the manufacturer's instructions. The isolated DNA was kept at 4°C and applied for polymerase chain reaction (PCR).

Following PCR mastermixes were prepared for CD27, CD70 and Apoe genotyping reactions:

	Stock concentration	Volume in µl
Dnase-/Rnase-free H_2O	-	12.75
GoTaq Flexi buffer	5x	5
$MgCl_2$	25 mM	2
dNTP mix	10 mM each	0.5
forward Primer	10 µM	1.25
reverse Primer	10 µM	1.25
GoTaq DNA Polymerase	5 U/µl	0.25
Genomic DNA	100 ng/µl	2

GoTaq Flexi DNA polymerase and GoTaq Flexi buffer were obtained from Promega (Promega, Fitchburg, WI, USA). Dnase-/Rnase-free H_2O, primer, magnesium chloride ($MgCl_2$), and the deoxynucleotide triphosphate (dNTP, containing deoxyadenosine/-guanosine/-cytidine/-thymidine triphosphate) mix were obtained from Sigma (Sigma Aldrich, St. Louis, USA).
Two mastermixes each were prepared for CD27 and CD70 genotyping containing either wildtype- or mutant allele-detecting primer.
The PCR program for CD27 DNA detection was composed of an initial step at 94°C for 2 min followed by 35 cycles of each 30 sec at 94°C, 30 sec at 60°C, and 1 min at 72°C. Subsequently, the samples were incubated at 72°C for 5 min and 21°C for 5 min.

Primer sequences for CD27 genotyping:

CD27 wildtype forward	5' CAA ACT CTG GTC CTC TGG AG 3'
CD27 wildtype reverse	5' AGG GCA GTG CTA TCC CTA TC 3'
CD27 mutant forward	5' CGT CTG TCG AGA AGT TTC TG 3'
CD27 mutant reverse	5' AGA AGA AGA TGT TGG CGA CC 3'

The amplified PCR products were each electrophoretically separated applying the QIAexcel Advanced System (Qiagen) according to the manufacturer's instructions. Expected results are a wildtype product at 390 base pair (bp) length and a mutant

product at 680 bp length. DNA samples from heterozygous mice would yield a product at 390 bp and 680 bp length.
Also for CD70 and Apoe genotyping two mastermixes were prepared with the common CD70 or Apoe forward primer and either the wildtype reverse primer or the mutant reverse primer. The PCR program was composed of an initial step at 94°C for 5 min followed by 35 cycles of each 30 sec at 94°C, 30 sec at 60°C, and 1 min at 72°C. Subsequently, the samples were incubated at 72°C for 5 min and 21°C for 5 min.

Primer sequences for CD70 genotyping:

CD70 common forward	5' ACA GGC CTG CTT CAG TTT GT 3'
CD70 wildtype reverse	5' TGC TTT AGC GCT TTC TCT CC 3'
CD70 mutant reverse	5' TCA AGT GTA TGG CCA GAT CG 3'

Expected results for CD70 are a wildtype product at 406 bp length and a mutant product at 472 bp length. DNA samples from heterozygous mice would yield a product at 406 bp and 472 bp length.

Primer sequences Apoe genotyping:

Apoe common forward	5’ GCC TAG CCG AGG GAG AGC CG 3’
Apoe wildtype reverse	5’ TGT GAC TTG GGA GCT CTG CAG C 3’
Apoe mutant reverse	5’ GCC GCC CCG ACT GCA TCT 3’

Expected results for Apoe are a wildtype product at 150 bp length and a mutant product at 245 bp length. DNA samples from heterozygous mice would yield a product at 150 bp and 245 bp length.

2.3.2 Surgical procedure

Mice were administered a normal chow diet and at the age of 18 and 28 weeks, mice were euthanized i.p. with Ketamine/Xylazine and blood was obtained via cardiac puncture. Spleen, abdominal aorta, liver, aortic root, and lymph nodes were harvested after perfusion of the arterial tree with sodium nitroferricyanide(III) dehydrate (Sigma Aldrich) followed by 1% paraformaldehyde (PFA) in phosphate-buffered saline (PBS) perfusion (Sigma Aldrich). Parts of the tissue were stored in RNAlater (Life Technologies, Carlsbad, USA) for 24 h at room temperature and afterwards at -80°C. Hearts were isolated and frozen in Tissue-tek (Sakura Finetek, Torrance, USA). The aortic arch and its main branch points were excised, fixed overnight in 1% PFA in PBS, and embedded in paraffin.

2.3.3 Bone marrow transplantation

Bone marrow cells were isolated from femurs and tibiae of *Cd27*$^{+/+}$*Apoe*$^{-/-}$ and *Cd27*$^{-/-}$ *Apoe*$^{-/-}$ or *Cd70*$^{+/+}$*Apoe*$^{-/-}$ and *Cd70*$^{-/-}$*Apoe*$^{-/-}$ and a single-cell suspension was prepared, followed by lysis of red blood cells (see 2.8). The bone marrow from the donor mice was stored at 5x10^{7}/ml in Roswell Park Memorial Institute 1640 (RPMI1640) (Life Technologies) medium containing 10% fetal bovine serum (FBS) (Life Technologies) and 10% dimethylsulfoxid (DMSO) (Sigma Aldrich) in liquid nitrogen until further use. Six to seven-week-old recipient *Apoe*$^{-/-}$ mice (Jackson laboratory) received drinking water containing antibiotics (polymyxin B sulfate, 6000 U/ml and neomycin, 100 µg/ml, Life Technologies) from 1 week prior to the bone marrow transplantation until 4 weeks after. Recipient mice were lethally-irradiated with 6 Gy (0.5 Gy/min; MU15F/225 kV; Philips, Eindhoven, The Netherlands) on two consecutive days. Following the second round of irradiation recipient mice were reconstituted intravenously with 1.5x10^{6} thawed and washed bone marrow cells from either *Cd27*$^{+/+}$*Apoe*$^{-/-}$ and *Cd27*$^{-/-}$*Apoe*$^{-/-}$ or *Cd70*$^{+/+}$*Apoe*$^{-/-}$ and *Cd70*$^{-/-}$*Apoe*$^{-/-}$ mice, respectively. Recipient mice were allowed to recover for 6 weeks and received a cholesterol-rich diet (HFD) containing 16% fat and 0.15% cholesterol (Western type diet 4021.13, Hope Farms, The Netherlands) for 7 weeks until their sacrifice was performed as described above.

2.4 Protein assays

2.4.1 Flow cytometry

Aortas were digested with an enzymatic cocktail (Collagenase I, 450 U/ml; collagenase XI, 250 U/ml; hyaluronidase, 120 U/ml; deoxyribonuclease (DNase) I, 120 U/ml; all Sigma Aldrich) in PBS containing 20 mM 4-(2-hydroxyethyl)-1-piperazineethanesulfonic acid (HEPES) (Thermo Scientific) for 30 min at 37°C as previously described.[209] Single cell suspensions of the aortic lysates were prepared by filtering the aortic tissue through a 50 µm cell strainer (BD Biosciences). Aortic lysates were washed with 1x PBS and resuspended in 100 µl 1x PBS/staining mix (maximum 2 staining panels were applied due to low abundance of leukocytes). Cell suspensions were prepared from harvested spleens and lymph nodes by tearing the tissues apart. Single cell suspensions were prepared by meshing the tissue through a 70 µm cell strainer (BD Biosciences). Splenic cells were erylysed (6 ml for a whole spleen) for 3 min on ice, washed and filtered through a 70 µm cell strainer. Freshly-drawn blood was incubated with red blood cell lysis buffer (5 ml for 1 ml blood) for 10 min at room temperature and subsequently washed. If the pellet was still containing too many red blood cells, another lysis step was performed (3 ml, 3 min, wash). Wash steps were performed with

1x PBS. Pellets from lymph nodes were resuspended in 1 ml PBS and pellets from whole spleens in 6 ml PBS. Blood leukocytes were resuspended in 100 µl/staining mix. Subsequently, 100 µl of cell suspension were stained with a viability dye (Live/Dead fixable Aqua/Violet/Near-Infrared; Life Technologies) to discriminate between living and dead cells according the manufacturer's instruction concomitantly with Fc-Block (anti-CD16/32-antibody, functional grade, clone:93, 1:100, eBioscience, San Diego, CA, USA). 1x PBS was used for Live/Dead staining as protein components of buffers, such as bovine serum albumin (BSA) FACS buffer, could reduce staining efficacy thus producing false negative results. Single cell suspensions were incubated (20 min, dark, room temperature) and washed with FACS buffer to remove remnant Live/Dead dye. Subsequently, cells were incubated for 20 min on ice with 50 µl of antibody mixes with antibodies from BD Biosciences, eBioscience, Biolegend (San Diego, CA, USA), or Novus Biologicals (Littleton, CO, USA). An extended list of antibodies applied in staining panels can be found below. An additional washing step was performed after antibody-staining with FACS buffer to remove unbound antibodies. In case intracellular stainings were performed the Foxp3/Transcription Factor Staining Buffer Set was used according the manufacturer's instructions (eBioscience). To determine the level of apoptosis, stainings were performed for fluorochrome-conjugated Annexin V (Biolegend) and simultaneous exclusion of dead cells determined by Live/Dead staining (Life Technologies) according the manufacturer's protocol. Apoptosis stainings were analyzed immediately. Other stainings were fixed with 1% PFA in FACS buffer and analyzed within the following days. Single cell suspensions were analyzed using a FACS Canto II (BD Biosciences) and data were analyzed using Flowjo v.10 (Flowjo, LLC, Ashland, USA).

2.4.2 Table 2: Antibodies used for flow cytometry

Antigen	Source and reactivity	Clone	Dilution	Source
CD45 APCe780	Rat-anti-mouse (IgG2b, κ)	30-F11	1:400	eBioscience
CD4 V500	Rat-anti-mouse (IgG2a, κ)	RM4-5	1:200	BD Biosciences
CD8a e450	Rat-anti-mouse (IgG2a, κ)	53-6.7	1:200	eBioscience
Foxp3 PE	Rat-anti-mouse/rat/pig/canine/bovine (IgG2b, κ)	FJK-16s	1:40	eBioscience
CD3 FITC	Armenian Hamster-anti-mouse (IgG)	45-2C11	1:200	eBioscience
CD25 APC	Rat-anti-mouse (IgG1, λ)	PC61.5	1:300	eBioscience
CD44 APC	Rat-anti-mouse/human (IgG2b, κ)	IM7	1:1000	eBioscience
Ki-67 FITC	Rat-anti-mouse/rat/canine/human (IgG2a, κ)	SolA15	1:100	eBioscience
BCL-2 PE	Rat-anti-mouse (IgG1, κ)	10C4	1:40	Biolegend
CD70 PE	Rat-anti-mouse (IgG2b, κ)	FR70	1:100	eBioscience
αβ-TCR e450	Armenian Hamster-anti-mouse (IgG)	H57-597	1:200	eBioscience
γδ–TCR APC	Armenian Hamster-anti-mouse (IgG)	eBioGL3	1:200	eBioscience
CD11b PerCp-Cy5.5	Rat-anti-mouse (IgG2b, κ)	M1/70	1:300	eBioscience
F4/80 BV510	Rat-anti-mouse (IgG2a, κ)	BM8	1:300	Biolegend
CD27 PE-Cy7	Armenian Hamster-anti-mouse/rat/human (IgG)	LG.3A10	1:300	Biolegend
ABCA-1 PE	Rabbit	polyclonal	1:200	Novus Biologicals
ABCG-1 FITC	Rabbit	polyclonal	1:200	Novus Biologicals

APC =Allophycocyanin, PE=Phycoerythrin, FITC = Fluorescein Isothiocyanate, PerCp = Peridinin chlorophyll, Cy = Cyanine

2.4.3 Plasma preparation and lipid analysis

Plasma was isolated by centrifugation (500 x g, 15 min, 4°C) of EDTA-anticoagulated blood. Plasma cholesterol concentration was determined using a colorimetric assay (Roche, Basel, Switzerland). In brief, the plasma samples were diluted 1:5 with 0.9% saline on ice. For a calibration of the machine a standard (Roche/Hitachi; 152 mg/dl accordingly 3.95 mmol/l) was serially diluted 1:2, 1:4, 1:8, 1:16 and 1:32 with 0.9%

saline on ice. Subsequently, 2 µl of each standard, sample and blank (0.9% saline) were transferred to a flat bottom microtiterplate (BD Biosciences) on ice. To increase the range of the standard 2 µl and 4 µl undiluted standard was added to the respective wells. After adding 200 µl reagent CHOD-PAP (Roche) to each well the microtiter-plate was gently mixed. Following incubation at room temperature for 30 min absorbance at 505 nm wavelength was measured using a 96-well plate reader (Tecan GENios). For calculating the cholesterol content of the sample the following equation was used:

$$\text{Concentration (mmol/l)} = \frac{\text{Sample (mean) x standard-concentration (mmol/l)}}{\text{Standard (mean)}}$$

Lipoproteins were isolated by sequential ultracentrifugation from 60 µl of plasma at d < 1.006 g/ml [very LDL (VLDL)], 1.006 ≤ d ≤ 1.063 g/ml [intermediate-density lipoprotein and LDL], and d > 1.063 g/ml [HDL] in an Optima LE 80K ultracentrifuge (Beckman, Brea, CA, USA). Cholesterol concentration in the respective lipoprotein fraction was determined enzymatically using a colorimetric assay (Roche). Hematologic analysis was performed with a ScilVet abc Plus+ (ScilVet, Viernheim, Germany).

2.4.4 Plasma analysis

Murine plasma was analyzed for cytokine levels, general Ig levels and oxLDL-reactive Ig using multiplex bead-based assays (eBioscience) and enzyme-linked immunosorbent assays (ELISA).

2.4.4.1 Anti-oxLDL-Ig ELISA

The abundance of antibodies detecting oxLDL in plasma of *Cd70*$^{+/+}$*Apoe*$^{-/-}$ and *Cd70*$^{-/-}$ *Apoe*$^{-/-}$ mice was detected via ELISA. In brief, a 96-well polystyrene microplate (Costar 3690, Corning, Corning NY, USA) was incubated with 50 µl per well of 10 µg/ml oxLDL in PBS pH 7.4 at 4°C overnight. Wells were washed twice with PBS, blocked 1h at room temperature with 1% gelatin (Sigma Aldrich) in PBS and washed twice with PBS. Subsequently, 50 µl of pre-diluted mouse plasma (1:20, 1:200, 1:1000) in 0.1% gelatin/Tris-buffered saline (TBS) were added per well and incubated for 2 h at room temperature. After incubation, wells were washed thrice with 0.05% PBS-Tween (PBS-T) and 50 µl of the biotinylated anti-mouse IgG-antibodies listed below were added (each antibody was diluted 1:25000 in 0.1% gelatin/TBS):

- Biotin-SP-conjugated Goat anti-mouse IgG1,
- Biotin-SP-conjugated Goat anti-mouse IgM, µ chain,
- Biotin-SP-conjugated Goat anti-mouse total IgG,

- Biotin-SP-conjugated Goat anti-mouse total IgG2b,
- Biotin-SP-conjugated Goat anti-mouse total IgG3,
- Biotin-SP-conjugated Goat anti-mouse total IgG2a,

All antibodies were obtained from Jackson ImmunoResearch Labs and handled according the manufacturer's data sheets. Subsequent to incubation for 1 h at room temperature with biotinylated antibodies, wells were washed thrice in 0.05% PBS-T and 50 µl of streptavidin conjugated to horse radish peroxidase (HRP, 1:1000 in 0.1% gelatin/TBS) were added (1 h ,room temperature, dark). After washing with 0.05% PBS-T (4x), 50 µl 3,3',5,5'-Tetramethylbenzidin (TMB) substrate (1-Step Ultra TMB ELISA substrate, Thermo Scientific) were added for 2-10 min depending of titers. The substrate is converted into blue product in presence of HRP activity. The addition of 1 M hydrochloric acid (HCL) stopped the reaction and changes the substrate to a yellow color. Absorbance was analyzed with an ELISA-well plate reader (Tecan GENios) at 450 nm wavelength with reference wave length set at 570 nm.

2.4.4.2 TGFβ1 ELISA

TGFβ1 concentration was determined in murine plasma employing a specific ELISA (Thermo Scientific). The manufacturer's protocol was followed. In brief, a 96-well plate was coated with a monoclonal antibody detecting murine TGFβ1. Murine plasma samples and control regimen were incubated in duplicates on the 96-well plate followed by incubation with a biotinylated antibody detecting TGFβ1. Several washing steps were performed between each incubation step. Subsequently, a streptavidin-HRP conjugate was added and colorimetric conversion of a substrate based on the enzymatic activity of HRP was analyzed with an ELISA well plate reader (Tecan GENios) at 450 nm wavelength with reference wave length set to 570 nm.
Of note, total TGFβ was analyzed after activation of latent TGFβ with acidic treatment, since concentrations of active TGFβ alone are below the detection limit in murine plasma.

2.4.4.3 Bead Arrays

Murine plasma from 18-week-old *Cd27*$^{+/+}$*Apoe*$^{-/-}$, *Cd27*$^{-/-}$*Apoe*$^{-/-}$, *Cd70*$^{+/+}$*Apoe*$^{-/-}$, *Cd70*$^{-/-}$ *Apoe*$^{-/-}$ and from 28-week-old *Cd27*$^{+/+}$*Apoe*$^{-/-}$and *Cd27*$^{-/-}$*Apoe*$^{-/-}$ mice was analyzed for T helper cytokine abundance with the mouse Th1/2/17/22 13-plex kit FlowCytomix Multiplex Kit (eBioscience) which allows for the simultaneous detection of IL-13, IL-1α, IL-2, IL-22 IL-5, IL-21, IL-6, IL-10, IL-27, IFNγ, TNFα, IL-4, and IL-17. Levels of circulating Ig subclasses (IgA, IgG1, IgG2a, IgG2b, IgG3, IgM) from 18-week-old

Cd70$^{+/+}$*Apoe*$^{-/-}$ and *Cd70*$^{-/-}$*Apoe*$^{-/-}$ mice were assessed with the mouse Ig isotyping 6-plex kit (eBioscience). Both assays are bead-based and follow a similar principal as a sandwich ELISA. Analysis was performed with a flow cytometer (BD FACS Canto II, BD Biosciences). In brief, fluorescently-marked polystyrol beads were pre-coupled with antibodies specifically detecting the respective analyte(s) of interest. A single bead population was only coupled with one specific capturing antibody. A mixture of different bead populations was incubated with plasma samples for 2 h. The bead-bound-analyte from the plasma sample was detected by a biotinylated detection antibody. Subsequent 1h incubation with streptavidin conjugated PE binding to the biotinylated analyte-bead-complex allowed for quantification of the respective analyte. The bead samples were acquired with a BD FACS Canto II (BD Biosciences). Up to 20 bead sets could be analyzed in one fluorescent channel as the beads are distinguishable by size (4 µm and 5 µm) and different intensities of the fluorochrome labeling the bead populations. Here, beads were labeled with a fluorochrome emitting in the far-red channel at 690 nm wavelength. First beads were separated by size by displaying size (front scatter) and granularity (side scatter). Gating on the size-separated bead populations allowed for further discrimination in fluorescence intensity by displaying fluorescence emitted in the APC channel. Mean fluorescence intensities (MFI) of each bead population for fluorescence emitted in the PE channel were acquired and standard curves based on the MFI obtained from standard cytokine beads were used for quantification of sample analyte concentration. Flow cytometer data was analyzed with the FlowCytomix Pro 3.0 analysis software to obtain plasma cytokine or Ig concentrations.

During the course of this thesis the manufacturer replaced the bead array technology analyzed by flow cytometry with the ProcartaPlex immunoassays using Luminex xMAP technology for the multi-analyte detection. Here, we applied the ProcartaPlex mouse Th1/Th2/Th9/Th17/Th22/Treg cytokine panel (17 plex) to simultaneously analyze plasma concentration of IL-12, IL-23, IL-27, GM-CSF, IFNγ, TNFα, IL-1β, IL-10, IL-13, IL-17A, IL-18, IL-2, IL-22, IL-4, IL-5, IL-6, and IL-9. Plasma was obtained from *Cd27*$^{+/+}$*Apoe*$^{-/-}$, *Cd27*$^{-/-}$*Apoe*$^{-/-}$, *Cd70*$^{+/+}$*Apoe*$^{-/-}$ or *Cd70*$^{-/-}$*Apoe*$^{-/-}$ bone-marrow transplanted *Apoe*$^{-/-}$ mice. The xMAP technology is also a bead-based technique which applies beads which are internally labeled with fluorescent dyes to produce a specific spectral address. The beads are magnetized thus allowing for convenient washing steps in a 96-well plate. The beads are coupled with antibodies which will capture the specific analyte which in turn will be bound by a biotinylated detection antibody. Quantification will follow the binding of streptavidin-PE-conjugates to the detection antibody. Again, MFI of each bead population for fluorescence emitted in the PE channel were acquired and standard curves based on the MFI obtained from standard

cytokine beads were used for quantification of sample analyte concentration. The samples were analyzed with the Luminex platform MAGPIX (Luminex). Data was analyzed with the xPONENT software controlling the MAGPIX platform (Luminex).

2.4.5 Histochemistry (morphometry and histology)

Hearts were cut in 8 µm-thick serial sections beginning from the onset of the aortic valves until the valves disappeared. Serial sections were stained with Oil Red O (Sigma to determine lipid depositions and analyzed with a Leica DM6000 microscope (Leica Microsystems) equipped with a computerized morphometry system (LAS 4.6 analysis, Leica Microsystems). In brief, air-dried cryostat sections were pre-incubated with 60% 2-propanol (10x dipping) and subsequently kept 15 min in the Oil Red O-working solution (180 ml Oil red O-stock solution and 120 ml distilled water filtered 1 h after mixing to remove precipitated salts). Excess Oil Red O solution was washed away by dipping 10 x in 60% 2-propanol. The sections were rinsed 5 min in tap water and counterstained with hemalaun in distilled water for 30 s followed by rinsing 5 min in tap water. Oil red O-stained sections were embedded in Immu-Mount (Thermo Scientific).
H&E-stained sections were classified as initial or advanced according the histological criteria determined by Virmani *et al.*[208] A picrosirius red staining was applied to visualize collagen content in atherosclerotic lesions. Phosphomolybdic acid (0.2%, Merck, Darmstadt, Germany) was used to block unspecific binding and sections were analyzed using brightfield light microscopy. Tissue sections with insufficient quality were excluded from further analysis, which influences the individual parameter group size.

2.4.6 Immunohistochemistry

Selected murine tissue cryosections were fixed in ice-cold acetone prior to incubation with antibodies against CD68 (AbD Serotec), alpha smooth muscle actin (α-SMA), CD3, CD4, Foxp3, ICAM-1, and VCAM-1. The primary antibody binding of non-fluorescent conjugated antibodies was detected either by incubation with fluorochrome-(Alexa Fluor 488, Alexa Fluor 594, Cy3 or horse-radish peroxidase-conjugated secondary antibodies and diaminobenzidine (ABC kit, Vector Labs, Burlingame, USA). To amplify signal strength for α-SMA staining, a primary antibody against α-SMA conjugated with FITC and secondary antibody directed against FITC and conjugated with Alexa Fluor 488 were used. Tissue sections were counterstained with hematoxylin or 4',6-Diamidino-2-phenylindol (DAPI, Life Technologies), respectively, mounted with DAKO fluorescent mounting medium (Dako, Agilent Technologies, Santa Clara, CA, USA), and images were recorded with a Leica DM6000 microscope equipped with a

DFC295 and DFC365FX camera (Leica). CD3-, CD4-, and Foxp3-stained cells were counted. CD68-, α-SMA-, ICAM-1-, and VCAM-1-positive areas were analyzed by applying color threshold measurements. ICAM-1 staining in sections of the aortic sinus is specifically correlating with endothelium. However, SMC are also expressing VCAM-1 besides EC. Thus, to specifically assess endothelial VCAM-1 staining, additional CD31 staining with a directly-conjugated antibody was performed. The CD31 positive area in the aortic root was subsequently assessed for VCAM-1 staining. The ICAM-1- and VCAM-1-positive area was correlated to plaque endothelial length. Tissue sections with insufficient quality were excluded from further analysis, which influences the individual parameter group size.

2.4.7 Confocal microscopy

Selected tissue cryosections from *Apoe*$^{-/-}$ mice were fixed in ice-cold acetone prior to incubation with antibodies against CD4, Foxp3, α-SMA, CD8, MAC3, CD68 (Abcam, Cambridge, United Kingdom), CD70, and CD27. The primary antibody binding was detected by incubation with fluorochrome-conjugated secondary antibodies (Alexa Fluor 488, Cy3; Abberior STAR 635 P). Tissue sections were counterstained with DAPI (Life Technologies) and mounted in DAKO fluorescence mounting medium. Confocal laser scanning microscopy was performed with a Leica SP8 3X microscope equipped with a 100xNA1.40 (Leica) oil immersion objective. Optical zoom was utilized where applicable. For fluorescence excitation, a UV laser (405 nm), and a tunable white light laser (488 nm, 552 nm, and 635 nm) were used to excite DAPI, Alexa Fluor 488, Cy3, Abberior Star 635p, respectively. Emitted fluorescence signal was sequentially detected using hybrid diode detectors spectrally set to minimize bleed-through between the sequentially recorded channels: 420-470 nm for DAPI, 515-540 nm for Alexa Fluor 488, 590-660 nm for Cy3, and 655-750nm for Abberior STAR 635 P. Image processing was performed using Leica LAS X software, image deconvolution (CMLE algorithm) was conducted with the Huygens Professional 15.05 software package (Scientific Volume Imaging, The Netherlands). The obtained 3D datasets are presented as extended depth of field projections based on maximum intensity contrast.

2.4.8. Table 3: Primary antibodies used in immunohistochemistry

Antigen	Source and reactivity	Clone	Dilution	Source
CD3	Armenian Hamster-anti-mouse (IgG1, κ)	145-2C11	1:100	BD Biosciences
CD4	Rat-anti-mouse (IgG2a, κ)	RM4-5	1:100	BD Biosciences
Foxp3	Rat-anti-mouse/rat/pig/canine/bovine (IgG2b, κ)	FJK-16s	1:50	eBioscience
α–SMA	Mouse-anti-mouse/rabbit/human/pig (IgG2a) FITC conjugated	1A4	1:1000	Sigma Aldrich
CD8	Rat-anti-mouse (IgG2a)	YTS105.18	1:100	AbD Serotec, Puchheim, Germany
MAC3	Rat-anti-mouse (IgG1, κ)	M3/84	1:200	BD Biosciences
CD68	Rat-anti-mouse (IgG2a)	FA-11	1:200	AbD Serotec,
CD68	Rabbit-anti-mouse/human	Polyclonal	1:200	Abcam
CD27	Armenian Hamster-anti-mouse/rat/human (IgG)	LG.3A10	1:100	eBioscience
CD70	Rat-anti-mouse (IgG2b, κ)	FR70	1:100	eBioscience
ICAM-1	Armenian Hamster-anti-mouse (IgG)	3E2B	1:100	Thermo Scientific
VCAM-1	Rat-anti-mouse (IgG1)	6C7.1	1:500	Novus Biologicals
CD31-PE	Rat-anti-mouse (IgG2a, κ)	MEC13.3	1:300	BD Biosciences

2.4.9. Table 4: Secondary antibodies used in immunohistochemistry

Source and Reactivity	Conjugate	Dilution	Source
Donkey-anti-rat	Alexa Fluor488	1:300	Thermo Scientific
Mouse-anti-FITC	Alexa Fluor488	1:400	Jackson ImmunoResearch, West Grove, PA, USA
Goat-anti-armenian hamster	Cy3	1:300	Thermo Scientific
Goat-anti-mouse	Alexa Fluor594	1:300	Thermo Scientific
Goat-anti-rabbit	Star 635P	1:300	Abberior, Goettingen, Germany

2.4.10 Western blot

At day 7 bone marrow-derived macrophages (BMDM) were loaded with 15 µg/ml oxLDL for 48 h. Subsequently, BMDM were lysed using radioimmunoprecipitation assay (RIPA) buffer supplemented with a protease inhibitor cocktail (Complete Mini, Roche). Aliquots (30 µg) of total protein were then size-fractioned by sodium dodecyl sulfate (SDS)-polyacrylamide gel electrophoresis (4-12% Tris-Glycine Mini Protein gels, Novex, Thermo Scientific) and transferred to nitrocellulose membranes. After blocking for 1h in Tris-buffered saline containing 0.1% Tween 20 and 3-5% skim milk, membranes were probed overnight at 4°C with primary antibodies against ABCA1 or ABCG1 (both from Abcam). Target protein expression was normalized to glycerinaldehy-3-phosphat-dehydrogenase (GAPDH) (Abcam) to correct for loading and band densities were analyzed using ImageJ software.

2.5 Cell culture and functional assays

Cell culture was performed under sterile conditions in a laminar flow hood. Cells were maintained in a carbon dioxide (CO_2)-incubator at 37°C and a humidified 5% CO_2 atmosphere. FBS was incubated at 56°C for 30 min to inactivate the complement proteins and stored at -20°C until use. According to cell types specific media were used.

2.5.1 $CD4^+$ T cell isolation

T cells were sorted isolated from spleen and lymph nodes. $CD4^+$ T cells were negatively sorted using antibody-conjugated magnetic beads (Dynabeads Untouched Mouse CD4, Life Technologies) and dynal isolation buffer. In brief, an antibody-mix

was used to label non-$CD4^+$ T cells. The addition of Fc-binding magnetic beads bound the labeled cells in the tube while separating untouched $CD4^+$ T cells. Tregs were sorted by either flow cytometry sorting for $CD3^+CD4^+CD25^{high}$ cells (BD FACS Aria III, BD Biosciences) or using an untouched CD4 negative magnetic bead-sort followed by a CD25 positive magnetic bead sort according to the instructions of the manufacturer (Dynabeads Flowcomp Mouse $CD4^+CD25^+$ Treg cells kit, Life Technologies). T Cells were cultured in T cell medium (see 2.9).

2.5.2 Treg suppression assay

Sorted $CD4^+$ T cells from *Apoe*$^{-/-}$ mice were stained with carboxyfluorescein succinimidyl ester (CFSE, Life Technologies). In brief, T cells were adjusted to $1x10^6$/100 µl in 37°C pre-warmed and stained with 3 µM CFSE for 15 min at 37°C in a water bath while shaking the tube every 2 min. Subsequently, the T cells were washed twice with T cell medium and adjusted to $1x10^6$/ml. $5x10^4$ CFSE-labeled T cells were co-cultured in a 1:1 ratio with anti-CD3/CD28 antibody-conjugated beads (Life Technologies) and varying concentrations of Tregs from *Cd27*$^{+/+}$*Apoe*$^{-/-}$ or *Cd27*$^{-/-}$*Apoe*$^{-/-}$ mice for 72 h. T cell proliferation was determined by CFSE dilution measured by flow cytometry.

2.5.3 Treg chemotaxis assay

For chemotaxis assays $CD4^+$ T cells from either *Cd27*$^{+/+}$*Apoe*$^{-/-}$ or *Cd27*$^{-/-}$*Apoe*$^{-/-}$ mice were sorted (Dynabeads Untouched Mouse CD4, Life Technologies) and applied on top of a HTS transwell plate (5 µm pore size, Corning, New York, USA) containing in the lower compartment varying concentrations of murine CCL19 or CCL21 (R&D Systems, Minneapolis, USA). Cells were incubated for 2 h and migration was assessed by determining the absolute number of migrated cells using CountBright beads (Life Technologies) and flow cytometry (BD FACS Canto II, BD Biosciences).

2.5.4 L929-conditioned medium

L929 is a murine fibrosarcoma cell-line that secretes macrophage-colony stimulating factor (M-CSF) into the medium, a growth factor for macrophage development and essential for differentiation BMDMs *in vitro*. In brief, L929 cells were cultured in D10 medium until monolayers reached confluence and were expanded in several culture flasks. If cells reached confluence in 162 cm² culture flasks (Corning), L929 cells were harvested and combined in a 10-STACK culture flask (Corning). The volume is approximately 1300 ml. The L929 culture was again allowed to gain confluence upon which another 500 ml D10 medium was added (total volume in 10-STACK: ~1800 ml).

The culture was continued for another 10 days during which the L929 cells secreted M-CSF into the supernatant. Subsequently, the conditioned medium was sterile filtered and aliquots were stored at -80°C until usage. As the exact concentration of M-CSF in the medium is unknown, bone marrow-derived macrophage cultures were started (see 2.5.5) to determine an appropriate amount of L929 as supplement. A range of concentrations (5%, 10%, 15%, 25%) of L929-conditioned medium were tested. At day 8 of the culture, BMDMs were replated, allowed to attach for 4h, and stimulated with LPS at 0, 1, 10, 100 ng/ml. Subsequently, the cultured cells were assayed for nitric oxide (NO) production (see 2.5.7) and analyzed for macrophage marker expression to determine the appropriate amount of L929 as supplement to induce macrophage differentiation.

2.5.5 Bone marrow-derived macrophages

Bone marrow cells were flushed from tibia and femur with cold RPMI 1640 medium (Life Technologies) and subjected to red blood cell lysis as described above. The cells were resuspended in macrophage differentiation medium (see 2.9). On day 3 of the culture, fresh macrophage differentiation medium was added without removing the old medium. At day 6 the medium was exchanged by fresh medium. At day 8 the cells were detached by incubating 5 min at 37°C in 10 ml citrate saline buffer. After washing, the cells were counted and plated or used for additional assays.
When stated the cells were cultured with 50 µg/ml oxLDL for 24-48 h on day 8. Consecutively, cells were labeled with propidium iodide (PI) (Biolegend) and Annexin V (Biolegend) for 15 min according to the manufacturer's protocol. The percentage of live (Annexin V^-/PI^-), apoptotic (Annexin V^+/PI^-), and necrotic (Annexin V^+/PI^+) cells was analyzed using a BD FACS Canto II (BD Biosciences).

2.5.6 Metabolic analysis

At day 8 of the BMDM culture 50000 cells were seeded per well in an XFe96 cell culture microplate in 100 µl culture medium. 24 h after plating the cells extracellular acidification rates (ECAR) and oxygen consumption rates (OCR) were measured in real-time in an XF-96 Flux Analyzer (Seahorse Bioscience, Agilent Technologies) as described in detail previously.[100] ECAR changes in response to glucose and oligomycin (OM) injections were used to assess glycolysis and OCR changes in response to OM, carbonyl cyanide-p-trifluoromethoxyphenylhydrazone (FCCP) and rotenone + antimycin A injections were used to assess mitochondrial oxidative phosphorylation (OXPHOS) characteristics. After completion of the extracellular flux analysis, DNA

content was measured with CyQuant (Thermo Scientific) using a spectrophotometer at 508 nm excitation and 527 emission to normalize ECAR and OCR data.

2.5.7 Nitric oxide production

At day 8 of BMDM culture the supernatant was collected and 50 µl transferred to a 96-well plate. A standard dilution series was made with sodium nitrite. 50 µl Griess reagent (Sigma Aldrich) was added to each sample and the absorption was read using a spectrophotometer at 550 nm wavelength.

2.5.8 Reactive oxygen species production

At day 8 of BMDM culture cells were exposed to 10 ng/ml LPS (Sigma Aldrich) for 24 h. Subsequently, the supernatant was removed and 100 µl 5 µM CM-H2DCFDA (Life Technologies) in serum-free RPMI medium were added, followed by 30 min incubation at 37°C. The attached BMDMs were washed with PBS and detached using citrate buffer. Following another washing step, the BMDMs were analyzed using a BD FACS Canto II (BD Biosciences).

2.5.9 Uptake of fluorescent E. coli particle

At day 8 of BMDM culture, the culture medium was removed and replaced by culture medium containing 1 mg/ml bioparticle suspension (pHrodo Green E. coli BioParticles, Thermo Scientific). After incubation (1 h) the cells were washed, detached using citrate buffer and analyzed for fluorescence resembling bioparticle uptake with a BD FACS Canto II (BD Biosciences).

2.5.10 Uptake of Dil-conjugated oxLDL

At day 8 of BMDM culture, the culture medium was removed and replaced by culture medium containing 50 µg/ml Dil-oxLDL (Biotrend, Cologne, Germany). Subsequent incubation (4 h) the cells were washed, detached using citrate buffer, and analyzed with a BD FACS Canto II (BD Biosciences).

2.5.11 Cholesterol efflux analysis

At day 7 of the BMDM culture, 0.5×10^6 cells were replated per well in a 24-well plate and allowed to adhere overnight in culture medium. The next day the culture medium was replaced by culture medium containing tritium (^{3}H)-cholesterol (1 µCi/well; PerkinElmer, Waltham, MA, USA) and oxLDL (50 µg/ml, Biotrend) for 24 h. After loading the cells were equilibrated for 2 h in RPMI medium containing 0.2% BSA (both

Life Technologies). The equilibrated BMDM were subsequently incubated for 6 h with RPMI medium containing 0.2% BSA and ApoA1 (15 µg/ml, Sigma Aldrich) or HDL (50 µg/ml, Sigma Aldrich) or received no further treatment. The medium was removed, collected, and the cells were lysed at 37°C with 0.3 M sodium hydroxide (NaOH) solution for 15 min. The cell lysate was collected and both, the lysate and the supernatant were transferred to scintillation medium (Zinsser Analytic, Frankfurt, Germany) and radioactivity measured with a scintillator (PerkinElmer). Counts from cellular lysate added with counts from supernatant represent total cholesterol uptake whereas counts only for supernatant represent cholesterol efflux.

2.6 Biomolecular methods

2.6.1 RNA isolation

All reagents were obtained from Qiagen if not stated otherwise. Total ribonucleic acid (RNA) was isolated from tissue stored in RNAlater (Ambion, Thermo Scientific) at -80°C according to the protocol of Qiagen RNeasy Mini Kit II. The entire procedure was performed under RNase-free conditions and partly on ice. The tissue samples were thawed and the amount of tissue was determined to use a maximum of 100 mg per sample. A stainless steel bead (7 mm diameter) was added along with the tissue sample removed from RNAlater to a 2 ml tube and kept on ice. Before placing the tube in the TissueLyser with a 12-Tube LT Adapter 1 ml Qiazol Lyses Reagent was added. Lysis was performed for 5 min at 50 Hz. The lysate was transferred to a new microcentrifuge tube and incubated at room temperature for 5 min so nucleoprotein complexes were able to dissociate. After incubation 200 µl Roti® - Phenol/C I (Roth, Karlsruhe, Germany) was added and the tube was shaken vigorously for 15 s. Another incubation step for 3 min. at room temperature was performed and thereafter all samples were centrifuged at 12,000 x g for 15 min at 4°C. After centrifugation 3 (or 4) Phases appeared in the tube: a) an upper, colorless, aqueous phase containing RNA b) a white interphase c) a lower, red, organic phase and d) a clear phase below the red phase (only in tissues with high fat content).

The upper, aqueous phase was transferred gently to a new tube without interfering with DNA- and protein-containing phases. One volume of 70% ethanol was added to the transferred RNA-containing phase and the tube was vortexed. Up to 700 µl of sample was transferred to an RNeasy Mini spin column placed in a supplied 2 ml tube. After closing the lid, the sample was centrifuged for 15 sec at 8,000 x g at room temperature. The flow-through was discarded. This procedure was repeated until the entire remainder of the sample was used. For digestion of potentially contaminating genomic

DNA the ribonuclease (RNase)-Free DNase set supplied with DNase I, buffer RDD and RNase-free water was used. Lyophilized DNase I was dissolved in 550 µl of RNase-free water to prepare a DNase I stock solution. After adding 350 µl of buffer RW1 to the RNeasy spin column the column was centrifuged at 5000 x g for 15 sec at room temperature. For each sample 10 µl DNase I stock solution were added to 70 µl buffer RDD. Subsequently, 80 µl of DNase I incubation mix was directly added to the middle of the RNeasy spin column membrane and incubated for 15 min at room temperature. Following incubation 350 µl RW1 buffer was applied to the RNeasy spin column and the column centrifuged for 15 sec at 8000 x g. The obtained flow-through was discarded. The membrane of the RNeasy spin column was washed twice with 500 µl buffer RPE supplied with 96% Ethanol. Following centrifuging the column for 15 sec at 8000 x g, a second drying step at 8000 x g for 2 min was performed. All flow-through was discarded. For elution of the RNA the RNeasy spin column was placed in a new 1.5 ml collection tube and 50 µl of RNase-free water was added to the membrane. The column was centrifuged for 1 min at 8000 x g.
Purity and yield of total RNA of each preparation were assessed spectrophotometrically at OD_{260}/OD_{280} employing a nanodrop (Peqlab). A value of OD_{260}/OD_{280} lower than 1.7 led to the disqualification of these samples. Samples were stored at -80°C until further use.

2.6.2 cDNA synthesis

RNA isolated from aortas was reverse transcribed with the SuperScript® VILO™ complimentary DNA (cDNA) Synthesis Kit (Invitrogen) according to the manufacturer's instructions. In brief, 4 µl 5X VILO™ Reaction Mix and 2 µl 10X SuperScriptR Enzyme Mix were added on ice. The concentration of RNA adjusted to the sample with the lowest concentration with DNAse-/RNAse-free water (Sigma Aldrich) for equal amounts of starting material, and 14 µl of RNA were added. The total reaction volume was 20 µl. The content of the tubes was mixed gently and incubated at 25°C for 10 min. Subsequently, the mixture was incubated at 42°C for 1 h and the reaction stopped at 85°C for 5 min.

2.6.3 Real-time polymerase chain reaction

Quantitative PCR (qPCR) was performed with a SYBR Green Fast Master mix (Life Technologies) on a ViiA7 real-time PCR system (Life Technologies). Primers were obtained from Sigma Aldrich. Primer sequences are listed below (see 2.6.4).

For a single real-time PCR reaction the following reagents were mixed on ice.

2 µl	2 ng/µl cDNA,
4 µl	Sybr Green Fast Master mix,
1.84 µl	DEPC-treated H_2O,
0.08 µl	300 nM forward primer, and
0.08 µl	300 nM reverse primer

If higher sample numbers were processed a master mix was prepared in a tube on ice and kept in the dark. Each PCR reaction was pipetted in duplicate. The PCR program was composed of an initial step at 95°C for 20 sec followed by 40 cycles of each 1 sec at 95°C and 20 sec at 60°C. Subsequently, a dissociation cycle was performed with 15 sec at 95°C, 1 min at 60°C, and followed by 15 sec at 95°C with a 2% ramp rate. The obtained data from real-time PCR for the respective genes and tissues was analyzed by applying the $2^{-\Delta\Delta C_T}$ method.[210] β-actin expression was considered to be equal in a respective tissue upon administration of atherogenic diet and therefore was used as reference.

2.6.4 Table 5: List of genes and primer sequences applied for gene expression analysis

Gene	Forward primer sequence 5' → 3'	Reverse primer sequence 5' → 3'
IL-1β	AAAGAATCTATACCTGTCCTGTGTAATGAAA	GGTATTGCTTGGGATCCACACT
ICAM-1	CTACCATCACCGTGTATTCGTTTC	CGGTGCTCCACCATCCA
Gata3	CAGCTCATGTGGAACCTCTG	TGCACCTGATACTTGAGGCACTCT
IL-6	GCTACCAAACTGGATATAATCAGGAAA	CTTGTTATCTTTTAAGTTGTTCTTCATGTACTC
VCAM-1	GTGTTGAGCTCTGTGGGTTTTG	TTAATTACTGGATCTTCAGGGAATGAG
CCL1	ATGGGCTCCTCCTGTCCTGAT	CCACGTTTTGTTAGTTGAGGCG
IL-12p35	GGAACTACACAAGAACGAGAG	AAGTCCTCATAGATGCTACCA
STAT6	TTTCTGCCAAAGACCTGTCC	TCTGTTCGGGCTTATAGTGAC
CCL5	GGAGTATTTCTACACCAGCAGCAA	GCGGTTCCTTCGAGTGACA
Rorγt	ACAGCCACTGCATTCCCAGTTT	TCTCGGAAGGACTTGCAGACAT
MCP1	CTTCTGGGCCTGCTGTTCA	CCAGCCTACTCATTGGGATCA
IL-12p40	GGTGCAAAGAAACATGGACTTG	CACATGTCACTGCCCGAGAGT
IL-23p19	GGATTCCCGTCCCTCGGTCTC	GGGCCAAGGCGCTTGGCACAG
IRF4	CAGCTCATGTGGAACCTCTG	CACTCTTGGATGGAAGAATGAC
CXCL10	CTGCCCACGTGTTGAGATCA	TGGTCTTAGATTCCGGATTCAGA
IL-2	TGCGGCATGTTCTGGATTTG	TGGCACTCAAATGTGTTGTCAG
Foxp3	CCCAGGAAAGACAGCAACCTT	TTCTCACAACCAGGCCACTTG
T-Bet	GCCAGGGAACCGCTTATATG	GACGATCATCTGGGTCACATTGT
STAT3	CTTCGAGACTGAGGTGTACCACC	TACCACAGGATTGATGCCCAA
IL-17α	TCCCTCTGTGATCTGGGAAG	CTCGACCCTGAAAGTGAAGG
IFNγ	TGGCTGTTTCTGGCTGTTACTG	GCTCTGCAGGATTTTCATGTCA
β-actin	GACAGGATGCAGAAGGAGATTACTG	CCACCGATCCACACAGAGTACTT

2.7 Statistical analysis

Data is presented as average ± standard error mean (SEM) or standard deviation (SD). Student's t test was used to analyze data for statistical significance with GraphPad Prism v.5 software (GraphPad Software Inc., La Jolla, USA). A p value of <0.05 was considered statistical significant.

For gene expression analysis, a false discovery rate approach (FDR set to 10%) was applied to control for type I errors[6] and a 2-tailed p value of <0.1 was considered statistical significant.

2.8 Buffers

Tissue lysis buffer

10 mM Tris

10 mM EDTA

10 mM Sodium chloride (NaCl)

0.5% Sarcosyl (N-Lauroylsarcosine sodium salt)

adjusted to 0.5 Liter with distilled H_2O.

Erythrocyte lysis buffer

10 mM Potassium hydrogen carbonate ($KHCO_3$)

150 mM Ammonium chloride (NH_4Cl)

0.1 mM EDTA

adjusted to 1 Liter with distilled H_2O and pH 7.2-7.4.

FACS buffer

1x PBS

0.5% BSA

0.01% Sodium azide (NaN_3)

Westen Blot blocking buffer

Tris-buffered saline

0.1% Tween 20

3-5% skim milk.

Fixation/Permeabilization working solution (from Foxp3 staining set, eBioscience)

1 part of fixation/permeabilization concentrate was diluted with 3 parts of fixation/permeabilization diluent.

Permeabilization buffer (from Foxp3 staining set, eBioscience)

Dilute the 10x Permeabilization Buffer (00-8333-56) 10 times in distilled water.

Dynal isolation buffer

1x PBS

0.1% BSA

2 mM EDTA

CFSE label buffer

1x PBS

0.1% BSA

Citrate saline buffer

135 mM Potassium chloride

15 mM Sodium citrate

In distilled H_2O. Autoclave before usage.

Antigen retrieval buffer

1M Tris

0.1 M EDTA

pH 8 in distilled H_2O

Oil Red O-stock solution

1 g Oil Red O (Sigma Aldrich)

200 ml 99% 2-propanol

RIPA buffer

50 mM Tris, pH 7.2-7.4

150 mM NaCl

0.1% SDS

0.5% sodium deoxycholate

1% Triton X 100

2.9 Media

T cell medium

All reagents were obtained from (A) Thermo Scientific and (B) Sigma Aldrich.

RPMI1640 with Glutamax (A)

10% FCBS (A)

100 U/ml Penicillin (A)

100 µg/ml Streptomycin (A)

10 mM Hepes (B)

1x MEM non-essential amino acids (B)

1 mM Sodium pyruvate (B)

50 µM 2-Mercaptoethanol (B)

D10 medium

DMEM (Dulbecco's Modified Eagle Medium) with 4,5 g/L glucose and pyruvate (Life Technologies)

10% FBS

100 U/ml Penicillin

100 µg/ml Streptomycin

Macrophage differentiation medium

All reagents were obtained from Thermo Scientific, except the L929-conditioned medium which was self-made, see 2.5.4

RPMI1640

2mM L-Glutamine

10% FBS

100 U/ml Penicillin

100 µg/ml Streptomycin

20 % filtered L-929 cell (ATCC,CCL-1)-conditioned medium containing M-CSF

Bone marrow freeze medium

RPMI1640

10% FBS

10% DMSO

3 RESULTS

3.1 CD27 co-localizes with T lymphocytes and associates with ruptured human atherosclerotic lesions.

Human carotid atherosclerotic plaques, histologically classified as ruptured, display a higher CD27 expression compared to stable carotid atherosclerotic plaques (Figure 3 A). CD27 is almost exclusively expressed on $CD3^+$ T cells in human atherosclerotic lesions (Figure 3 B).

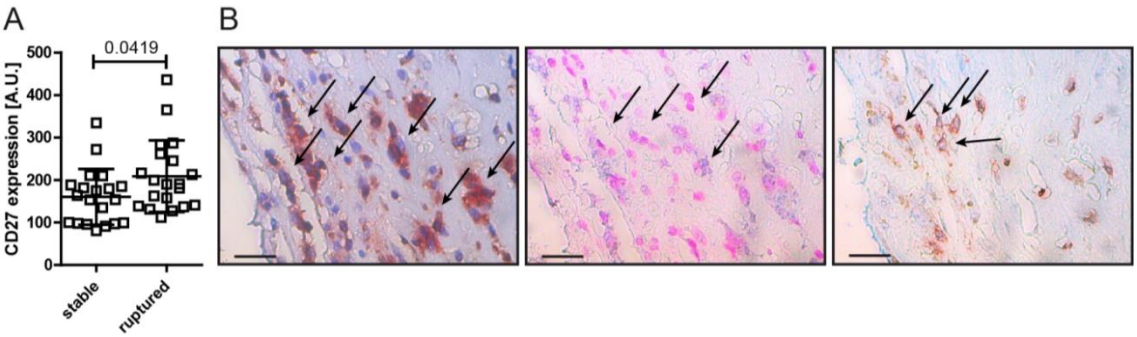

Figure 3. CD27 expression is increased in ruptured human atheroma and associates with T cells. (**A**) CD27 mRNA expression in stable and ruptured human atherosclerotic lesion analyzed by gene array (n=20). (**B**) Adjacent sections of human atherosclerotic lesions stained for (left) CD3 (red) and counterstained with hematoxylin (nuclei; blue); (middle) for CD27 (blue) and counterstained with Nuclear Red (red); (right) for CD3 (red) and CD27 (blue). Arrows indicate $CD3^+$, $CD27^+$, or $CD3^+CD27^+$ cells, respectively; Scale bar = 25 µm. Data are mean ± SD.

Immunohistochemistry demonstrated specific staining of CD27 colocalizing with $CD4^+$ T cells in murine atheroma (Figure 4 A-C).

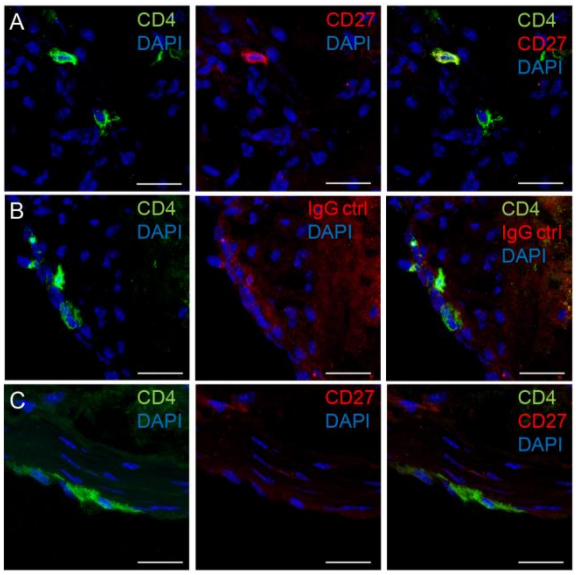

Figure 4. CD27 colocalizes with CD4 T cells. (**A-C**) Immunofluorescent images for CD4 and CD27 staining (**A**), CD4 combined with a CD27 isotype-specific antibody (**B**) microscopy in cross-sections of the aortic root of a 28-week-old *Cd27*$^{+/+}$*Apoe*$^{-/-}$ mouse and CD4 and CD27 colocalization staining on aortic sections of a 28-week-old *Cd27*$^{-/-}$*Apoe*$^{-/-}$ mouse (**C**). Scale bar = 20 µm.

Additionally, CD8$^+$ T cells and Foxp3$^+$ cells, which per definition are a subset of CD4$^+$ T cells, are positive for CD27. Non-lymphoid cells of atherosclerotic lesions as macrophages and SMC did not express CD27 (Figure 5).

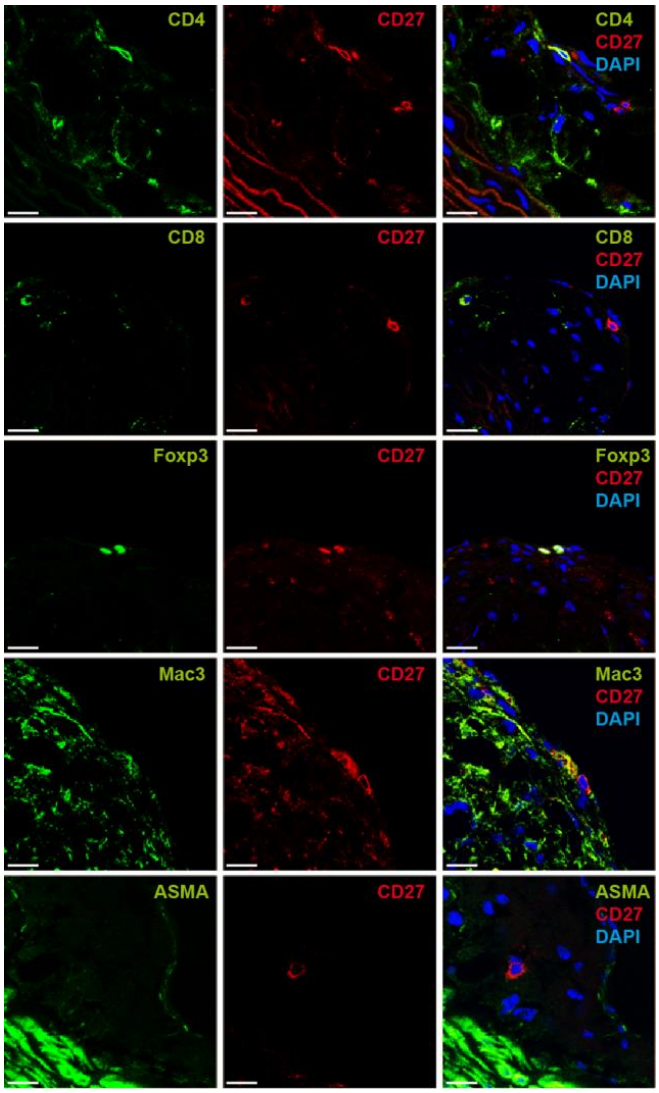

Figure 5. CD27 colocalizes exclusively with T cells in atherosclerotic lesions of murine aortas. Immunofluorescent images for CD8, Foxp3, Mac3, ASMA, and CD27 obtained by confocal microscopy in cross-sections of the aortic root of a 28-week-old *Apoe*$^{-/-}$ mouse; Scale bar = 20 µm.

Flow cytometry of aortic suspensions of hyperlipidemic *Apoe*$^{-/-}$ mice demonstrated high abundance of $\alpha\beta$T cells, B cells, and macrophages whereas $\gamma\delta$T cells were only a minority (Figure 6 A). Among aortic T cells, CD4$^+$ and CD8$^+$ T cells were equally distributed. As expected, CD4$^+$ Treg were only minor fraction of aortic leukocytes (Figure 6 D). Further analysis of the respective leukocyte and lymphocyte subsets revealed exclusive and specific CD27 expression on T cells and subsets thereof, whereas myeloid and B cells did not express CD27. CD27 deficient mice do not harbor CD27 expression on aortic T cells (Figure 6 B,C,E,F). Interestingly, CD27 expression was similar between T cell subsets (Figure 6 E,F). A significant reduction in aortic Treg

was observed in hyperlipidemic *Cd27*$^{-/-}$*Apoe*$^{-/-}$ compared to *Cd27*$^{+/+}$*Apoe*$^{-/-}$ mice (Figure 6 D). A mechanistic explanation will follow below.

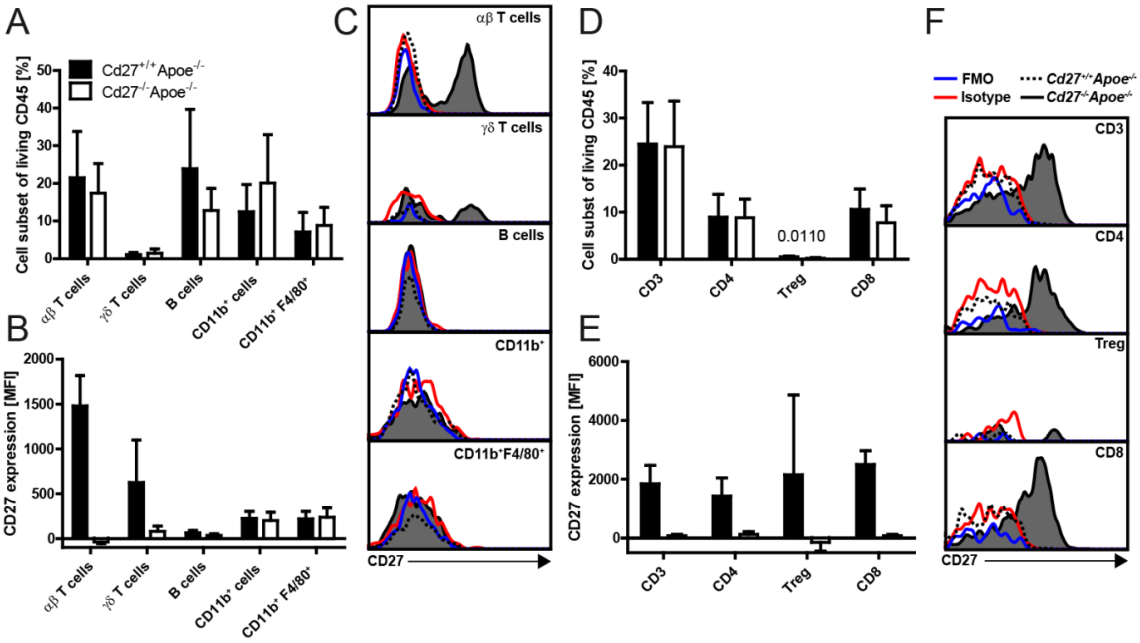

Figure 6. Aortic T cells exclusively express CD27.
Flow cytometry was applied to determine (**A,D**) leukocyte abundance and CD27 expression (**B,E**) on the respective subset in the aorta of hyperlipidemic *Cd27*$^{+/+}$*Apoe*$^{-/-}$ (solid line with grey fill) or *Cd27*$^{-/-}$*Apoe*$^{-/-}$ (dashed line) mice (age=28 weeks; n=3). (**C,F**) Representative histograms are displayed. An isotype control (red line) and fluorescence minus one (FMO) control (blue line) were included. Data is presented as mean±SD.

3.2 Hematopoietic CD27 deficiency increases atherosclerosis and promotes a pro-inflammatory plaque phenotype.

Cd27$^{-/-}$*Apoe*$^{-/-}$ bone marrow was transplanted into lethally-irradiated *Apoe*$^{-/-}$ recipient mice. Upon recovery for 6 weeks recipient mice consumed a cholesterol-rich diet for 7 weeks until assessment of atherosclerosis. Absolute and relative lesion size in the aortic root increased 2.2-fold in *Cd27*$^{-/-}$*Apoe*$^{-/-}$ bone marrow chimeras compared *Cd27*$^{+/+}$*Apoe*$^{-/-}$ bone marrow chimeras (Figure 7 A-C).

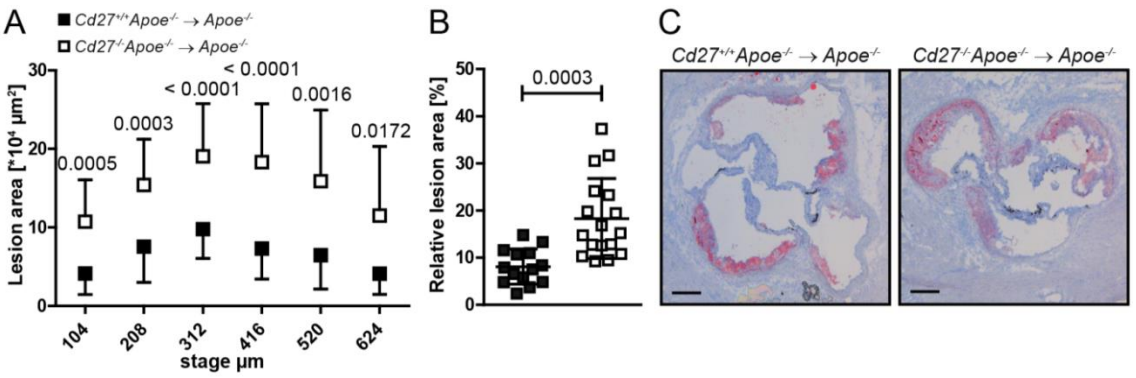

Figure 7. Lack of hematopoietic CD27 aggravates atherosclerosis.
(**A**) Atherosclerotic plaque area in cross-sections at indicated positions of the aortic root from irradiated *Apoe*$^{-/-}$ mice reconstituted with *Cd27*$^{+/+}$*Apoe*$^{-/-}$ or *Cd27*$^{-/-}$*Apoe*$^{-/-}$ bone marrow. (n=10-14 (Donor: *Cd27*$^{+/+}$*Apoe*$^{-/-}$); n=13-18 (Donor: *Cd27*$^{-/-}$*Apoe*$^{-/-}$)) (**B**) Average of lesion area in stages 312-518 as percentage of total vessel area. (**C**) Representative photomicrographs showing Oil Red O-stained sections; Scale bar = 200 µm. Data is presented as mean±SD.

This exacerbation of plaque area was accompanied by an increase in necrotic core area (Figure 8 A), reflecting accelerated plaque progression. Indeed, phenotypic classification according to Virmani guidelines[208] revealed more advanced lesion characteristics in *Cd27*$^{-/-}$*Apoe*$^{-/-}$ bone marrow chimeras corroborating aggravated atherosclerosis (Figure 8 B).

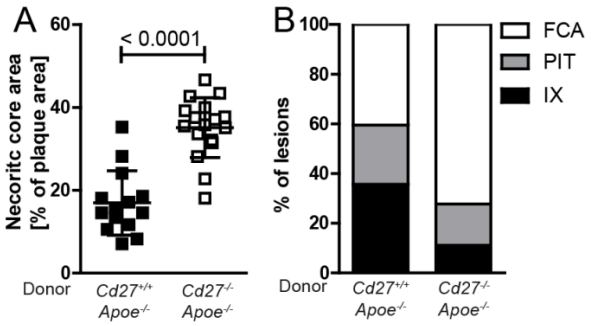

Figure 8. Lack of hematopoietic CD27 increases necrotic core area and causes advanced lesions.
(**A**) Relative lesional necrotic core area in atherosclerotic lesions of the ascending aorta from irradiated *Apoe*$^{-/-}$ mice reconstituted with *Cd27*$^{+/+}$*Apoe*$^{-/-}$ or *Cd27*$^{-/-}$*Apoe*$^{-/-}$ bone marrow. (**B**) Phenotypic characterization of lesions. FCA, fibrous cap atheroma; IX, intimal xanthoma; PIT, pathologic intimal thickening; n=10-14 (Donor: *Cd27*$^{+/+}$*Apoe*$^{-/-}$); n=13-18 (Donor: *Cd27*$^{-/-}$*Apoe*$^{-/-}$)). Data is presented as mean±SD.

Interestingly, the deficiency of CD27 in hematopoietic cells led to significantly increased macrophage content accompanied by decreased lesional Treg numbers assayed by immunohistochemistry staining for CD68 and Foxp3, respectively (Figure 9 A,C). Although lesional abundance of Treg was reduced, abundance of the entire parental CD4^{+} T cell population was only mildly affected by hematopoietic CD27 deficiency (Figure 9 B). The content of SMC (Figure 9 D) and collagen (Figure 9 F) did not change between groups. However, endothelial expression of the adhesion molecule ICAM-1 significantly increased (Figure 9 E). These data suggest a pro-inflammatory plaque milieu with less anti-inflammatory Tregs present in atherosclerotic lesions of

hyperlipidemic CD27-deficient bone marrow-transplanted mice resulting in potentially enhanced leukocyte recruitment and subsequently accelerated plaque progression.

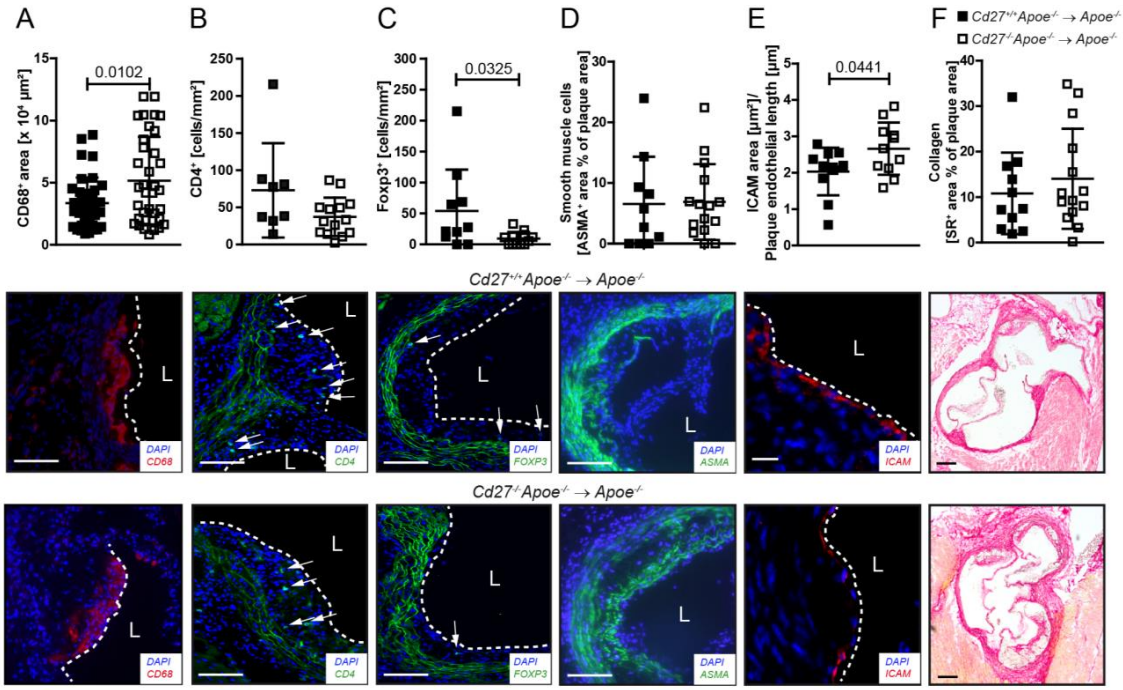

Figure 9. Lack of hematopoietic CD27 affects cellular plaque composition and increases endothelial adhesion molecule expression.
Quantifications (left) and representative photomicrographs (right) are displayed for each staining. The dashed line separates the atherosclerotic lesion from the lumen (L). (**A-E**) Immunofluorescent staining in cross-sections of the aortic root from irradiated *Apoe*$^{-/-}$ mice reconstituted with *Cd27*$^{+/+}$*Apoe*$^{-/-}$ or *Cd27*$^{-/-}$ *Apoe*$^{-/-}$ bone marrow analyzed for (**A**) CD68^{+} area, (**B**) CD4^{+} T cells, (**C**) Foxp3^{+} T cells (Treg), (**D**) α-SMA; A-D scale bar = 100 µm. (**E**) ICAM-1^{+} area was quantified on the lesions endothelial area and further correlated to endothelial length; Scale bar= 25 µm. (**F**) Percentage of sirius red positive stained area in aortic lesions; Scale bar = 200 µm. Data is presented as mean±SD.

3.3 Hematopoietic CD27 deficiency decreases systemic Treg abundance and promotes vascular inflammation.

Cd27$^{-/-}$*Apoe*$^{-/-}$ bone marrow chimeras showed reduced abundance of Tregs in the spleen and aorta (Figure 10 A,B, and data not shown). Of note, splenic Tregs of *Cd27*$^{-/-}$ *Apoe*$^{-/-}$ bone marrow chimeras proliferated less as assayed by Ki-67 staining whereas aortic Tregs did not differ compared to control (Figure 10 C-E).

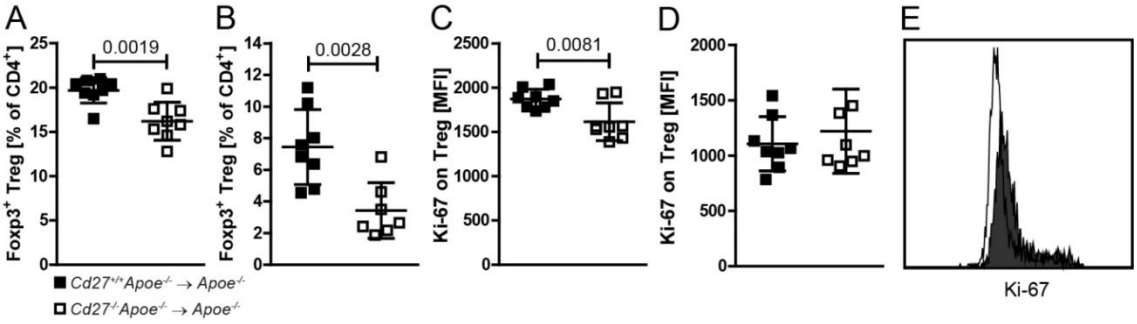

Figure 10. Hematopoietic CD27 deficiency decreases splenic and aortic Treg abundance.
Flow cytometric analysis of splenic (**A,C**) and aortic suspensions (**B,D**) of irradiated *Apoe*$^{-/-}$ mice reconstituted with *Cd27*$^{+/+}$*Apoe*$^{-/-}$ or *Cd27*$^{-/-}$*Apoe*$^{-/-}$ bone marrow for (**A,B**) Foxp3^{+} Treg and (**C,D**) Ki-67 expression of Treg. (**E**) Representative flow cytometric histograms depicting Ki-67 expression on splenic Treg. Data is presented as mean±SD.

Gene expression analysis of abdominal aortae from mice transplanted with *Cd27*$^{-/-}$ *Apoe*$^{-/-}$ bone marrow revealed a significant increase in pro-inflammatory genes. The Th2–associated marker *Gata-3* was significantly increased in the aorta, whereas *Rorγt* and *Foxp3* were only mildly reduced displaying a potential shifting of T cell subsets in the aorta compared to *Cd27*$^{+/+}$*Apoe*$^{-/-}$-transplanted controls (Figure 11 A,B). Furthermore, the pro-inflammatory chemokines *Ccl1* and the adhesion molecules *Icam1* and *Vcam1* were significantly increased potentially promoting leukocyte influx into the lesion, leading to macrophage accumulation and perpetuating atherosclerosis (Figure 11 A). Indeed, CD27-deficient transplanted mice displayed a higher ICAM-1 staining on the plaque endothelium as demonstrated by immunohistochemistry (Figure 9 E). In addition, the pro-inflammatory cytokines *Il1b*, *Il6*, and *Il12p35* were significantly increased (Figure 11 A). These data indicate the presence of a persistent inflammatory reaction in the arterial wall of *Cd27*$^{-/-}$*Apoe*$^{-/-}$ bone marrow chimeras likely due to reduced abundance of Tregs.

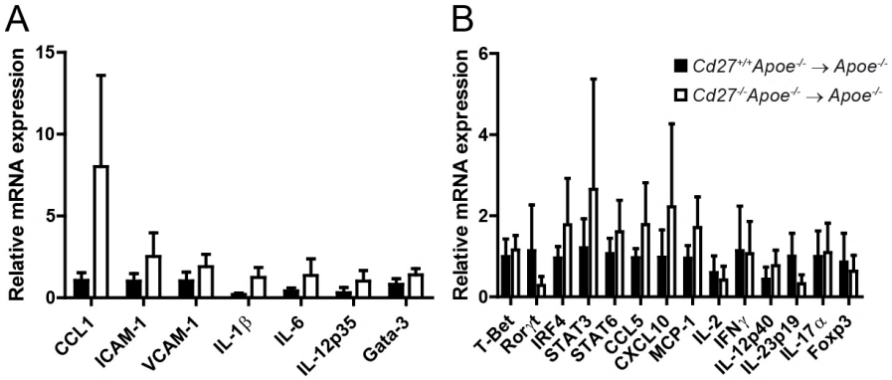

Figure 11. Hematopoietic CD27 deficiency causes vascular inflammation.
Relative mRNA expression analyzed by quantitative PCR in murine aortas, (**A**) *q* value after FDR correction < 0.1 for all genes presented. (**B**) Relative mRNA expression of genes that did not reach statistical significance but were included in a multiple testing approach. n=5 (Donor: *Cd27*$^{+/+}$*Apoe*$^{-/-}$), n=9 (Donor: *Cd27*$^{-/-}$*Apoe*$^{-/-}$). A table displaying probability values for comparisons of differences in mRNA expression levels can be found in the appendix (Table VIII). Data is presented as mean±SD.

To investigate whether systemic reduction of Treg numbers also causes changes in plasma cytokine expression, multiplex-bead based assays and ELISA were applied. Since Tregs are potent source for TGFβ, decreased Treg numbers may account for systemically lower concentrations of this anti-inflammatory cytokine. Indeed, plasma TGFβ was reduced (Figure 12 A). The plasma abundance of other cytokines was not affected (Figure 12 B).

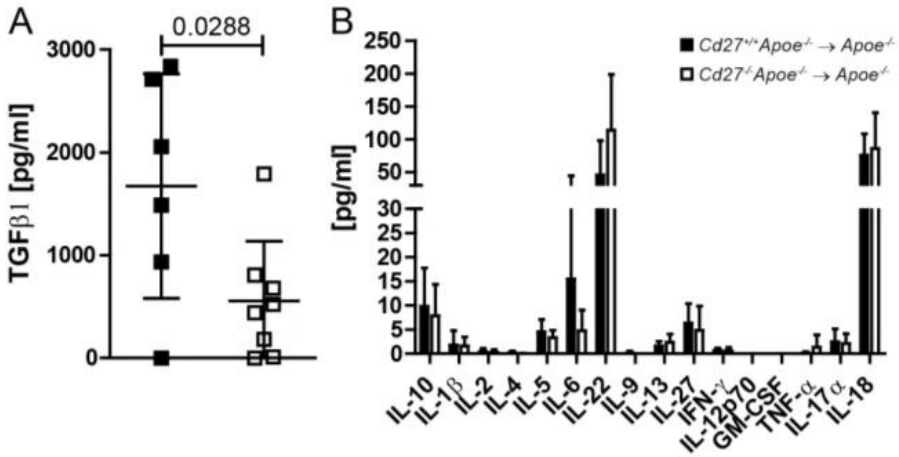

Figure 12. Hematopoietic CD27 deficiency decreases plasma TGFβ concentration.
(**A**) Plasma cytokine concentration of TGFβ measured by ELISA of irradiated *Apoe*$^{-/-}$ mice reconstituted with *Cd27*$^{+/+}$*Apoe*$^{-/-}$ or *Cd27*$^{-/-}$*Apoe*$^{-/-}$ bone marrow. (**B**) Plasma cytokine expression levels analyzed by multiplex bead-based technology. (n=8 (Donor: *Cd27*$^{+/+}$*Apoe*$^{-/-}$), n=7-8 (Donor: *Cd27*$^{-/-}$*Apoe*$^{-/-}$)). Data is presented as mean±SD.

3.4 CD27 deficiency increases nTreg apoptosis but does not affect their migratory or suppressive capacity.

Reduced abundance of Tregs in lymphoid organs may be a consequence of reduced CCR7 expression leading to decreased sensitivity of Tregs to the lymph node-homing chemokines CCL19 and CCL21. Interestingly, CCL19 seemed not to affect Treg migration in transwell assays at any concentration (Figure 13 A), however, caused total CD4^{+} cell migration (data not shown). In contrast, CCL21 promoted migration of Treg although the migratory capacity was not different between genotypes (Figure 13 B) thus excluding altered migratory capacity as a potential mechanism for reduced lesional and systemic Treg abundance.

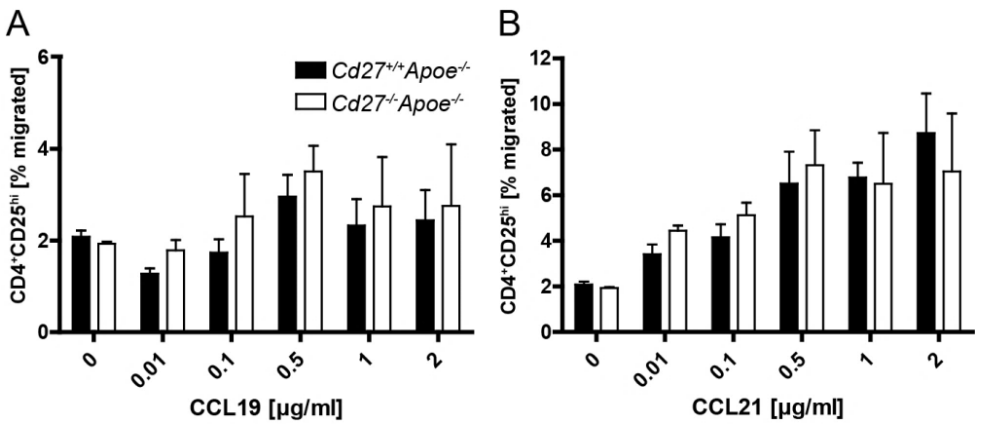

Figure 13. CD27 deficiency does not affect Treg chemotaxis towards CCL19 and CCL21.
Migration of CD4$^+$ T cells isolated from spleens of *Cd27$^{+/+}$Apoe$^{-/-}$* or *Cd27$^{-/-}$Apoe$^{-/-}$* mice through a transwell plate towards various concentrations of murine (**A**) CCL19 and (**B**) CCL21 during a 2h culture. Migrated cells were counted, analyzed for their CD25 expression by flow cytometry and displayed as ratio of the cellular input. Data is representative for two individual experiments. Data is presented as mean±SD.

Next, we addressed whether the mild pro-inflammatory and pro-atherosclerotic phenotype relates to an overall reduction of Treg frequency or whether the suppressive capacity per single Treg differs. Co-culture of CFSE-labeled and anti-CD3/CD28-stimulated CD4$^+$ T cells with varying numbers of Tregs from *Cd27$^{+/+}$Apoe$^{-/-}$* or *Cd27$^{-/-}$Apoe$^{-/-}$* mice did not show any difference in the fraction of divided conventional T cells indicating similar suppressive capacity between wildtype- and CD27-deficient Tregs (Figure 14 A,B).

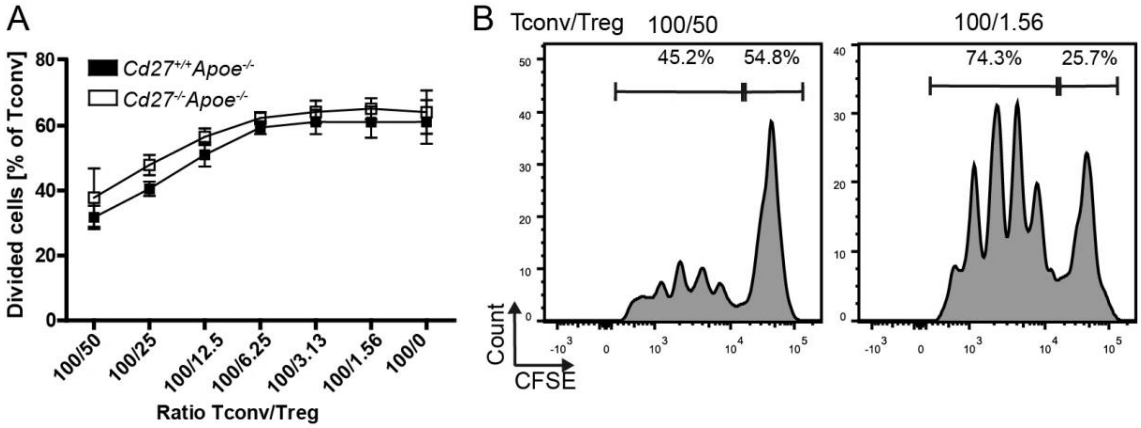

Figure 14. CD27 deficiency does not influence the suppressive capacity of Treg.
(**A**) Varying numbers of Tregs isolated from spleens of *Cd27$^{+/+}$Apoe$^{-/-}$* or *Cd27$^{-/-}$Apoe$^{-/-}$* mice were co-cultured with CFSE-labeled CD4$^+$CD25$^-$ conventional responder T cells (Tconv) from *Cd27$^{+/+}$Apoe$^{-/-}$* mice and anti-CD3/CD28 stimulatory beads for 3 days. CFSE dilution was measured and frequency of divided responder T cells is displayed. n=3 (*Cd27$^{+/+}$Apoe$^{-/-}$*), n=4 (*Cd27$^{-/-}$Apoe$^{-/-}$*) (**B**) Representative histograms for CFSE dilution of *Cd27$^{+/+}$Apoe$^{-/-}$* effector T cells. Data is presented as mean±SD.

Recent studies demonstrated impaired Treg survival upon disruption of CD27 signaling[156, 196] prompting us to investigate whether *Cd27$^{-/-}$Apoe$^{-/-}$* mice show a similar phenotype in this hyperlipidemic mouse model. Indeed, flow cytometric analysis of the thymus revealed a significant reduction in CD4$^+$CD25$^+$ cells (Figure 15 A) whereas the

fraction of Foxp3^{+} cells among those cells was 50% and remained unchanged between genotypes (data not shown). This was accompanied by increased Annexin-V staining demonstrating increased apoptosis of thymic but not splenic CD4^{+}CD25^{high} Treg from *Cd27$^{-/-}$Apoe$^{-/-}$* mice (Figure 15 B,C). Moreover, splenic Tregs in the bone marrow transplantation model displayed significantly reduced Ki-67 staining indicating less proliferation of these cells (Figure 10 C). Thus, our observation of increased atherosclerosis in *Cd27$^{-/-}$Apoe$^{-/-}$* mice may stem from overall limited numbers of Treg caused by reduced survival in the thymus and impaired proliferation in the periphery.

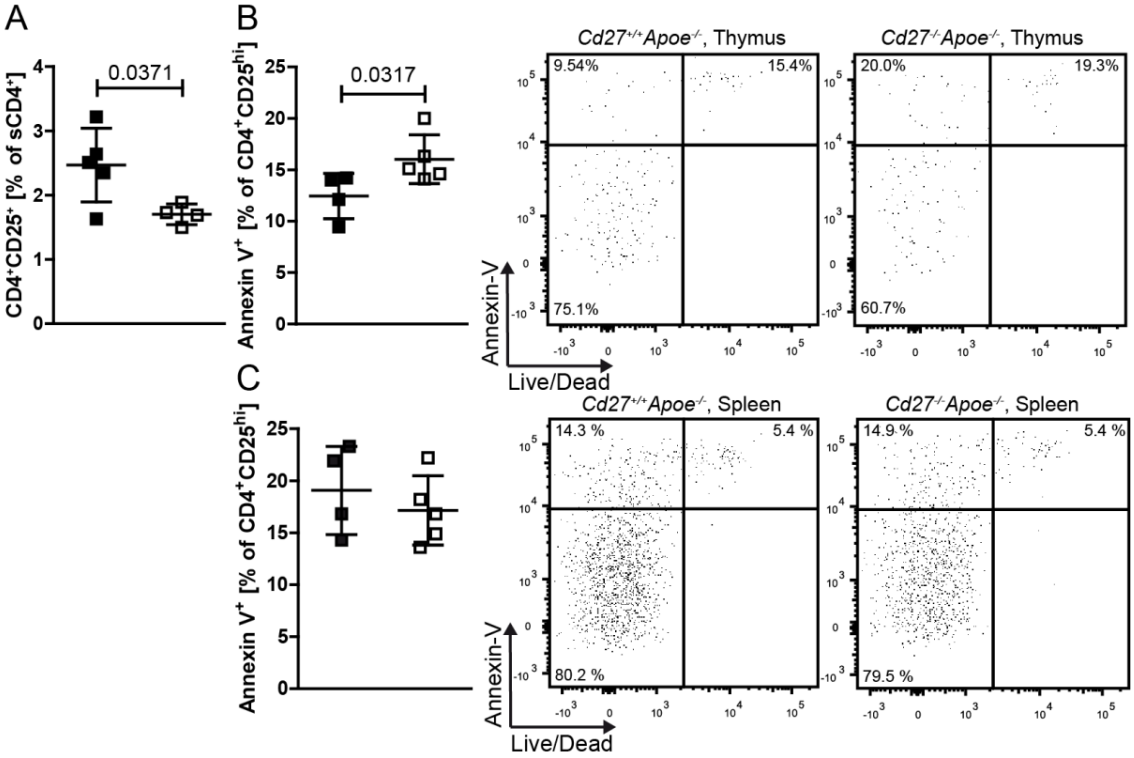

Figure 15. CD27 deficiency reduces thymic Treg abundance by increasing their apoptosis.
(**A**) Abundance of thymic CD4^{+}CD25^{+} cells in *Cd27$^{+/+}$Apoe$^{-/-}$* or *Cd27$^{-/-}$Apoe$^{-/-}$* mice assayed by flow cytometry. Tregs (CD4^{+}CD25^{+}) of (**B**) thymic and (**C**) splenic suspensions from were analyzed by flow cytometry for apoptosis by Annexin-V binding and live/dead fixable staining exclusion. Representative plots gated on CD4^{+}CD25^{+} cells are displayed. Data is presented as mean±SD.

3.5 Systemic CD27 deficiency aggravates early atherogenesis, but does not affect advanced atherosclerosis.

Absolute and relative lesion area was increased in *Cd27$^{-/-}$Apoe$^{-/-}$* mice compared to littermate controls at the age of 18 weeks (Figure 16 A-D).

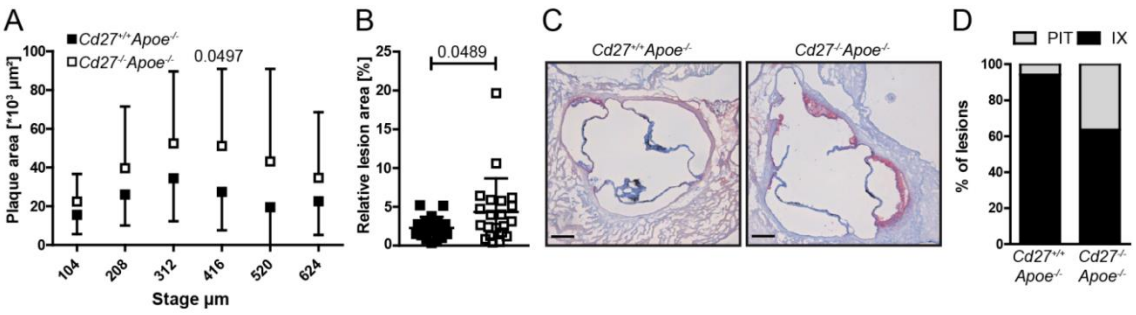

Figure 16. Early atherosclerosis is accelerated in *Cd27$^{-/-}$Apoe$^{-/-}$* compound-deficient mice.
(**A**) Atherosclerotic plaque area in cross-sections at indicated positions of the aortic root at different stages from 18-week-old, male *Cd27$^{+/+}$Apoe$^{-/-}$* or *Cd27$^{-/-}$Apoe$^{-/-}$* mice. n=15-17 (*Cd27$^{+/+}$Apoe$^{-/-}$*), n=16-21 (*Cd27$^{-/-}$Apoe$^{-/-}$*). (**B**) Average lesion area in stages 312-520 as percentage of total vessel area. (**C**) Representative photomicrographs of Oil Red O-stained sections; Scale bar = 200 µm. (**D**) Phenotypic characterization of lesions. Data is presented as mean±SD.

CD3$^+$ T cells and CD4$^+$ T cells appeared less frequent in atherosclerotic lesions of CD27 deficient compared to littermate control mice (Figure 17 A,B). In addition, increased macrophage content was observed corroborating the phenotype observed in the bone marrow chimeras (Figure 17 C). Furthermore, the collagen content in atherosclerotic lesions did not change among groups while lesions seemed phenotypically more advanced in accordance with increased lesion size (Figure 17 D).

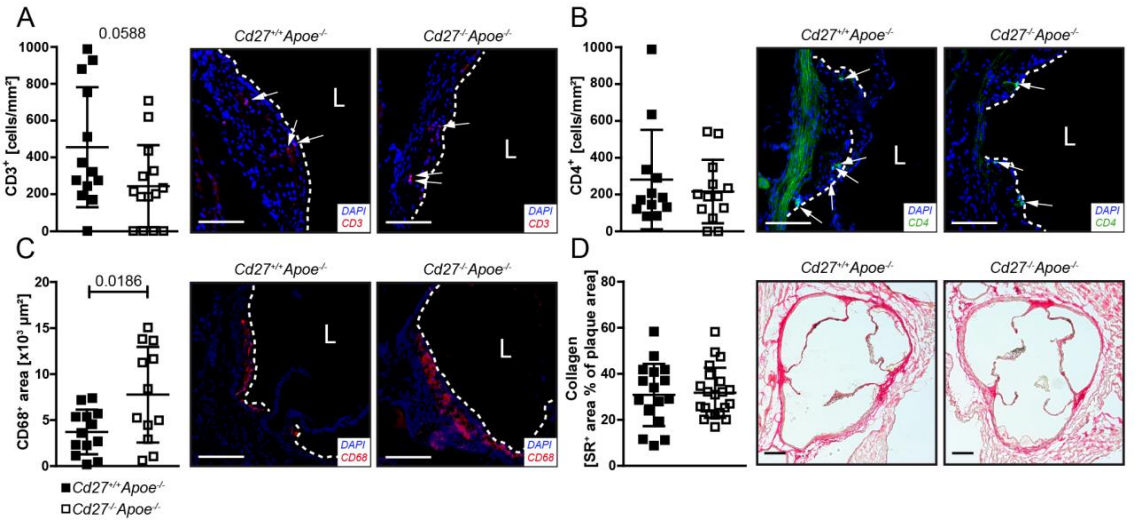

Figure 17. Macrophage area is increased in atherosclerotic lesions of young *Cd27$^{-/-}$Apoe$^{-/-}$* compound-deficient mice.
Immunofluorescent staining in cross-sections of the aortic root for (**A**) CD3$^+$ T cells, (**B**) CD4$^+$ T cells, (**C**) CD68$^+$ macrophage area. Quantifications (left) and respective representative photomicrographs (right) are displayed for each staining. Arrows indicate positive stained cells, the dashed line separates the atherosclerotic lesion from the lumen (L) Scale bar = 100 µm. (**H**) Percentage of sirius red-positive stained area in aortic root lesions; Scale bar = 200 µm. Data is presented as mean±SD.

Although at this early stage of plaque development no Tregs could be detected histologically, flow cytometry of splenic and aortic suspensions, lymph nodes, and blood (Figure 18 A-D) demonstrated a significant decrease of Treg abundance in *Cd27$^{-/-}$Apoe$^{-/-}$* mice.

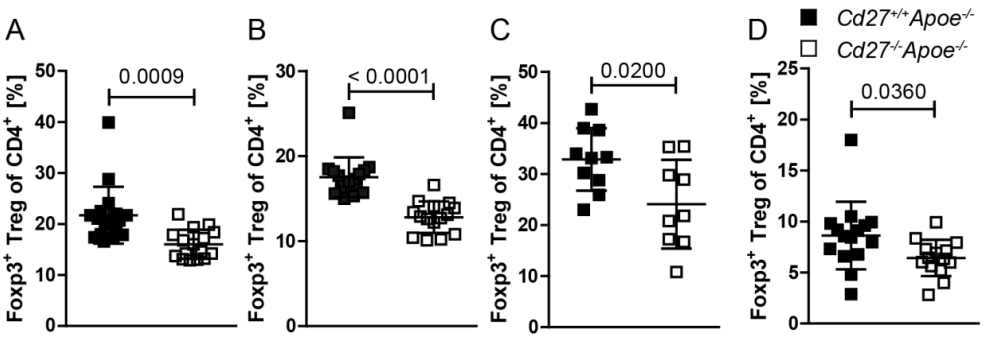

Figure 18. CD27 deficiency decreases systemic Treg abundance in young hypercholesterolemic mice.
Flow cytometric analysis of Foxp3^{+} Treg of (**A**) splenic, (**B**) lymph node, (**C**) aortic suspensions, (**D**) and in blood of 18-week-old *Cd27$^{+/+}$Apoe$^{-/-}$* and *Cd27$^{-/-}$Apoe$^{-/-}$* mice. Data is presented as mean±SD.

In contrast, 28-week-old *Cd27$^{+/+}$Apoe$^{-/-}$ and Cd27$^{-/-}$Apoe$^{-/-}$* did not display alteration in absolute and relative plaque size (Figure 19 A-C). In addition, the classification of atherosclerotic lesions of 28-week-old *Cd27$^{-/-}$Apoe$^{-/-}$* and control mice did not yield any relevant differences (Figure 19 D).

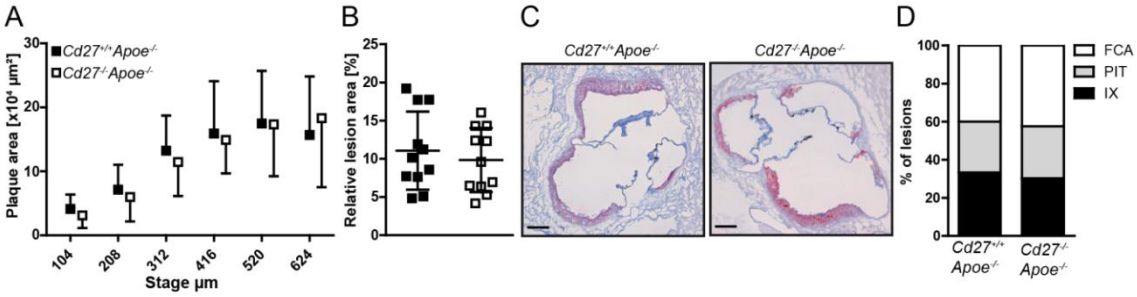

Figure 19 CD27 deficiency does not influence advanced atherosclerosis.
(**A**) Atherosclerotic plaque area in cross-sections at indicated positions of the aortic root at different stages from 28-week-old, male *Cd27$^{+/+}$Apoe$^{-/-}$* or *Cd27$^{-/-}$Apoe$^{-/-}$* mice. n=10-11 (*Cd27$^{+/+}$Apoe$^{-/-}$*), n=9-11 (*Cd27$^{-/-}$Apoe$^{-/-}$*) (**B**) Average lesion area in stages 312-520 as percentage of total vessel area. (**C**) Representative photomicrographs of Oil Red O-stained sections; Scale bar = 200 µm. (**D**) Phenotypic characterization of lesions. Data is presented as mean±SD.

Besides lesion size and phenotype, the content of lesional CD3^{+} T cells, CD4^{+} T cells, Tregs, macrophages, or collagen did not change between 28-week-old *Cd27$^{-/-}$Apoe$^{-/-}$* and control mice (Figure 20 A-E).

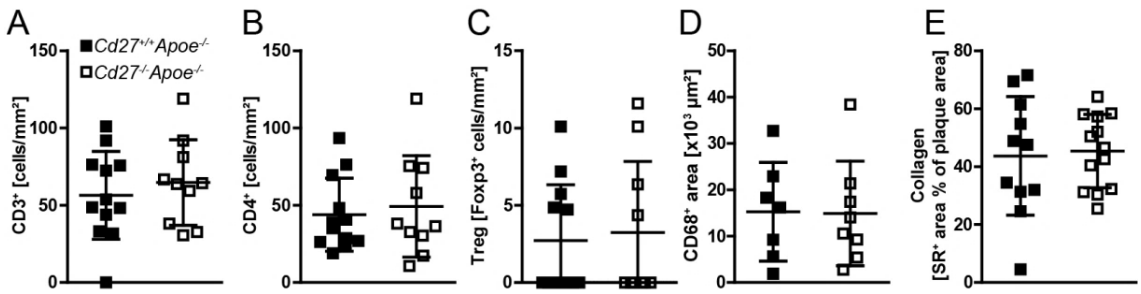

Figure 20. CD27 deficiency does not influence cellular composition in aged hypercholesterolemic mice.
(**A-D**) Immunofluorescent staining in cross-sections of the aortic root of 28-week-old, male *Cd27*$^{+/+}$*Apoe*$^{-/-}$ or *Cd27*$^{-/-}$*Apoe*$^{-/-}$ mice for (**A**) CD3^{+} T cells, (**B**) CD4^{+} T cells, (**C**) Foxp3^{+} Treg cells, and (**D**) CD68^{+} macrophage area. (**E**) Percentage of sirius red positive stained area in aortic root lesions. Data is presented as mean±SD.

Concomitantly, flow cytometry demonstrated similar abundance of Tregs in spleen, lymph nodes, and in circulation between groups (Figure 21).

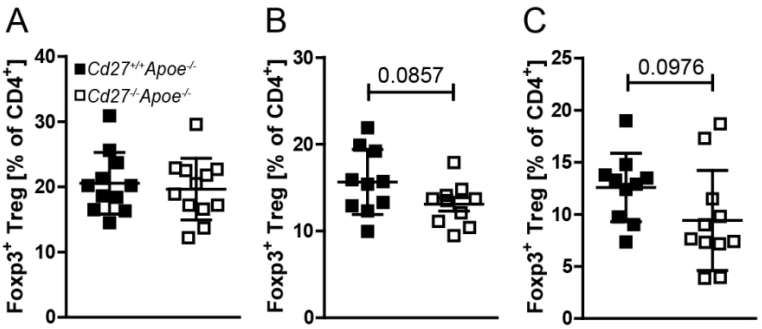

Figure 21. CD27 deficiency does not affect systemic Treg abundance in aged hypercholesterolemic mice.
Flow cytometric analysis of Foxp3^{+} Treg of (**A**) splenic, and (**B**) lymph node suspensions and in (**C**) blood of 28-week-old *Cd27*$^{+/+}$*Apoe*$^{-/-}$ and *Cd27*$^{-/-}$*Apoe*$^{-/-}$ mice. Data is presented as mean±SD.

The transplantation of CD27-deficient bone marrow leads to leukocytosis which we can confirm in our model (Table 6).[211] Since leukocytosis promotes atherosclerosis[212]**,** we could not determine whether either leukocytosis or reduced Treg frequency are the underlying causes for exacerbated atherosclerosis. To exclude leukocytosis we applied a milder model of atherosclerosis without the need for bone marrow transplantation using *Cd27*$^{+/+}$*Apoe*$^{-/-}$ and *Cd27*$^{-/-}$*Apoe*$^{-/-}$ compound-mutant mice consuming a chow diet. Indeed, neither 18-week-old nor 28-week-old *Cd27*$^{-/-}$*Apoe*$^{-/-}$ mice displayed relevant changes in hematological parameters (Table 6).

Table 6. Body weight, hematological parameters, and plasma cholesterol content in CD27 deficient mice and bone marrow chimeras.

	18 weeks			28 weeks			Bone marrow transplant		
	Cd27$^{+/+}$ *Apoe*$^{-/-}$	*Cd27*$^{-/-}$ *Apoe*$^{-/-}$	*p*	*Cd27*$^{+/+}$ *Apoe*$^{-/-}$	*Cd27*$^{-/-}$ *Apoe*$^{-/-}$	*p*	*Cd27*$^{+/+}$ *Apoe*$^{-/-}$ → *Apoe*$^{-/-}$	*Cd27*$^{-/-}$ *Apoe*$^{-/-}$ → *Apoe*$^{-/-}$	*p*
n	18	16		11	12		16	18	
Body weight [g]	30.94 ± 1.31	29.94 ± 3.62	n.s.	33.45 ± 1.92	32.92 ± 1.38	n.s.	29.09 ± 1.57	29.58 ± 1.27	n.s.
Platelets [10³/µl]	1306 ± 338	1401 ± 431	n.s.	1702 ± 366	1854 ± 528	n.s.	382 ± 165	481 ± 85	n.s.
Erythrocytes [10⁶/µl]	8.44 ± 0.94	8.60 ± 1.10	n.s.	8.43 ± 0.52	8.28 ± 0.46	n.s.	14.78 ± 2.19	17.16 ± 0.64	n.s.
Leukocytes [10³/µl]	3.79 ± 1.98	3.51 ± 1.60	n.s.	3.62 ± 1.04	2.83 ± 0.70	n.s.	5.30 ± 2.30	10.89 ± 5.08	0.0003
Lymphocytes [%]	68.07 ± 7.67	70.63 ± 10.74	n.s.	68.00 ± 10.88	71.08 ± 7.38	n.s.	60.83 ± 12.90	59.65 ± 15.60	n.s.
Monocytes [%]	6.22 ± 1.98	6.01 ± 1.79	n.s.	6.78 ± 3.32	6.08 ± 2.19	n.s.	5.51 ± 2.08	5.29 ± 1.61	n.s.
Granulocytes [%]	25.71 ± 6.67	23.37 ± 9.37	n.s.	25.22 ± 7.90	22.84 ± 5.89	n.s.	33.66 ± 11.14	35.03 ± 14.22	n.s.
Lymphocytes [10³/µl]	2.49 ± 1.31	2.37 ± 1.01	n.s.	2.40 ± 0.75	1.95 ± 0.43	n.s.	3.34 ± 1.86	6.61 ± 3.83	0.004
Monocytes [10³/µl]	0.17 ± 0.14	0.16 ± 0.12	n.s.	0.20 ± 0.15	0.13 ± 0.08	n.s.	0.21 ± 0.10	0.49 ± 0.22	< 0.0001
Granulocytes [10³/µl]	1.13 ± 0.63	0.99 ± 0.68	n.s.	1.02 ± 0.43	0.75 ± 0.33	n.s.	1.74 ± 0.64	3.79 ± 2.12	0.0008
Plasma Cholesterol [mM]	5.61 ± 1.45	6.28 ± 1.21	n.s.	7.56 ± 1.64	6.36 ± 0.80	n.s.	11.73 ± 6.86	10.32 ± 2.17	n.s.

Mean ± SD. Statistical significance was calculated for groups pairwise by 2-tailed *t* test. ***$p < 0.001$, ****$p < 0.0001$

Of note, CD27 deficiency did neither change body weight nor total plasma cholesterol or distribution among lipoprotein fractions in CD27-compund deficient mice or bone marrow chimeras (Table 6 and Figure 22).

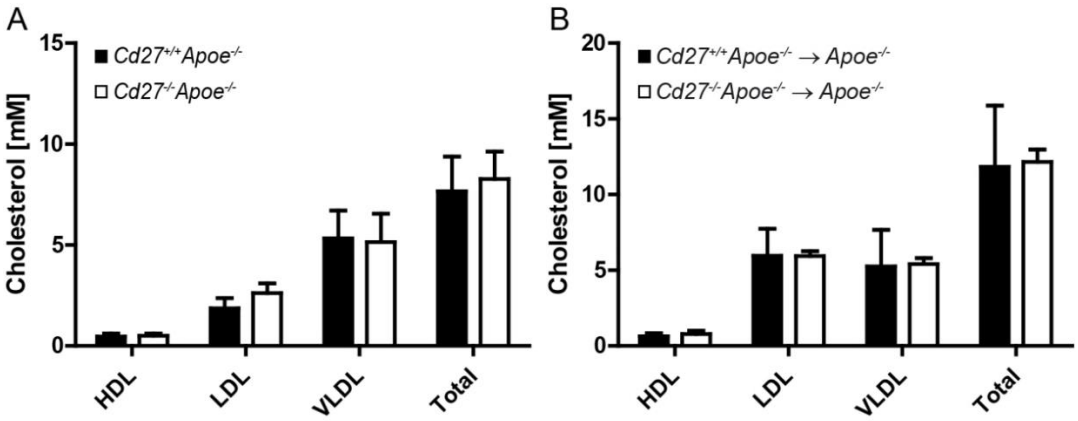

Figure 22. CD27 deficiency does not affect plasma lipoprotein cholesterol distribution.
Cholesterol distribution in different lipoprotein fractions separated by ultracentrifugation. Plasma from (**A**) 18-week-old *Cd27*$^{+/+}$*Apoe*$^{-/-}$ and *Cd27*$^{-/-}$*Apoe*$^{-/-}$ mice (n=6/group) and from (**B**) *Apoe*$^{-/-}$ mice reconstituted with *Cd27*$^{+/+}$*Apoe*$^{-/-}$ or *Cd27*$^{-/-}$*Apoe*$^{-/-}$ bone marrow (n=4/group) was analyzed. Data is presented as mean±SD.

In sum, deficiency of the co-stimulatory receptor CD27 exacerbates atherosclerosis preferentially in early stages of disease by reducing thymic T cell survival and development. However, data describing the function of CD70, the ligand of CD27, is missing. We thus we sought to investigate the role of CD70 in atherosclerosis.

3.6 CD70 is predominantly expressed on macrophages in human and murine atherosclerotic lesions.

Transcriptional profiling revealed that ruptured human carotid atherosclerotic plaques display higher CD70 expression compared to stable plaques (Figure 23) suggesting participation of this molecule in the inflammatory process in atherosclerosis.

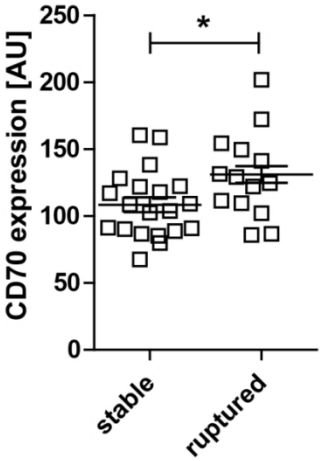

Figure 23. Increased CD70 expression in ruptured human atheroma. CD70 mRNA expression in stable and ruptured human atherosclerotic lesions analyzed by gene array (n=20). Data is presented as mean±SEM. *$p < 0.05$

Furthermore, flow cytometric analysis of atherosclerotic aortas of *Apoe*$^{-/-}$ mice identified macrophages as the predominant CD70-expressing immune cells whereas T cells are only expressing little amounts of CD70, if any (Figure 24).

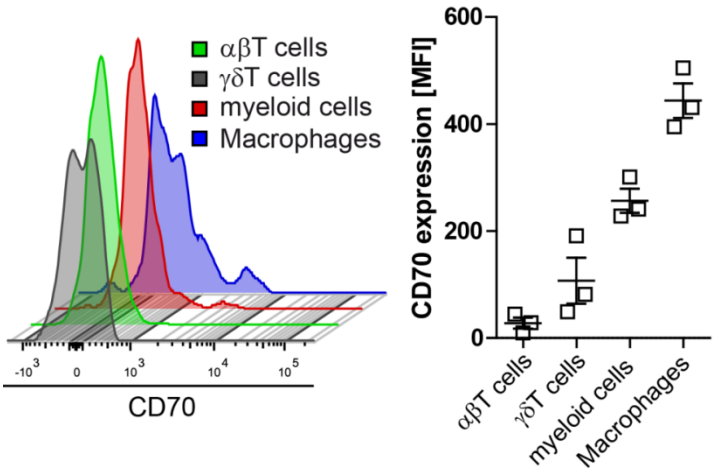

Figure 24. Macrophages are the predominant CD70 expressing cells in the murine aorta of atherosclerotic mice. CD70 expression determined by flow cytometry on leukocyte subsets in the aorta of *Apoe*$^{-/-}$ mice (age=28 weeks; n=3). Representative histograms (left) and quantifications (right). Myeloid cells are live CD11b^{+} cells. Macrophages are live CD11b^{+}F4/80^{+} cells. Data is presented as mean±SEM.

Immunohistochemistry corroborated that CD70 localized primarily to macrophages in atherosclerotic lesions of the ascending aorta of hyperlipidemic *Apoe*$^{-/-}$ mice (Figure 25). Notably, splenic and aortic T cells of hyperlipidemic mice did not express CD70.

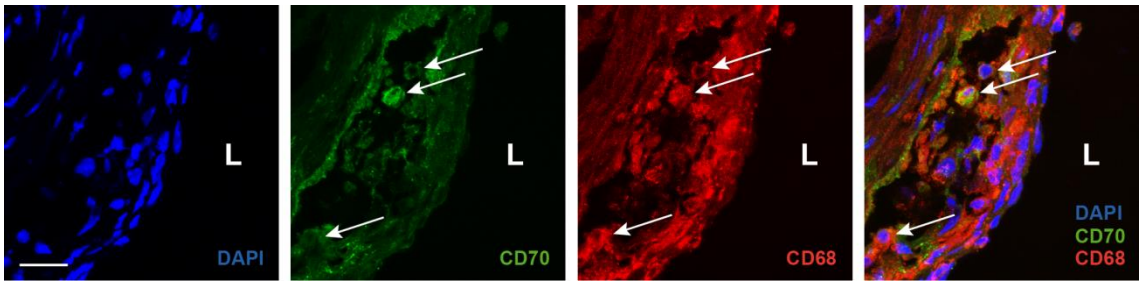

Figure 25. CD70 colocalizes predominantly with macrophages in murine atherosclerotic plaques. Immunofluorescent staining (maximum intensity projections) for CD68 and CD70 recorded by confocal microscopy in cross-sections of the aortic root of a 28-week-old *Apoe*$^{-/-}$ mouse; Scale bar = 20 µm. L = lumen.

3.7 CD70-deficient macrophages are less inflammatory and metabolically active.

The macrophage-dominant expression of CD70 led us to investigate its function in this cell type. Flow cytometry revealed that on an *Apoe*$^{-/-}$ background, CD70-deficient BMDM had increased expression of M1 macrophage markers CD64 and MHCII compared to littermate control CD70-proficient BMDM. However, they also expressed more CD301 and produced more IL-10, both characteristics of M2 macrophages (Figure 26 A-D).

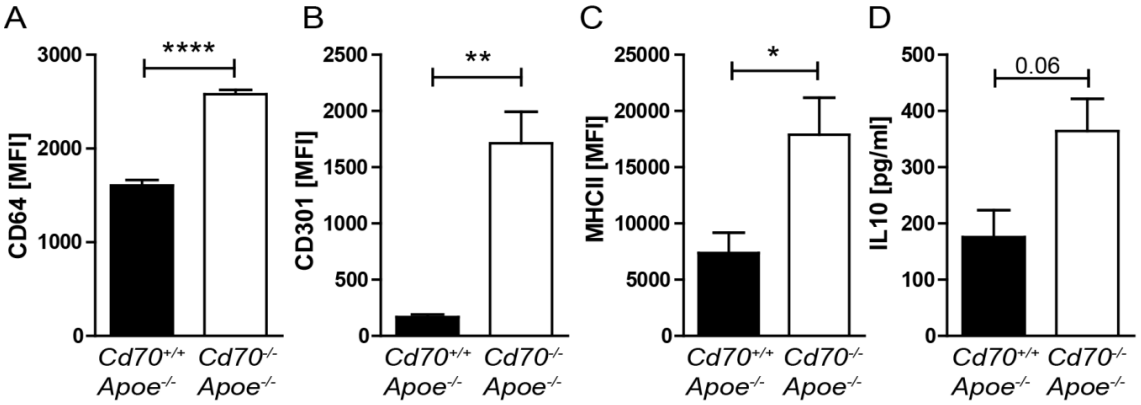

Figure 26. CD70-deficient macrophages harbor M1 and M2 marker expression. BMDM were derived from *Cd70*$^{+/+}$*Apoe*$^{-/-}$ or *Cd70*$^{-/-}$*Apoe*$^{-/-}$ mice. Flow cytometric analysis for (**A**) CD64, (**B**) CD301, and (**C**) MHCII. (**D**) IL-10 concentration in culture supernatant. Data is presented as mean±SEM (n=3). *$p < 0.05$, **$p < 0.01$, ****$p < 0.0001$

Furthermore, CD70-deficiency led to reduced production of ROS and NO by BMDM, pointing towards a diminished inflammatory capacity and an impaired M1 macrophage functionality (Figure 27 A,B). In general, CD70-deficient BMDM displayed a higher rate of apoptosis (Figure 27 C).

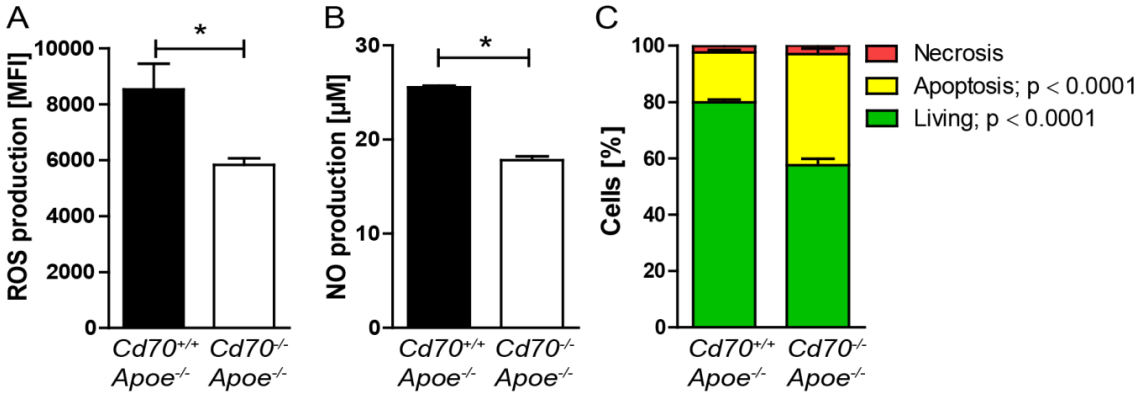

Figure 27. CD70-deficient macrophages are less inflammatory and prone to apoptosis
BMDM were derived from *Cd70*$^{+/+}$*Apoe*$^{-/-}$ or *Cd70*$^{-/-}$*Apoe*$^{-/-}$ mice. (**A**) ROS production was assayed by production of the fluorescent adduct of CM-H2DCFDA by flow cytometry. (**B**) NO production was assayed by enzymatic assay. (**C**) Cell viability assayed by Annexin-V and PI staining by flow cytometry. Data is presented as mean±SEM (n=3). *$p < 0.05$

Interestingly, *Cd70*$^{-/-}$ BMDM showed impaired mitochondrial function as demonstrated by the reduced basal respiration, OM-sensitive mitochondrial ATP synthesis, and FCCP-induced maximal respiration in *Cd70*$^{-/-}$ BMDM (Figure 28 A). *Cd70*$^{-/-}$ BMDM displayed similar glycolysis as evident from the recorded ECAR (Figure 28 B). Glycolysis is rather associated with M1 macrophages whereas M2 macrophages are considered to depend more on oxidative phosphorylation.

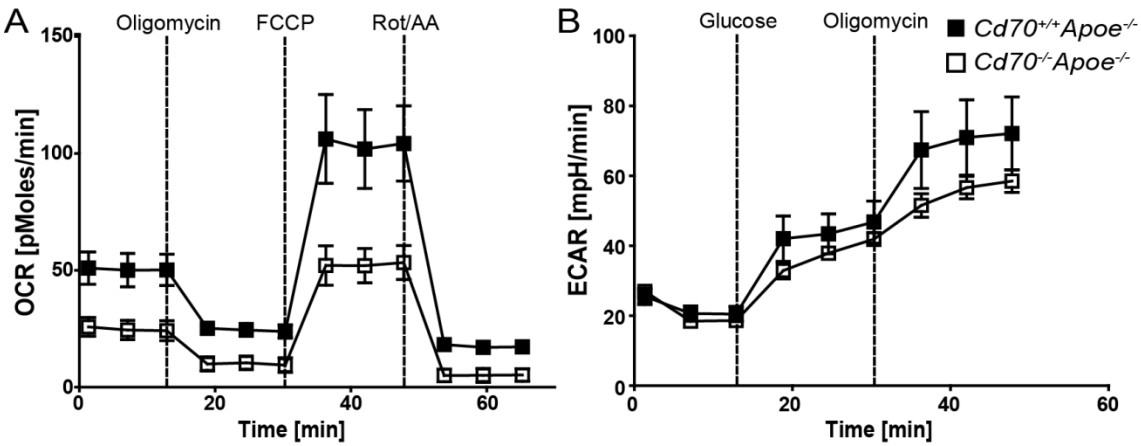

Figure 28. CD70-deficient macrophages are less inflammatory and metabolically active.
BMDM were derived from *Cd70*$^{+/+}$*Apoe*$^{-/-}$ or *Cd70*$^{-/-}$*Apoe*$^{-/-}$ mice and subsequently treated with (**A**) Oligomycin, FCCP, and rotenone (Rot) and antimycin (AA) or (**B**) glucose and OM. Vertical dotted lines indicate application of respective reagent. Bioenergetic profiles were assessed by (**A**) mito-stress test and (**B**) glycolysis stress test and are presented as (**A**) OCR and (**B**) ECAR, respectively. Data is presented as mean±SEM (n=3).

3.8 CD70-deficiency reduces scavenging and cholesterol efflux capacities of macrophages.

Next, we examined whether metabolic impairment of CD70-deficient BMDM also led to functional deficits. Indeed, CD70-deficient BMDM scavenged less fluorescently-labeled *E.coli* and oxLDL particles suggesting reduced phagocytic activity in absence of CD70 (Figure 29 A,B). Supporting this finding, CD70-deficient BMDMs expressed lower levels of the scavenger receptor CD36 and transformed less efficiently into foam cells reflecting their reduced cholesterol uptake capacity (Figure 29 C,D).

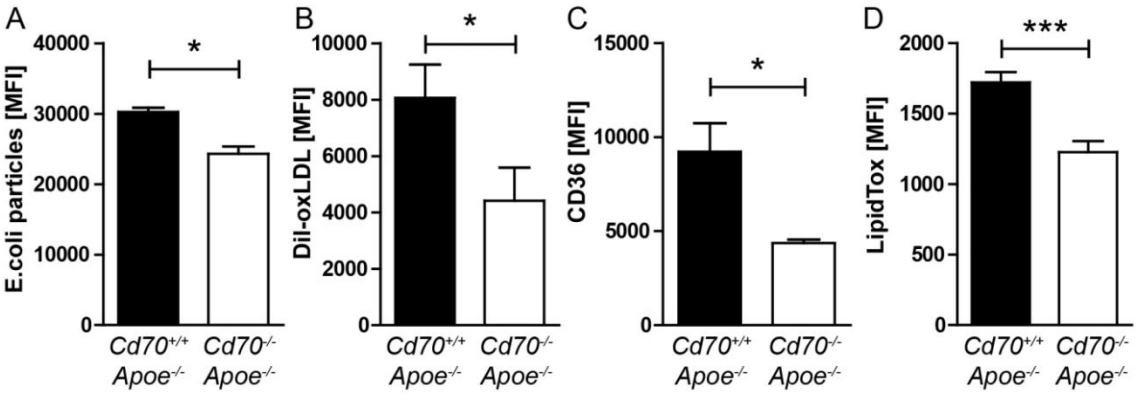

Figure 29. CD70-deficient macrophages display reduced particle uptake and foam cell formation capacity.
BMDM from *Cd70*$^{+/+}$*Apoe*$^{-/-}$ or *Cd70*$^{-/-}$*Apoe*$^{-/-}$ mice were incubated with (**A**) fluorescently-conjugated *E. coli* particles or (**B**) Dil-oxLDL. Uptake of aforementioned agents and (**C**) CD36 expression was analyzed by flow cytometry. (**D**) BMDMs were incubated with oxLDL and intracellular accumulation of neutral lipids was analyzed by LipidTox staining applying flow cytometry. Data is presented as mean±SEM (n=3). *$p < 0.05$, ***$p < 0.001$

Furthermore, lack of CD70 led to reduced cholesterol efflux towards HDL whereas ApoA1-directed efflux remained unchanged (Figure 30 A). Of note, cholesterol efflux to ApoA1 is mediated by ABCA1 whereas efflux to HDL relies mainly on ABCG1. In line with the functional data, western blot analysis of cellular lysates revealed a reduced expression of ABCG1 while ABCA1 expression in oxLDL-treated CD70-deficient BMDMs remained unchanged (Figure 30 B). Flow cytometry corroborated reduced ABCG1 expression on macrophages lacking CD70, further substantiating impaired HDL-mediated cholesterol efflux of CD70-deficient BMDM (Figure 30 C,D).

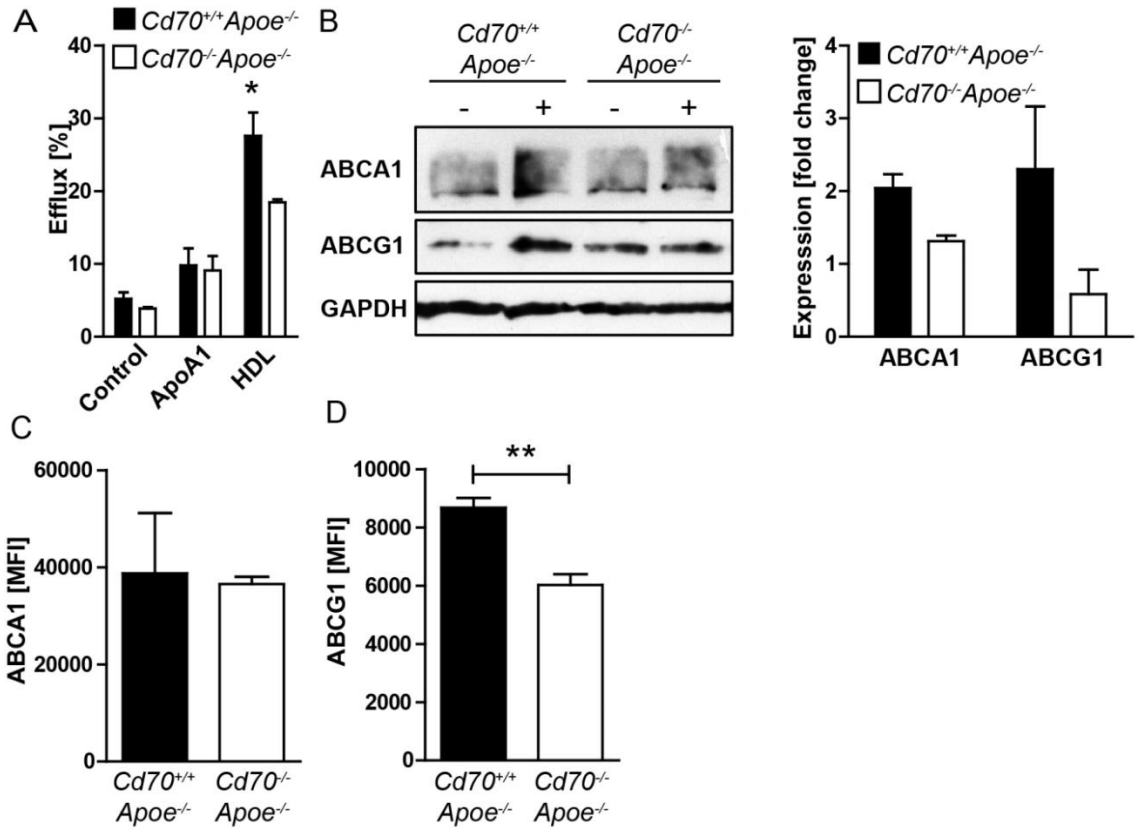

Figure 30. CD70-deficient macrophages display reduced cholesterol efflux capacity by reduced ABCG-1 expression.
BMDM were generated from *Cd70*$^{+/+}$*Apoe*$^{-/-}$ or *Cd70*$^{-/-}$*Apoe*$^{-/-}$ mice. (**A**) Cholesterol efflux to ApoA1 and HDL of BMDMs preloaded with [^{3}H]cholesterol. (**B**) Western blot analysis of protein extracts from BMDMs either non-treated or incubated with oxLDL for 48h. Immunoblots were probed for ABCA1, ABCG1, or GAPDH. Representative blots (left) and quantitative analysis (right) expressed as fold change oxLDL vs. untreated cells. Flow cytometric analysis for (**C**) ABCA1 and (**D**) ABCG1 expression of BMDMs. Data is presented as mean±SEM (n=3). *$p < 0.05$, **$p < 0.01$

3.9 CD70 deficiency aggravates atherosclerosis in bone marrow transplanted mice.

To gauge the contribution of CD70 on hematopoietic cells to atherosclerosis, we transplanted *Cd70*$^{+/+}$*Apoe*$^{-/-}$ or *Cd70*$^{-/-}$*Apoe*$^{-/-}$ BM into lethally-irradiated *Apoe*$^{-/-}$ recipient mice. Following administration of cholesterol-rich diet for 7 weeks atherosclerotic plaque size was increased 2-fold in the ascending aorta of *Apoe*$^{-/-}$ mice receiving CD70-deficient BM compared to controls (Figure 31 A,B).

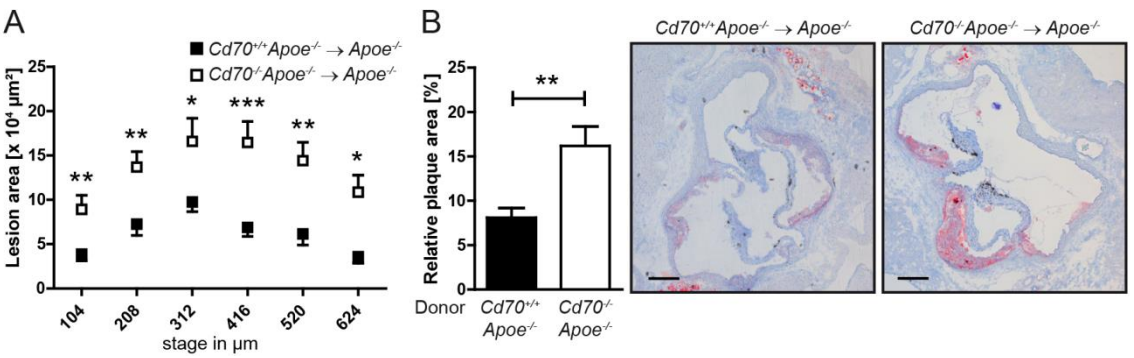

Figure 31. Hematopoietic CD70 deficiency aggravates atherosclerosis.
Irradiated *Apoe*$^{-/-}$ mice were reconstituted with bone-marrow from *Cd70*$^{+/+}$*Apoe*$^{-/-}$ or *Cd70*$^{-/-}$*Apoe*$^{-/-}$ mice. (**A**) Atherosclerotic plaque area in cross-sections at indicated positions of the ascending aorta. (**B**) Quantification of average lesion area in stages 312-520 as percentage of total vessel area (left) and representative photomicrographs showing Oil Red O-stained sections (right); Scale bar = 200 µm. Data is presented as mean±SEM (n=12-15). *$p < 0.05$, **$p < 0.01$, ***$p < 0.001$

Increased lesion size was accompanied by a larger necrotic core (Figure 32 A). Phenotypic classification according to Virmani guidelines[208] demonstrated advanced lesion characteristics in CD70-deficient BM chimeras confirming exacerbated atherosclerosis (Figure 32 B).

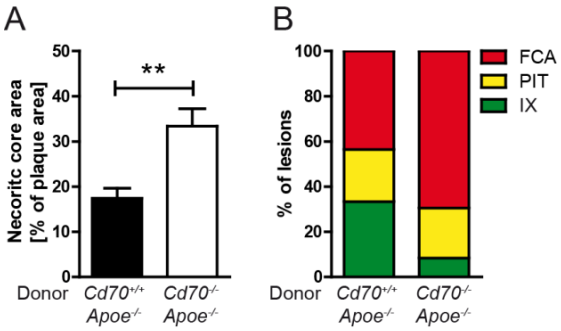

Figure 32. Hematopoietic CD70 deficiency aggravates atherosclerosis.
Irradiated *Apoe*$^{-/-}$ mice were reconstituted with bone-marrow from *Cd70*$^{+/+}$*Apoe*$^{-/-}$ or *Cd70*$^{-/-}$*Apoe*$^{-/-}$ mice. (**A**) Relative lesional necrotic core area. (**B**) Phenotypic characterization of lesions. Data is presented as mean±SEM (n=12-15). **$p < 0.01$

In agreement, lesional macrophage content was increased when CD70 was absent on hematopoietic cells (Figure 33 F). Of note, the content of collagen, SMC, CD4^{+} T cells in the lesions, as well as expression of ICAM-1 and VCAM-1 on EC in lesions did not differ between the two experimental groups (Figure 33 A-E).

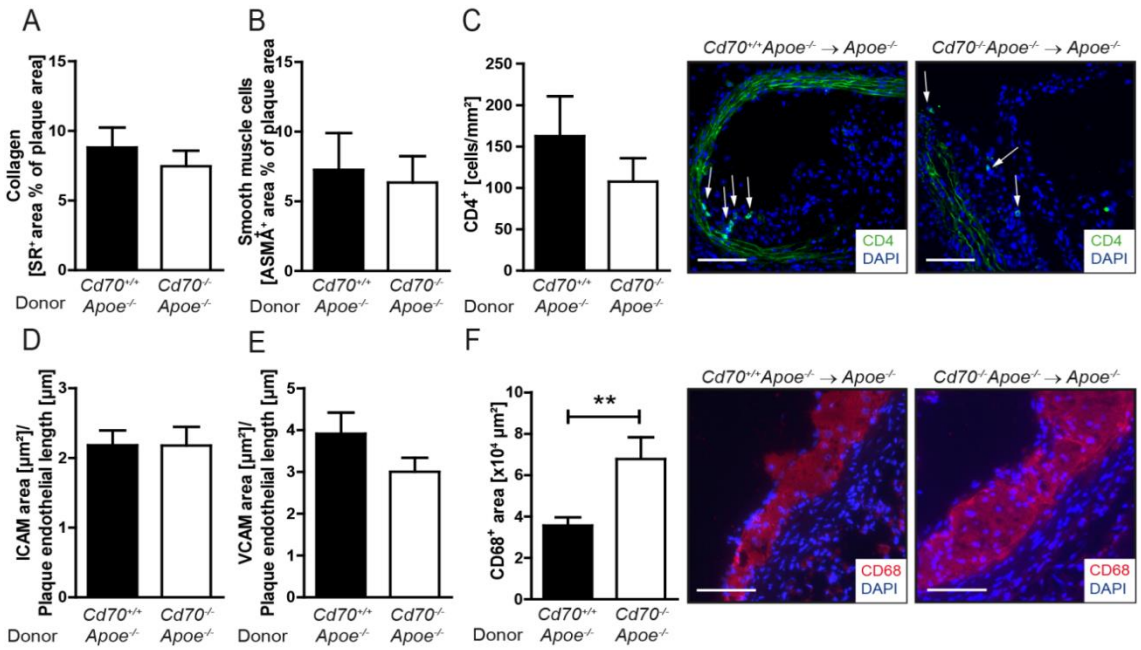

Figure 33. Lack of hematopoietic CD70 increases lesional macrophage area.
Irradiated *Apoe*$^{-/-}$ mice were reconstituted with *Cd70*$^{+/+}$*Apoe*$^{-/-}$ or *Cd70*$^{-/-}$*Apoe*$^{-/-}$ bone marrow (n=10-14 (Donor: *Cd70*$^{+/+}$*Apoe*$^{-/-}$), n=12-15 (Donor: *Cd70*$^{-/-}$*Apoe*$^{-/-}$)). (**A**) Percentage of sirius red positive stained area in lesions of the ascending aorta. (**B-F**) Immunofluorescent staining for (**B**) α-SMA, (**C**) CD4, quantification (left) and representative photomicrographs (right), (**D**) ICAM-1, (**E**) VCAM-1, and (**F**) CD68^{+} macrophage area, quantification (left) and representative photomicrographs (right) in cross-sections of the ascending aorta. (**D,E**) ICAM-1^{+} and VCAM-1^{+} area was quantified on the lesions endothelial area and further correlated to endothelial length. Data is presented as mean±SEM. $^{**}p < 0.01$. Scale bar = 100

3.10 CD70 deficiency only mildly affects systemic Treg abundance in bone marrow-transplanted mice.

CD70 and CD27 are exclusive interaction partner. As CD27 deficiency impairs Treg development and increases atherosclerosis (see aforementioned data) systemic Treg abundance was investigated in CD70-deficient bone marrow-chimeric mice hypothesizing that CD70 deficiency reduces Treg content contributing to exacerbated atherosclerosis. In our study, we only observed a moderate decrease in splenic Tregs in mice transplanted with *Cd70*$^{-/-}$*Apoe*$^{-/-}$ BM compared to mice receiving *Cd70*$^{+/+}$*Apoe*$^{-/-}$ BM (Figure 34 B). Concomitantly, Treg in CD70-deficient bone marrow chimeric mice displayed lower expression of proliferative and anti-apoptotic markers, Ki67 and BCL-2, respectively (Figure 34 D,F) which might explain the mild reduction in splenic Treg abundance. However, aortic Treg abundance and Treg Ki67 and BCL-2 expression on Treg was not affected by lack of hematopoietic CD70 (Figure 34 A,C,E). Furthermore, Treg abundance in atherosclerotic lesions did not change in mice transplanted with *Cd70*$^{-/-}$*Apoe*$^{-/-}$ BM (Figure 34 G) suggesting CD70 in Treg development and function appears negligible in our model of atherosclerosis and altered Treg numbers are unlikely to underlie those effects caused by CD70-deficiency observed here. Indeed, in

the BM transplantation set-up, CD70 is not expressed by thymic DC but still expressed on mTECs and thus Treg development is only mildly affected.

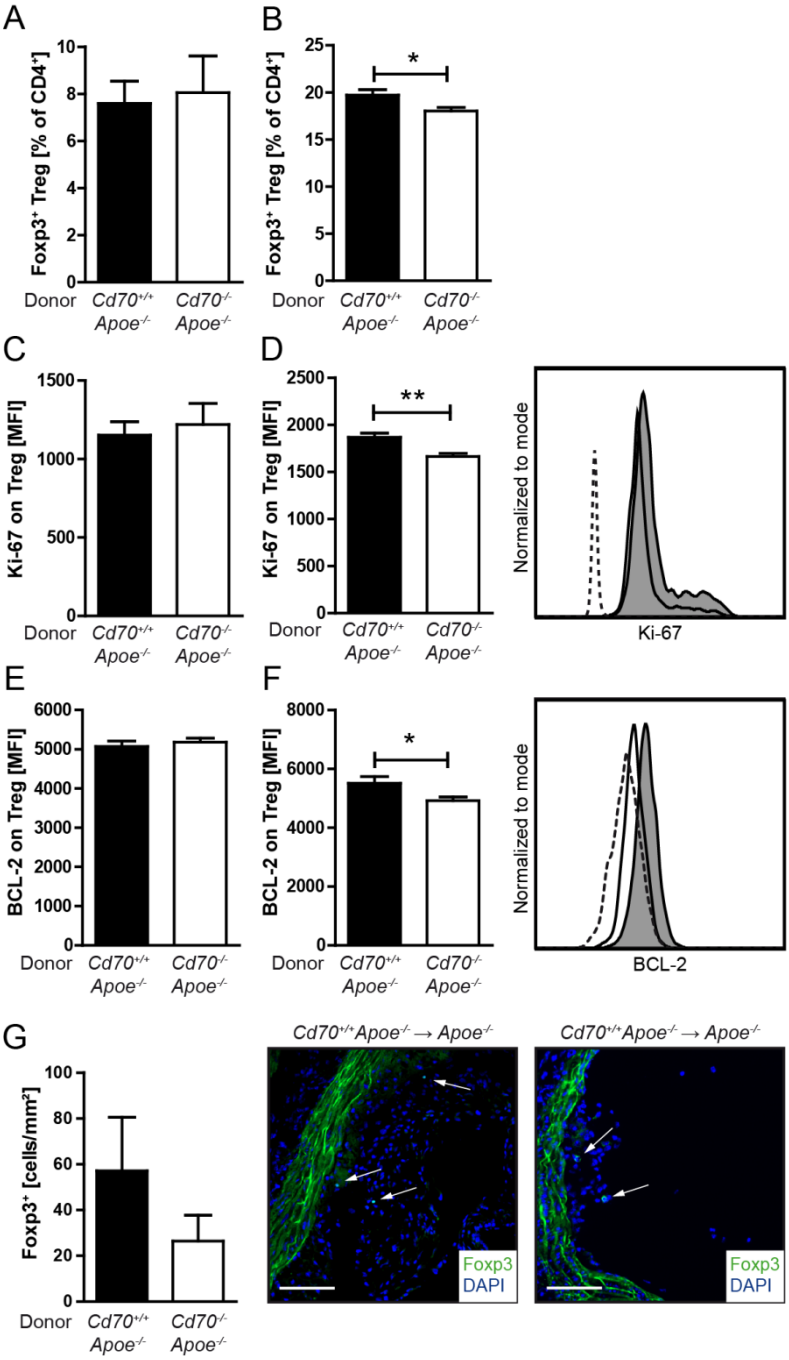

Figure 34. CD70 deficiency reduces splenic but not aortic Treg abundance.
(**A-G**) Irradiated *Apoe*$^{-/-}$ mice were reconstituted with *Cd70*$^{+/+}$*Apoe*$^{-/-}$ or *Cd70*$^{-/-}$*Apoe*$^{-/-}$ bone marrow. Flow cytometric analysis of (**A**) aortic and (**B**) splenic suspensions for Foxp3^{+} Treg. Ki-67 expression of (**C**) aortic and (**D**) splenic Treg. Representative flow cytometric histograms depicting Ki-67 expression on splenic Treg (right). BCL-2 expression of (**E**) aortic and (**F**) splenic (middle) Treg. Representative flow cytometric histograms depicting BCL-2 expression on splenic Treg (right). (**G**) Immunofluorescent staining for Foxp3 in cross-sections of the ascending aorta. Quantifications (left) and representative photomicrographs (right) are displayed. Arrows indicate positive stained cells; Scale bar = 100 µm (n=7-10). Data is presented as mean±SEM. *$p < 0.05$, **$p < 0.01$.

To further investigate the systemic inflammatory status of hyperlipidemic mice lacking hematopoietic CD70 we assessed changes in plasma cytokine expression by immuno-assays. Paralleling a slight reduction in Tregs caused by lack of hematopoietic CD70 we observed only a mild reduction in TGFβ plasma (Figure 35 A). Interestingly, plasma levels of IL-18 were increased in CD70-deficient bone marrow chimeras (Figure 35 B). The abundance of other cytokines in plasma was not affected (Figure 35 C).

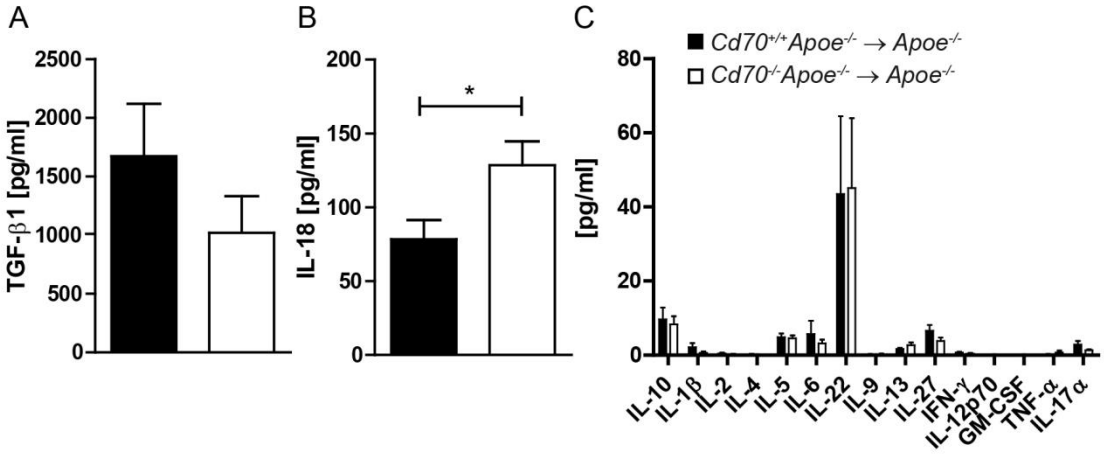

Figure 35. Hematopoietic CD70 deficiency increases plasma IL-18 concentration in hyperlipidemic mice.
Irradiated *Apoe*$^{-/-}$ mice were reconstituted with *Cd70*$^{+/+}$*Apoe*$^{-/-}$ or *Cd70*$^{-/-}$*Apoe*$^{-/-}$ bone marrow. (**A**) Plasma cytokine concentration of TGFβ measured by ELISA. (**B,C**) Plasma cytokine expression levels of analyzed by multiplex bead-based technology. (n=7 (Donor: *Cd70*$^{+/+}$*Apoe*$^{-/-}$), n=7-8 (Donor: *Cd70*$^{-/-}$*Apoe*$^{-/-}$)). Data is presented as mean±SEM. *$p < 0.05$

Although CD70-deficient macrophages displayed reduced phagocytic capacity and reduced cholesterol efflux plasma lipid levels were comparable in *Apoe*$^{-/-}$ mice that were transplanted with *Cd70*$^{+/+}$*Apoe*$^{-/-}$ or *Cd70*$^{-/-}$*Apoe*$^{-/-}$ BM (Table 7). Additionally, body weight and further hematologic parameters remained unchanged (Table 7). We only observed a mild increase in circulating monocytes of *Apoe*$^{-/-}$ mice transplanted with *Cd70*$^{-/-}$*Apoe*$^{-/-}$ bone marrow (Table 7), which may also contribute to enhanced atherosclerosis.

Table 7. Body weight, plasma cholesterol content, and hematological parameters in CD70 deficient mice and bone marrow chimeras.

	18 weeks			28 weeks			Bone marrow into $Apoe^{-/-}$		
	$Cd70^{+/+}Apoe^{-/-}$	$Cd70^{-/-}Apoe^{-/-}$	*p*	$Cd70^{+/+}Apoe^{-/-}$	$Cd70^{-/-}Apoe^{-/-}$	*p*	$Cd70^{+/+}Apoe^{-/-} \rightarrow Apoe^{-/-}$	$Cd70^{-/-}Apoe^{-/-} \rightarrow Apoe^{-/-}$	*p*
n	10	16		10	13		15	18	
Body weight [g]	27.60 ± 1.01	28.75 ± 0.53	n.s.	31.40 ± 0.45	29.92 ± 0.71	n.s.	29.13 ± 0.42	30.17 ± 0.51	n.s.
Platelets [10^3/µl]	1087 ± 140	1239 ± 100	n.s.	1844 ± 71	1548 ± 110	n.s.	397 ± 65	535 ± 73	n.s.
Erythrocytes [10^6/µl]	9.32 ± 0.21	8.52 ± 0.27	n.s.	8.26 ± 0.26	8.41 ± 0.29	n.s.	14.78 ± 0.83	16.16 ± 0.65	n.s.
Leukocytes [10^3/µl]	6.02 ± 1.01	4.59 ± 0.45	n.s.	3.53 ± 0.54	3.51 ± 0.41	n.s.	5.28 ± 0.61	7.67 ± 0.98	n.s.
Lymphocytes [%]	70.24 ± 3.65	75.74 ± 1.16	n.s.	69.01 ± 2.06	71.71 ± 4.14	n.s.	60.17 ± 3.37	63.31 ± 2.78	n.s.
Monocytes [%]	5.62 ± 1.03	5.00 ± 0.41	n.s.	7.13 ± 0.83	4.95 ± 0.54	*	5.71 ± 0.51	5.34 ± 0.40	n.s.
Granulocytes [%]	23.98 ± 2.61	19.26 ± 0.98	n.s.	23.86 ± 1.47	23.35 ± 3.92	n.s.	34.13 ± 2.94	31.36 ± 2.51	n.s.
Lymphocytes [10^3/µl]	4.16 ± 0.74	3.45 ± 0.36	n.s.	2.43 ± 0.40	2.26 ± 0.29	n.s.	3.30 ± 0.49	4.91 ± 0.73	n.s.
Monocytes [10^3/µl]	0.28 ± 0.07	0.18 ± 0.03	n.s.	0.16 ± 0.02	0.12 ± 0.03	n.s.	0.22 ± 0.02	0.34 ± 0.04	*
Granulocytes [10^3/µl]	1.59 ± 0.28	0.97 ± 0.09	n.s.	0.94 ± 0.13	1.02 ± 0.28	n.s.	1.75 ± 0.17	2.43 ± 0.32	n.s.
Plasma Cholesterol [mM]	8.35 ± 0.76	10.63 ± 1.40	n.s.	7.56 ± 0.62	6.36 ± 0.27	n.s.	11.73 ± 2.42	8.45 ± 1.14	n.s.

Mean ± SEM. Statistical significance was calculated for groups pairwise by 2-tailed *t* test. ***$p < 0.001$, ****$p < 0.0001$

3.11 Systemic CD70 deficiency aggravates atherosclerosis in young mice.

In a second model of mild hypercholesterolemia comparing compound-mutant CD70-proficient or deficient *$Apoe^{-/-}$* mice that had consumed a chow diet for 18 weeks we also did not observe any changes in body weight, hematological parameters, or plasma cholesterol content (Table 7). However, absolute and relative lesion area increased significantly in the ascending aorta of *$Cd70^{-/-}Apoe^{-/-}$* mice compared to littermate controls (Figure 36 A,B).

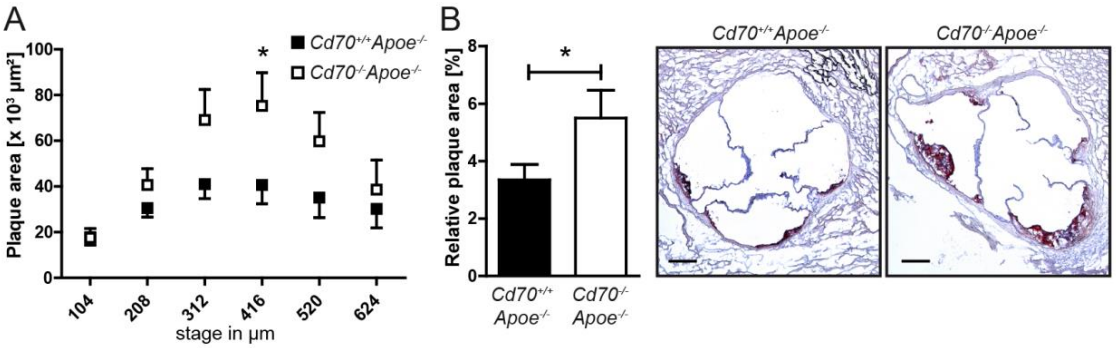

Figure 36. CD70 deficiency aggravates atherosclerosis in young hyperlipidemic mice.
(**A**) Atherosclerotic plaque area in cross-sections at indicated positions of the ascending aorta at different stages from 18-week-old, male *$Cd70^{+/+}Apoe^{-/-}$* or *$Cd70^{-/-}Apoe^{-/-}$* mice. (**B**) Average of lesion area in stages 312-520 as percentage of total vessel area (left) and representative photomicrographs showing Oil Red O-stained sections (right); Scale bar = 200 µm. Data is presented as mean±SEM (n=12-15). *$p < 0.05$

Although none of the rather initial plaques in these mice featured necrotic cores, lesions in *$Cd70^{-/-}Apoe^{-/-}$* mice had decreased cellularity as compared to controls (Figure 37 A). In addition, a larger proportion of lesions were classified as PIT, which are characterized by accumulation of extracellular lipids (Figure 37 B). The decrease in cellularity and the increase in extracellular lipid pools support the previous *in vitro* data

detailing dysfunctional lipid uptake and efflux by CD70-deficient macrophages. Although the absolute lesion area was increased in *Cd70*$^{-/-}$*Apoe*$^{-/-}$ mice, neither absolute macrophage infiltrate nor content of collagen, SMC, or CD4^{+} T cells was different from controls (Figure 37 C-E). These data further support the notion that enhanced extracellular lipid accumulation, reflecting the deficient lipid handling of the CD70-deficient macrophages *in vitro*, causes enhanced atherosclerotic burden in *Cd70*$^{-/-}$*Apoe*$^{-/-}$ mice.

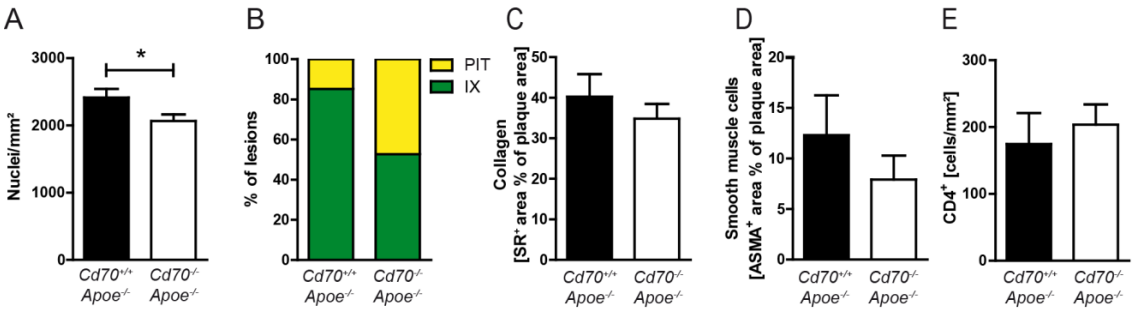

Figure 37. CD70 deficiency aggravates atherosclerosis and reduces cellular content in atherosclerotic lesions.
(**A**) Quantification of nuclei in cross-sections of the aortic root 18-week-old, male *Cd70*$^{+/+}$*Apoe*$^{-/-}$ or *Cd70*$^{-/-}$ *Apoe*$^{-/-}$ mice. (**B**) Phenotypic characterization of lesions. (**C**) Percentage of sirius red positive stained area in aortic lesions. Immunofluorescent stainings were analyzed for (**D**) α-SMA and (**E**) CD4 in cross-sections of the ascending aorta. Data is presented as mean±SEM (n=12-15). *$p < 0.05$

To further investigate the systemic inflammatory status of hyperlipidemic CD70-compoun-mutant mice in plasma cytokine expression was assessed by multiplex-bead based assays. No significant changes were observed between groups (Figure 38) which could be explained once by the mild chronic inflammatory nature of our atherosclerosis model and again highlights dysfunctional macrophages as underlying cause for aggravated atherosclerosis in *Cd70*$^{-/-}$*Apoe*$^{-/-}$ mice.

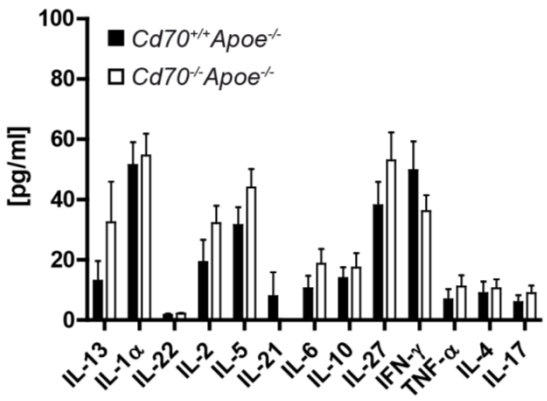

Figure 38. CD70 deficiency does not affect plasma cytokine concentration in young hyperlipidemic mice.
Plasma cytokine levels/concentrations of 18-week-old, male *Cd70*$^{+/+}$*Apoe*$^{-/-}$ or *Cd70*$^{-/-}$*Apoe*$^{-/-}$ mice analyzed by multiplex bead-based technology. Data is presented as mean±SEM (n=14-16).

CD70 is expressed by thymic DC and mTECs. Thus, a global CD70 deficiency might affect Treg development as these cells need to receive signals via CD27 during their development. Indeed, CD70-compound-mutant mice demonstrate a mild reduction in

splenic Treg abundance which further might contribute to exacerbated atherosclerosis (Figure 39 A).

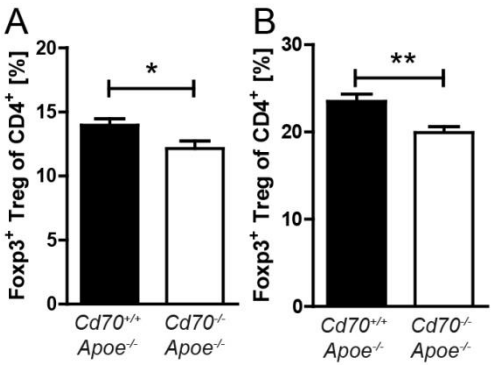

Figure 39. CD70 deficiency reduces splenic Treg abundance in 18- and 28-week-old mice.
Flow cytometric analysis Foxp3$^+$ Treg of splenic suspensions for (**A**) 18-week-old (n=7-10) and (**B**) 28-week-old (n=11-13), male *Cd70*$^{+/+}$*Apoe*$^{-/-}$ or *Cd70*$^{-/-}$*Apoe*$^{-/-}$ mice Data is presented as mean±SEM. *$p < 0.05$, **$p < 0.01$.

3.12 Systemic CD70 deficiency does only mildly affect systemic B cell abundance but increases titers of oxLDL-reactive Ig.

B cells are important immune cells and pivotal in establishing a humoral immune response. Furthermore, B cells and subsets are implicated in atherogenesis.[213] Activated B cells express CD70 and previous reports demonstrated a reduction in B cell responses and germinal center formation when CD70 was constitutively expressed on T cells.[214] Similarly, constitutive CD70 expression in B cells mediated a strong IFNγ response by T cells promoting B cell death in germinal centers thus reducing the humoral immune response.[153] The mere abundance of B cells and subsets thereof might influence the amount and subtype of Ig produced. However, we did not detect any changes in B cell abundance in blood, spleen, lymph nodes, or the peritoneum. We only observed increased abundance of circulating B1b cells and peritoneal B1a cells (Figure 40 A-D) which are considered to produce natural IgM antibodies that confer protection against atherosclerosis.

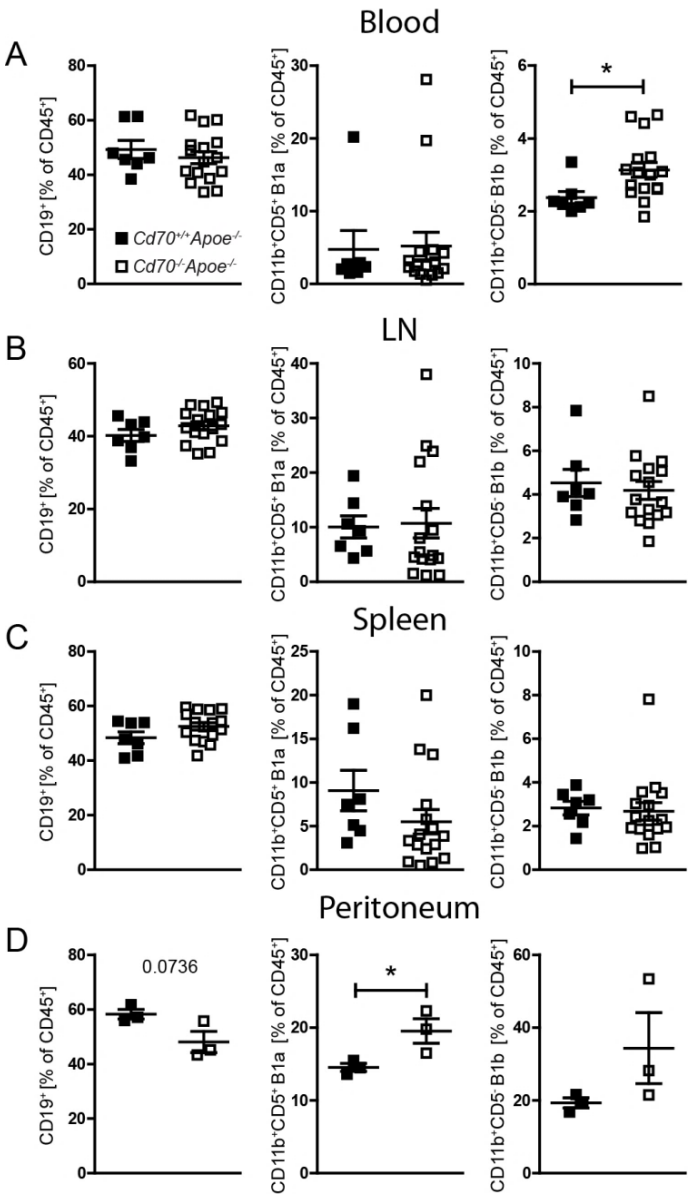

Figure 40. CD70 deficiency does not alter general B cell abundance and only mildly affects B cell composition at various sites.
Flow cytometric analysis for $CD19^+$ B cells, $CD11b^+CD5^+$ B1a and $CD11b^+CD5^-$ B1b of (**A**) blood, (**B**) lymph node suspensions, (**C**) splenic suspensions, and peritoneal exsudates of 18-week-old (male *Cd70*$^{+/+}$*Apoe*$^{-/-}$ or *Cd70*$^{-/-}$*Apoe*$^{-/-}$ mice Data is presented as mean±SEM. $*p < 0.05$

Blocking CD27/CD70 interaction employing a monoclonal anti-CD70 antibody after infection with LCMV enhanced the expression of neutralizing antibodies.[175] This led us to investigate how global CD70 deficiency would alter plasma Ig abundance in the atherosclerotic mice with a multiplex bead-based assay. Indeed, CD70-deficient hyperlipidemic mice had increased abundance of IgA, IgG3, and IgG2a in plasma (Figure 41). Yet, the assay did not detect IgG1.

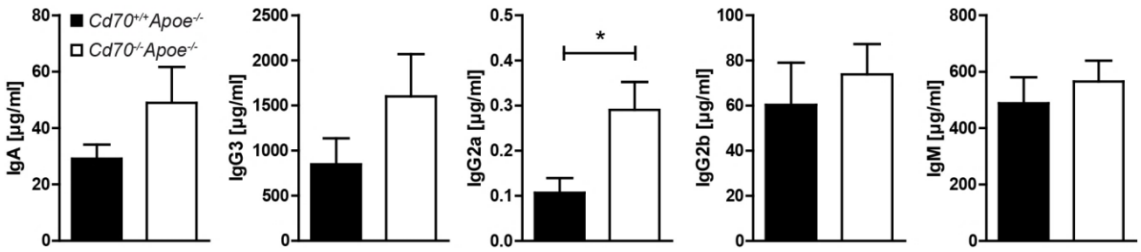

Figure 41. CD70 deficiency increases IgG2a plasma abundance in young hyperlipidemic mice.
Plasma expression levels for respective Ig of 18-week-old, male and female *Cd70*$^{+/+}$*Apoe*$^{-/-}$ (n=14) or *Cd70*$^{-/-}$*Apoe*$^{-/-}$ (n=17) mice analyzed by multiplex bead-based technology. Data is presented as mean±SEM. *$p < 0.05$

The general abundance of Ig and subclasses does not allow for extrapolation about reactivity and abundance of Ig specifically binding atherosclerosis-relevant antigens, such as oxLDL. Accordingly, we performed an oxLDL-specific ELISA detecting oxLDL binding Ig in plasma of hyperlipidemic *Cd70*$^{+/+}$*Apoe*$^{-/-}$ and *Cd70*$^{-/-}$*Apoe*$^{-/-}$ mice. Indeed, plasma of CD70-deficient mice harbored more oxLDL-specific total IgG, IgG1, and IgG2b whereas levels of IgM remained unchanged (Figure 42). These data indicate increased abundance of Ig subsets considered pro-atherogenic potentially contributing to exacerbated atherosclerosis. The assay failed to detect levels of oxLDL-specific IgG2a and IgG3.

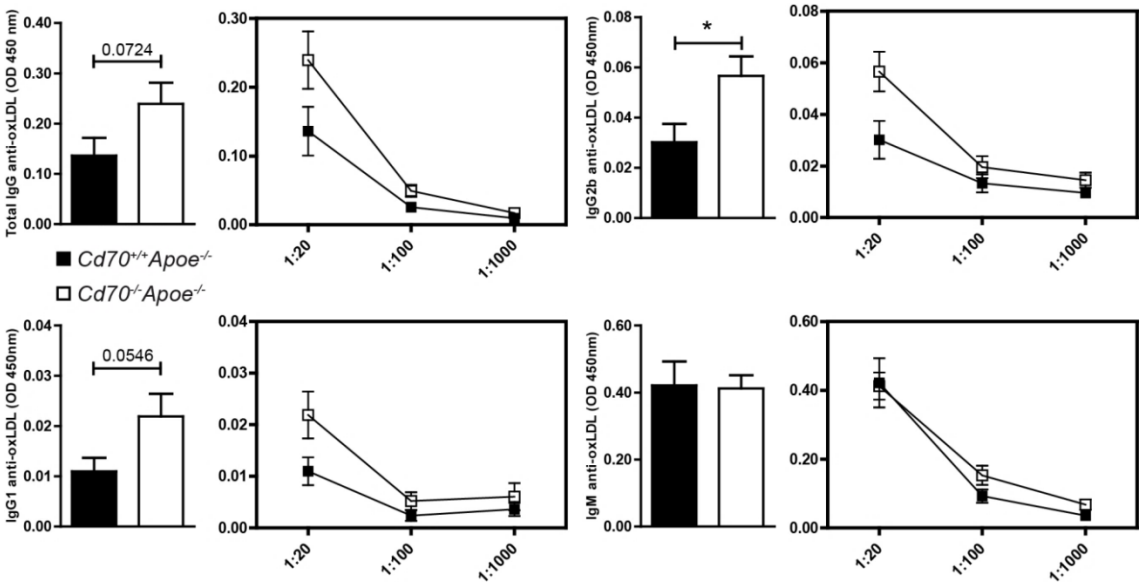

Figure 42. CD70 deficiency increases plasma abundance of Ig binding oxLDL in young hyperlipidemic mice.
Plasma abundance of antibodies detecting oxLDL of 18-week-old, male *Cd70*$^{+/+}$*Apoe*$^{-/-}$ (n=15) or *Cd70*$^{-/-}$*Apoe*$^{-/-}$ (n=17) mice. Antibody abundance was analyzed by ELISA and respective murine detection antibodies. Quantifications for optic density acquired at 450 nm wavelength of 1:20 diluted plasma is displayed in a bar graph (right), dilution series (1:20, 1:100, 1:1000) of plasma and respective ODs are displayed for each antibody (left). Data is presented as mean±SEM. *$p < 0.05$

To address the impact of CD70 deficiency on advanced atherosclerosis we sacrificed 28-week-old *Cd70*$^{+/+}$*Apoe*$^{-/-}$ and *Cd70*$^{-/-}$*Apoe*$^{-/}$ mice. Although exacerbation in young

CD70-compound deficient mice and bone marrow chimeric mice was observed, 28-week-old *Cd70*$^{-/-}$*Apoe*$^{-/}$ mice did not display alterations in absolute and relative plaque area compared to littermate controls (Figure 43 A,B). We did not observe any changes in body weight, hematological parameters, or plasma cholesterol content (Table 2). However, the relative abundance in circulating monocytes was reduced which would argue for reduced atherosclerotic burden.

3.13 Advanced atherosclerosis is not altered by global CD70 deficiency.

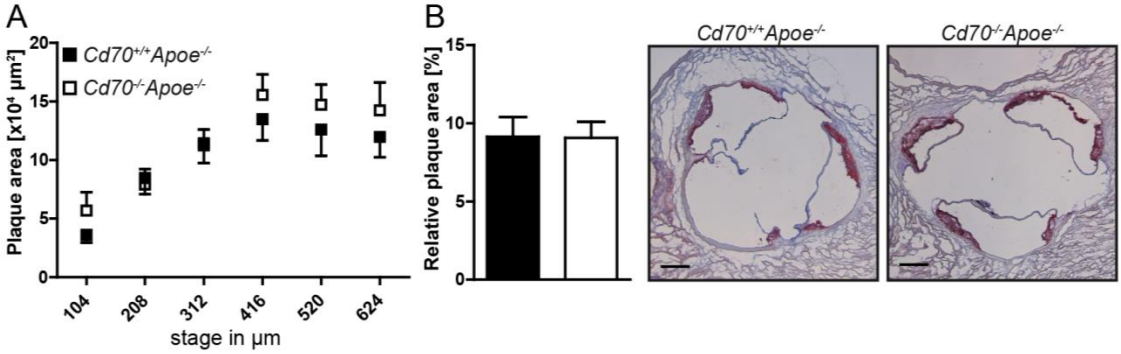

Figure 43. CD70 deficiency does not alter atherosclerotic burden in aged hyperlipidemic mice.
(**A**) Atherosclerotic plaque area in cross-sections at indicated positions of the ascending aorta at indicated stages from 28-week-old, male *Cd70*$^{+/+}$*Apoe*$^{-/-}$ or *Cd70*$^{-/-}$*Apoe*$^{-/-}$ mice. (**B**) Average of lesion area in stages 312-520 as percentage of total vessel area (left) and representative photomicrographs showing Oil Red O-stained sections (right); Scale bar = 200 µm. Data is presented as mean±SEM (n=10-12). *$p < 0.05$

Besides lesion size and phenotype, neither the content of CD68^{+} macrophage area, CD4^{+} T cells, Foxp3^{+} Tregs, SMC, nor collagen was altered between 28-week-old *Cd70*$^{-/-}$*Apoe*$^{-/-}$ and littermate control mice (Figure 44 A-E).

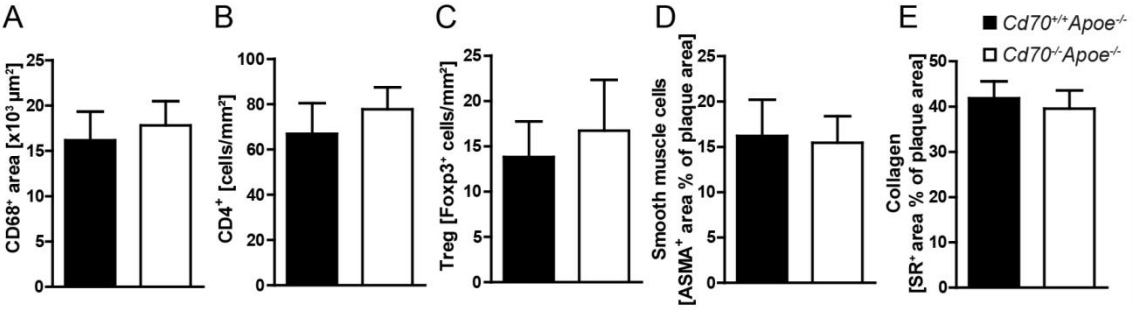

Figure 44. CD70 deficiency does not affect atherosclerotic plaque composition in aged hyperlipidemic mice.
Immunofluorescent stainings of cross-sections of the ascending aorta from 28-week-old, male *Cd70*$^{+/+}$*Apoe*$^{-/-}$ or *Cd70*$^{-/-}$*Apoe*$^{-/-}$ mice were analyzed for (**A**) CD68^{+} macrophage area, (**B**) CD4, (**C**) Foxp3^{+} cells, and (**D**) α-SMA. (**E**) Percentage of sirius red positive stained area in lesions of the ascending aorta. Data is presented as mean±SEM (n=10-12).

Although flow cytometry revealed a significantly reduced abundance of Tregs in blood, spleen, and lymph nodes of 28-week-old hyperlipidemic CD70-deficient mice (Figure

39 B, Appendix Table IV), atherosclerosis was unchanged. However, phenotypic and inflammatory changes in secondary lymphoid organs not necessarily reflect the inflammatory status of atherosclerotic lesions.

A comprehensive overview of immune cell abundance in *Cd27*$^{-/-}$*Apoe*$^{-/-}$ mice and *Cd70*$^{-/-}$*Apoe*$^{-/-}$ mice can be found in the Appendix (Appendix Tables I-IV). CD27 and CD70 interactions are indispensable for T cell memory formation and are needed for the fulminant induction of a T cell response. Indeed, we could observe reduced abundance of effector memory CD8^{+} T cells in blood and spleen of 18-week-old *Cd27*$^{-/-}$*Apoe*$^{-/-}$ mice and in lymph nodes of young *Cd70*$^{-/-}$*Apoe*$^{-/-}$ mice (Appendix Tables I, III). However, during aging these changes were not apparent anymore (Appendix Tables I, IV). *Cd70*$^{-/-}$ and *Cd27*$^{-/-}$ bone marrow chimeric mice also displayed reduced effector memory T cell abundance in the spleen (Appendix Tables VII), whereas only *Cd27*$^{-/-}$bone marrow chimeric mice also demonstrated less central memory CD8^{+} T cells in lymph nodes and spleen (Appendix Tables VI, VII). Of note, CD27 and CD70 deficiency did not influence CD4^{+} T cell memory formation (Appendix Tables I-VII).

4 DISCUSSION

Human atherosclerotic lesions harbor a substantial amount of T cells expressing CD27 and lesions classified as ruptured display increased expression of CD27 and CD70 compared to stable lesions thereby implicating this co-stimulatory dyad in atherogenesis. However, it is also possible that increased CD27 and CD70 transcript simply reflects an increased influx of activated immune cells or activation of lesional immune cells expressing those molecules. Hypercholesterolemia induces the infiltration of leukocytes such as T cells and monocytes in the arterial wall, which perpetuates inflammation. Monocytes will subsequently transform into macrophages. In models of murine atherosclerotic plaques CD27 colocalizes with T cells and subsets thereof whereas CD70 was highly expressed in macrophages.

4.1 Reduced Treg abundance in CD27-deficient mice causes exacerbated atherosclerosis.

The present study indicates that in atherosclerosis CD27 co-stimulation increases Treg responses, which is associated with reduced disease symptoms. In a model of bone marrow transplantation, CD27 deficiency caused a substantial increase in atherosclerotic lesion size accompanied by less Tregs and more macrophages in these lesions. Moreover, the majority of plaques displayed an advanced phenotype. In addition, CD27-deficiency in hematopoietic cells promoted inflammation in atherosclerotic lesions as also demonstrated by increased expression of pro-inflammatory chemokines, cytokines, and adhesion molecules in the murine aorta. This pronounced inflammatory phenotype is likely evoked by a systemic decrease in Treg abundance. However, the transplantation of CD27-deficient bone marrow cells induces leukocytosis and causes activation of stem cells which might further perpetuate aortic inflammation. Nonetheless, hyperlipidemic CD27-deficient mice display similar increment in atherosclerotic burden compared to mice transplanted with CD27-deficient bone marrow, however, do not develop leukocytosis, as also reported previously.[211, 212] Accordingly, our data suggest that systemic reduction of Tregs caused by CD27 deficiency majorly contributes to exacerbated atherogenesis. Indeed, Tregs are known to counter-balance inflammation and control peripheral immune homeostasis and their anti-inflammatory features in atherosclerosis are well-established.[56, 62, 215] Tregs exert their suppressive function in various ways. In particular, they are potent sources of the anti-inflammatory cytokines IL-10 and TGFβ and disruption of IL-10- and TGFβ-signaling on T cells and DC aggravated atherosclerosis.[74, 75, 216]

TGFβ can suppress MHCII expression on APC, stimulate SMC proliferation, collagen synthesis, and decrease matrix metalloproteinase expression, thus stabilizing the collagen content and the phenotype of the atherosclerotic lesion.[5] A decrease in plasma levels of TGFβ may be attributable to a systemic decrease of Tregs as the potential source and explain the increased pro-inflammatory status of *Cd27*$^{-/-}$ mice.

Since Tregs are in a balance with Th17 cells it is tempting to speculate that a decrease of Tregs could lead to a more pronounced Th17 response. Indeed, in experimental autoimmune encephalomyelitis, a murine model of multiple sclerosis, CD27 signaling decreased Th17 function and disease severity by suppressing IL-17 production and CCR6 expression in already committed Th17 cells.[190] However, plasma levels of IL-17 and the expression of the lineage-specific marker Rorγt in the aorta were unchanged in mice reconstituted with *Cd27*$^{-/-}$*Apoe*$^{-/-}$ bone marrow, indicating that changes in Th17 cell activity are unlikely to contribute to the increased inflammation.

Thus, decreased Treg numbers are the most likely cause of increased atherosclerosis in mice reconstituted with *Cd27*$^{-/-}$*Apoe*$^{-/-}$ bone marrow. Concomitantly, aortic expression of the IL-12p35 subunit increased, suggesting increased abundance of IL-12 whereas expression of the IL-23p19 subunit tended to decrease in mice transplanted with CD27-deficient bone marrow. This argues for a shift towards a Th1-dominated T cell response and a reduced Th17 response since IL-23 is needed for maintenance of Th17 cells.[217] Furthermore, the expression of GATA-3 is substantially increased. Yet, GATA-3 is expressed by Th2 T cells and M2 macrophages and its origin here remains elusive. The drastically elevated expression of IL-1β coinciding with increased macrophage content in aortae of mice receiving *Cd27*$^{-/-}$*Apoe*$^{-/-}$ bone marrow is not surprising considering that macrophages are potent sources for this pro-atherogenic cytokine.[98, 101]

Although the abundance of aortic Tregs was diminished in mice reconstituted with *Cd27*$^{-/-}$ bone marrow we were only able to detect a trend in reduced expression of the lineage transcription factor Foxp3. This discrepancy may derive from the analysis of whole tissue lysates which contain cells not only from the plaque but also from additional layers of the vessel, namely media and adventitia, thus diluting the abundance of Foxp3 mRNA.

IL-2 is an autocrine T cell survival factor important for peripheral Treg maintenance since Tregs are not able to synthetize IL-2 themselves.[218] Plasma IL-2 levels did not differ in *Cd27*$^{-/-}$ chimeric mice of the present study. However, systemic IL-2 levels require careful interpretation with regard to local Treg prevalence since a recent study demonstrated a necessity for IL-2 abundance in the micro-milieu for Treg maintenance.[219] Nonetheless, we propose that in the chronic inflammatory condition of

atherosclerosis, reduced production of IL-2 by activated conventional *Cd27*$^{-/-}$ T cells might lead to a reduced abundance of IL-2 in the atherosclerotic lesion.[160] This would impair Treg maintenance and the conversion of conventional T cells into iTregs further perpetuating lesional inflammation.[220]

A second pathway that most likely contributes to the pronounced inflammation in plaques of *Cd27*$^{-/-}$ mice in the present study is the systemic decrease in nTregs resulting from increased apoptosis of developing nTregs in the thymus. Indeed, ligation of CD27 by CD70 expressed on mTECs or DC was found to promote thymic output of nTregs during T cell development in wild-type mice.[156] The low though relevant abundance of Tregs in the atherosclerotic lesion complicates to delineate whether they originate from converted conventional T cells or underwent thymic development. Thus, it is not clear which of the two aforementioned mechanisms prevails and requires clarification in the future.

4.2 Tregs are anti-atherogenic and are reduced during atherogenesis.

Interestingly, patients suffering from non-ST-segment-elevated myocardial infarction harbor lower numbers of circulating Treg accompanied by enhanced apoptosis allowing for speculation regarding the clinical potential of counterbalancing Treg apoptosis.[221] Tregs have a distinct kinetic in atherosclerosis as recently demonstrated in *Ldlr*$^{-/-}$ mice.[80] Their presence in atherosclerotic lesions peaked upon 4 weeks of cholesterol-enriched diet. Sustained hyperlipidemia reduced their frequency accompanied by an increase in lesion size and inflammation. However, the underlying mechanisms remain undefined. Besides reduced survival other pathways might limit Treg abundance. One mechanism may be the conversion of Tregs into T cells lacking Foxp3 expression, which cannot be detected by the classical assays for this conventional lineage marker. Additionally, Tregs might actively egress from the atherosclerotic lesion during the progression of atherosclerosis. Recently, an elegant study demonstrated homing of peripheral Tregs to the thymus where they suppressed development of further progeny.[222] None of the aforementioned mechanisms has been formally demonstrated during the course of atherosclerosis. *Apoe*$^{-/-}$ mice were used in the present study and it seems likely that Tregs show similar kinetics as observed in *Ldlr*$^{-/-}$ mice. Thus, Tregs might play an essential and protective role particularly during early stages of atherosclerosis. However, upon progression of atherosclerosis other immune cells predominate and the influence of Treg becomes negligible, corroborating our finding of similar atherosclerotic burden yet continuously suppressed Treg numbers in 28-week-old mice. Direct comparison of results obtained by Maganto-Garcia *et al.* with this study

requires cautious interpretation as different hyperlipidemic mouse models were applied.[80]

This is the first study demonstrating the involvement of CD27 in atherosclerosis ascribing this co-stimulatory molecule a rather anti-inflammatory and athero-protective role by enhancing Treg survival and development.

4.3 *Cd70*$^{-/-}$ macrophages are metabolically less active and prone to apoptosis.

CD70-deficiency in *Apoe*$^{-/-}$ mice induces a unique macrophage phenotype including markers of M1- (CD64, MHCII) and M2- (CD301, IL-10) differentiation. During *in vitro* experiments, M1 macrophages are induced by LPS whereas M2 macrophages are induced by IL-4. Furthermore, CD70-deficient BMDM from *Apoe*$^{-/-}$ mice produce less ROS and NO. Of note, ROS production is usually associated with function and activation of M1 macrophages, and both ROS and NO are key components of the antimicrobial machinery of M1 macrophages.[223] Interestingly, NO production can inhibit oxidative metabolism which is pivotal for M2 macrophage survival and function.[224] Typically, lower ROS production would constitute a characteristic situation of M2 macrophages featuring an increased oxidative consumption rate. These features again reflect a unique phenotype of CD70-deficient BMDM which are not clearly classifiable solely as M1 or M2 macrophages. Of note, M1 macrophages conduct an increased glycolytic metabolism and reduced mitochondrial respiratory activity, whereas M2 macrophages are typically characterized by a high mitochondrial oxidative phosphorylation and enhanced spare respiratory capacity. Whereas glycolytic metabolism induces a pro-inflammatory M1 macrophage phenotype, inhibition of glycolysis by applying 2-desoxyglucose reduces inflammatory cytokine production.[225, 226] Inhibition of fatty acid oxidation prevents M2 macrophage polarization thus suggesting that macrophage polarization is linked to their metabolism and influencing each other.[227] In our model, we observed similar glycolytic capacity but reduced OCR of CD70-deficient BMDM supporting their unique identity as observed by phenotypic marker expression. Their lowered metabolic fitness is paralleled by increased apoptotic potential.

4.4 *Cd70*$^{-/-}$ macrophages harbor reduced lipid clearing capacity leading to pronounced atherosclerosis.

Additionally, CD70-deficient BMDMs harbored reduced capacity to scavenge bacterial and modified lipid particles, probably due to reduced CD36 expression, an important

scavenger receptor mediating phagocytosis. This is accompanied by reduced expression of the cholesterol transporter ABCG1. Hence, CD70-deficient macrophages display reduced cholesterol efflux towards HDL, which is the main cholesterol acceptor interacting with ABCG1. Interestingly, CD70 deficiency did not alter ABCA1 expression and ABCA1-mediated cholesterol efflux to its acceptor ApoA1.

The role of ABCG1 in atherosclerosis is controversially discussed and can exert anti- or pro-atherogenic functions depending on the mouse model and the disease stage assessed. Reports demonstrated increased or unchanged susceptibility towards atherosclerosis in ABCG-1 deficient (*Abcg1*$^{-/-}$) mice in different mouse models.[228, 229] This appears stage-dependent since administering HFD to *Abcg1*$^{-/-}$*Ldlr*$^{-/-}$ mice for 10 weeks increases atherosclerosis whereas 12 weeks causes reduction in atherosclerotic burden.[230] Transplantation of *Abcg1*$^{-/-}$ bone marrow into *Apoe*$^{-/-}$- or *Ldlr*$^{-/-}$-recipient mice decreased atherosclerotic burden by enhanced apoptosis of macrophages.[231] Furthermore, macrophages from *Abcg1*$^{-/-}$ mice produce more ApoE which is paralleled by an increase in circulating ApoE in *Abcg1*$^{-/-}$*Ldlr*$^{-/-}$ bone marrow chimeric mice compared to controls.[232] These controversial findings seem only be partially applying to the macrophage phenotype observed in the present study, since the here described mice lack ApoE and reduced ABCG1 expression does not protect against atherosclerosis. However, the exact underlying mechanism why CD70 deficiency influences ABCG1 expression and ABCG1-mediated cholesterol efflux remains to be further investigated.

Reduced metabolic activity cannot be excluded to further negatively influence phagocytic activity of macrophages upon CD70 deficiency. A plethora of work attributes macrophages a major role in atherosclerosis.[233] Accordingly, reduced fitness or function of macrophages likely contributes to exacerbated atherosclerosis.

The aforementioned features of *Cd70*$^{-/-}$ macrophages suggest an impaired capacity disburdening the arterial wall from lipid deposits thus fostering atherosclerotic lesion formation. Indeed, in two models of atherosclerosis we corroborate the anti-atherogenic role of CD70. Mice receiving *Cd70*$^{-/-}$ bone marrow display a substantial increase in atherosclerotic lesion size and the majority of plaques are of an advanced phenotype. Similar results were obtained in 18-week-old *Cd70*$^{-/-}$*Apoe*$^{-/-}$ mice supporting the anti-atherogenic role of CD70. Furthermore, lesions from *Cd70*$^{-/-}$*Apoe*$^{-/-}$ mice are bigger, display lower cellularity and were scored as PIT being characterized by the accumulation of extracellular lipids recapitulating the reduced lipid handling capacity of macrophages observed *in vitro*. However, during the progression of atherosclerosis CD70-deficiency does not affect atherosclerotic burden in hyperlipidemic *Apoe*$^{-/-}$ mice anymore. It seems likely that during advanced stages of atherosclerosis macrophages

from *Cd70*$^{+/+}$*Apoe*$^{-/-}$ and *Cd70*$^{-/-}$*Apoe*$^{-/-}$ mice are equally dysfunctional in clearing lipid depositions in the arterial wall thus explaining similar atherosclerotic burden.

4.5 Tregs are moderately affected by CD70 deficiency depending on the mouse model.

Another important function of CD70 pertains to Treg development in the thymus. CD70 on mTECs or DC in the thymus ligates CD27 on developing Tregs and thus fosters generation of natural Tregs as demonstrated by aforementioned data and suggested by others.[156] In our study, we only observed a moderate decrease in splenic Tregs in hyperlipidemic *Cd70*$^{-/-}$*Apoe*$^{-/-}$ bone marrow chimeric mice. Moreover, these Tregs displayed lower expression of proliferative and anti-apoptotic markers, Ki67 and BCL-2, respectively. In the BM transplantation set-up, CD70 is not expressed by thymic DC but still expressed on mTECs and thus Treg development is only mildly if at all affected as shown by unchanged numbers of aortic Tregs compared to control mice. Thus, the role of CD70 in Treg development and function appears negligible in this model of atherosclerosis and altered Treg numbers are unlikely to underlie those effects of CD70-deficiency observed in the bone marrow transplantation model. However, global CD70 deficiency reduces Treg frequencies in the spleen at early and advanced stages of atherosclerosis. As we did not assess aortic Treg abundance in those mice, we cannot exclude reduced frequency of aortic Treg contributing to pronounced atherosclerosis in *Cd70*$^{-/-}$*Apoe*$^{-/-}$ mice.

4.6 CD70 deficiency fosters oxLDL-IgG production by B cells.

Besides the aforementioned immune cells, B cells might be affected by CD70 deficiency as they express CD70 upon activation and maturation.[141] Furthermore, B cells and subsets are implicated in atherogenesis.[213] Previous reports demonstrated a reduction in B cell responses and germinal center formation when CD70 was constitutively expressed on T cells or B cells.[153, 214] B cell frequencies influence Ig expression. However, we did not observe any profound changes in B cell abundance at various sites in *Cd70*$^{-/-}$*Apoe*$^{-/-}$ mice. However, blocking CD27/CD70 interactions with a monoclonal anti-CD70 antibody after infection with LCMV enhanced the expression of virus-neutralizing antibodies.[175] Indeed, CD70-deficient hyperlipidemic mice showed increased IgG2a concentrations which is elicited by Th1 cytokine responses and considered pro-atherogenic.[113] However, data from this experiment requires careful interpretation. The analyzed mouse models are derived from a C57BL6/J background which harbors expression of the *Igh1-b* allele thus not bearing the genetic information

for IgG2a (which rather pertains to Balb/c mice). C57BL6/J mice instead express the IgG2c isotype which has a 16% amino acid difference compared to the IgG2a subtype.[234] Thus, the here used commercially available bead assay detecting IgG2a might inadequately cross-react with the IgG2c subtype underestimating the actual abundance. Overall increased abundance of immunoglobulins is not necessarily affecting the presence of antigen-specific immunoglobulins. Indeed, oxLDL-reactive IgG, IgG1, and IgG2b subclasses were increased whereas levels of IgM remained unchanged in plasma of hyperlipidemic *Cd70*$^{-/-}$*Apoe*$^{-/-}$ compared to littermate control mice. IgG, IgG1 and, IgG2b are considered pro-atherogenic and produced by B2 cells. Depletion of B2 cells reduced the aforementioned athero-reactive Ig subclasses and mice were protected from atherosclerosis.[113] Natural B cells, such as B1a cells, are potent sources of the IgM subclass which is encoded in the germ line and not generated by Ig class switching and affinity maturation such as IgG subclasses. Mice deficient for IgM display exacerbated atherogenesis.[235] Overall, CD70 deficiency increases the abundance of circulating pro-atherogenic Ig subclasses which potentially contribute to exacerbated atherosclerosis. However, future studies need to address the exact contribution of increased atherosclerotic antigen-specific antibodies to increased atherosclerosis in *Cd70*$^{-/-}$*Apoe*$^{-/-}$ mice.

4.7 CD27/CD70 interactions moderately influence T cell memory.

Although CD27/CD70 interactions are pivotal for T cell memory generation, the reduction in memory T cells was age-dependent and affected only CD8 T cells. However, the general population might not reflect the behavior of antigen-specific T cells overall influenced by CD27 or CD70 deficiency. Only recently, potential antigens in atherosclerosis were identified being derived from peptides of ApoB-100 or LDL.[236, 237] These peptides could also be used to load tetramers or dextramers to identify antigen-specific T cells in atherosclerosis, which will help to further investigate the timing and interplay of factors expressed by athero-reactive T cells. Furthermore, the application of tetramers that are consisting of a Streptavidin-core complex to which up to 4 biotinylated MHCII-complexes displaying the antigen of interest will bind to, may help to unravel the fate of antigen-specific T cells in atherosclerosis. However, these experiments are beyond the scope of this thesis and currently exerted at collaborative partner sites.

4.8 Why does this work contribute to novelty to the understanding of CD27/CD70 in atherosclerosis?

So far, this is the first study addressing the implications of CD27 and CD70 signaling in atherosclerosis. Previous work demonstrated that transgenic expression of CD70 on B cells led to a CD27-driven increase in the pro-atherogenic Th1 subset.[206] Nevertheless, amelioration of atherosclerosis in that model was likely caused by increased apoptosis of pro-atherogenic Ly6C$^+$ monocytes and chronic stimulation of CD27 on T cells which ultimately led to a gradual loss of the naïve T cell pool and a profound reduction of B cells. Although pioneering in its approach, this study employed a very non-physiological B cell-restricted overexpression of CD70 which led to a severe patho-inflammatory phenotype. This transgenic system emphasizes a potential consequence of chronic and systemic CD27/CD70 engagement, but cannot predict the consequence of natural CD27/CD70 interactions in atherosclerosis.[206]

Currently only CD27 is known as interaction partner of CD70. Although this study demonstrates CD27 expression only on T cells in atherosclerotic aortas and CD70 expression mainly on macrophages the exact cell types and subsets interacting via CD27/CD70 with each other remain unidentified. Furthermore, intrinsic CD70 signaling has been described[153] and future studies have to address the requirement and cellular origin of a putative CD27 signal interacting with macrophage CD70. Hematopoietic stem cells express CD27 thus potentially representing the cellular source for interactions with CD70 on developing macrophages in the BMDM culture. In addition, the absence of CD70 might also alter the CD27 expressing cell which in turn affects functionality of the interaction partner.

4.9 Future perspectives

The role of the co-stimulatory dyad CD27/CD70 remained so far elusive. In the present work, we were able to demonstrate CD27 expression by T cells in atherosclerotic lesions whereas CD70 was predominantly expressed by macrophages. This is the first study comprehensively demonstrating the effects caused by CD27 or CD70 on atherosclerosis. Young mice deficient for either CD27 or CD70 developed aggravated atherosclerosis whereas established atherosclerotic lesions remained unaffected. Of note, deficiency of hematopoietic CD27 or CD70 promoted most significantly atherosclerosis suggesting leukocytes causing the underlying changes. However, different mechanisms were observed in CD27- or CD70-compound mutant mice.

CD27-deficient mice display promoted progression of atherosclerosis accompanied by increased macrophage content and larger necrotic cores. Furthermore, the

endothelium covering atherosclerotic lesions and atherosclerotic aortas from CD27 bone marrow chimeric mice displayed increased expression of pro-inflammatory cytokines (IL-1β, IL-6), adhesion molecules (ICAM-1, VCAM-1), and chemokines (CCL1), thus, further fueling atherosclerosis. Interestingly, the pronounced pro-atherogenic phenotype was accompanied by systemic and local reduction of anti-inflammatory Tregs. CD27-deficent Tregs were not impaired in their suppressive capacity suggesting the mere reduction in abundance being responsible for pronounced atherosclerosis in CD27-deficient mice. The reduced systemic abundance of Tregs in CD27-deficient mice is caused by enhanced apoptosis of developing Tregs in the thymus where Tregs need to receive signals via CD27 and CD70 expressed by DCs and mTECs.

Although CD70 bone marrow chimeric mice displayed aggravated atherosclerosis, the abundance of Tregs was only mildly affected, as mTECs still covered CD70 expression. Thus, other mechanisms are coming into play. Indeed, CD70-deficient mice harbor a substantial increase in oxLDL-specific antibodies that might contribute to atheroprogression. However, it is likely that the pro-atherosclerotic effect is caused by the phenotype of the CD70-deficient macrophages. These macrophages are metabolically less active, less inflammatory, and prone to cell death. Furthermore, they exhibit reduced scavenging capacity, turn less into foam cells, and possess reduced cholesterol efflux capacity. This all further substantiates the pro-inflammatory plaque environment based on the substantially reduced capacity to clear lipids from the atherosclerotic vessel wall.

Considering all these pro-inflammatory effects in atherosclerosis based on either CD27 or CD70 deficiency, it appears desirable to promote function of these molecules, particularly during the early stages of disease development. However, we observed increased expression of CD27 and CD70 in human atherosclerotic lesions classified as ruptured, possibly reflecting and anti-inflammatory response, or the mere presence of T-effector cells and macrophages which bear expression of CD27 and CD70. Ongoing clinical studies are targeting CD27 or CD70 in patients suffering from tumors using biologicals. A broad range of tumor cells express high levels of CD70, thus a neutralizing antibody might proof successful in patients with advanced malignancies.[238] CD70-expressing Tregs are contributing to tumor immune evasion and thus blocking them might be beneficial for the patient. [238] Furthermore, agonistic CD27 antibodies were designed to promote anti-tumor immunity by enhancing a cytotoxic CD8 T cell response.[203] However, therapeutic intervention agonistically modulating CD27 might also enhance the suppressive capacity of tumor-resident Tregs. Although this might enhance tumor immune evasion, the data available indicates a successful anti-tumor

immune reaction after CD27 stimulation overweighing the potential negative effects. Nonetheless, the present work demonstrates potential side-effects on the cardiovascular system by modulating CD27 and CD70. So far, no study addressed the potential cardiovascular side effects of these therapeutical antibodies. Additionally, these antibodies should be tested in animal models under hyperlipidemic conditions. Furthermore, the progression of other inflammatory diseases should be investigated in animal models that were systemically treated with CD70 blocking or agonistic CD27 antibodies. Overall, the philosophical question arises, whether a patient suffering from advanced tumor malignancies could gain expanded lifetime when undergoing a modifying CD27-CD70 therapy on the cost of accepting a higher risk for cardiovascular complications.

5 SUMMARY

Atherosclerosis is a chronic patho-inflammatory condition of the arterial vessel wall. Hypercholesterolemia is a major risk factor and lipid depositions in the vessel wall drive formation of the nascent atherosclerotic lesion. During pathogenesis innate and adaptive immune cells play distinct roles. Depending on their general function these cells either contribute to disease progression or counterbalance atherogenesis. T cells are part of the adaptive immune system and contribute to atherosclerosis in a subset-dependent manner. T cells need to receive proper T cell receptor stimulation and co-stimulatory signals provided by antigen presenting cells for full activation. The present thesis summarizes the first studies elucidating implications of the costimulatory CD27/CD70 dyad in atherosclerosis.

Expression of both co-stimulatory molecules is increased in human atherosclerotic lesions classified as ruptured, suggesting implicating of this dyad in this patho-inflammatory process. Whereas CD27 colocalizes with T cells in aortae of hyperlipidemic mice macrophages display highest CD70 expression suggesting interactions between both cell types via the CD27/CD70 axis in atherosclerotic lesions. However, deficiency for either molecule causes enhanced atherosclerosis in bone marrow chimeric mice and in young compound-mutant mice via different pathways.

Mice transplanted with CD27-deficient bone marrow display increased atherosclerotic lesion size and accelerated disease progression. Besides an increase in necrotic core and macrophage area, we observed that endothelial cells covering atherosclerotic lesions expressed more intercellular adhesion molecule 1 (ICAM-1) in absence of hematopoietic CD27. Concomitantly, aortae from CD27 bone marrow chimeric mice displayed increased expression of pro-inflammatory cytokines (interleukin-1β, interleukin-6), adhesion molecules (ICAM-1, vascular adhesion molecule 1), and chemokines (chemokine C-C motif ligand 1). This pro-inflammatory milieu further fuels inflammation in the atherosclerotic lesion and leads to pronounced atheroprogression. Similar results were observed in young CD27/Apoe-compound-deficient mice. In both mouse models of atherosclerosis, Treg frequencies were diminished systemically and locally in atheroma. CD27-deficent Tregs were not impaired in their suppressive capacity suggesting the mere reduction in abundance responsible for aggravated atherosclerosis in CD27-deficient mice. The reduced systemic abundance of Tregs in CD27-deficient mice is caused by enhanced apoptosis of developing Tregs in the thymus where Tregs need to receive signals via CD27 and CD70 expressed by dendritic cells and thymic medullary epithelial cells. At later stages of atherosclerosis,

effects mediated by CD27-deficiency appear negligible since neither atherosclerotic burden nor systemic Treg abundance changed compared to littermate control mice.

Multiple pathways seem to contribute to enhanced atherosclerosis in CD70 deficient mice. Macrophages derived from CD70-deficient mice are metabolically less active and prone to apoptosis. Furthermore, they are less competent in the uptake and efflux of oxidized lipoproteins. The reduced lipid clearance capacity contributes to exacerbated atherosclerotic lesion development. Indeed, CD70 bone marrow chimeric mice and young CD70/Apoe-compound mutant mice display larger and more advanced atherosclerotic lesions. Concomitant to an increase in necrotic core formation, the overall cellularity in atherosclerotic lesions is reduced suggesting that also increased lipid deposition accounts for increased lesion size. In CD70 bone marrow chimeric mice, Treg abundance is only mildly affected since developing Tregs can still receive CD27 signals via CD70 expressed on radioresistant medullary thymic epithelial cells. Thus, exacerbated atherosclerotic lesion formation in CD70-apoecompound-deficient mice is also affected by reduced Treg frequencies as observed in the spleen. Furthermore, increased abundance of oxidized low-density lipoprotein-reactive Ig subclasses might further lead to enhanced atheroprogression. However, at later stages of atherosclerosis effects mediated by CD70 become less important and CD70-deficient mice have similar atherosclerotic lesion size and phenotype compared to littermate controls.

In sum, CD27 and CD70 exert atheroprotective effects, especially during early phases of atherosclerosis.

6 ZUSAMMENFASSUNG

Atherosklerose ist durch eine chronische pathologische Entzündung in der arteriellen Gefäßwand charakterisiert. Hypercholesterinämie ist hierbei ein entscheidender Risikofaktor und die auftretenden Lipidablagerungen in der Gefäßwand fördern die Entstehung und Progression atherosklerotischer Läsionen. Immunzellen des angeborenen und adaptiven Immunsystems üben während der Pathogenese der Atherosklerose distinkte Funktionen aus. T Zellen als Protagonisten des adaptiven Immunsystems tragen entsprechend ihrer charakteristischen Eigenschaften positiv oder negativ zum Fortschreiten der Atherosklerose bei. Zur vollständigen Aktivierung benötigen T-Zellen Signale, welche durch den T-Zellrezeptor und kostimulatorische Moleküle vermittelt werden. Die hier vorliegende Arbeit beschreibt erstmalig die Auswirkung von Interaktionen der kostimulatorischen CD27/CD70 Achse auf Atherosklerose.

Sowohl CD27 als auch CD70 Expression sind erhöht in rupturierten humanen, atherosklerotischen Läsionen, was für eine entscheidende Rolle in diesem Prozess spricht. Das Fehlen von CD27 oder CD70 verschlimmert die Atherogenese in knochenmarkstransplantierten oder jungen, gendefizienten Mäusen, wobei jeweils unterschiedliche Mechanismen zu greifen scheinen.

Die Transplantation von CD27-defizientem Knochenmark vergrößert atherosklerotische Läsionen und führt zu einem fortgeschrittenen Plaque-Phänotyp im Vergleich mit Wildtyp-transplantierten *Apoe*$^{-/-}$ Empfängermäusen. Ebenso findet sich eine vermehrte Nekrose in den atherosklerotischen Läsionen, welche mit einer erhöhten Ansammlung von Makrophagen einhergeht. Weiterhin exprimieren die Endothelzellen der atherosklerotischen Läsion mehr *intercellular adhesion molecule 1* (ICAM-1), was auf eine erhöhte Infiltration von inflammatorischen Leukozyten in den atherosklerotischen Plaques hindeutet. Aorten von CD27-defizienten Knochenmarkschimären weisen zudem gesteigerte Expression der pro-inflammatorischen Zytokine Interleukin-1β, Interleukin-6, der Adhäsionsmoleküle ICAM-1, *vascular adhesion molecule 1*, und des Chemokins *chemokine C-C motif ligand 1* auf. Dieses pro-inflammatorische Milieu fördert die Rekrutierung von Immunzellen in die atherosklerotische Läsion und trägt zur verstärkten Pathogenese bei. Ähnliche Prozesse konnten in jungen CD27-defizienten Mäusen beobachtet werden. Hyperlipidämische Mäuse, denen CD27-defizientes Knochenmark transplantiert wurde oder die global CD27-defizient sind, weisen nicht nur eine systemische, sondern auch eine lokale Reduktion von regulatorischen T Zellen (Treg) auf. Diese CD27-defiziente Tregs besitzen dabei jedoch dieselbe suppressive Kapazität wie solche aus Wildtyp-Mäusen. Daher scheint die erhöhte

Atherogenese durch CD27 Defizienz eher in der systemischen und lokalen Reduktion der Anzahl von Tregs begründet zu sein. Fehlende Interaktion von CD27 auf den sich entwickelnden Tregs im Thymus mit dendritischen Zellen und medullären thymischen Epithelzellen, welche CD70 exprimieren, führt zu einer gesteigerten Apoptose der sich entwickelnden Tregs. Diese vermehrte Apoptose führt zur systemischen Treg Reduktion. In späteren Stadien der Atherosklerose scheinen die durch CD27-Defizienz vermittelten Effekte eine vernachlässigbare Rolle zu spielen, da sich weder Ausmaß der Atherosklerose noch systemische Abundanz der Tregs ändern.

Multiple Mechanismen tragen zur erhöhten Atheroprogression CD70-defizienter Mäuse bei. Makrophagen, denen CD70 fehlt, sind metabolisch weniger aktiv und weisen eine erhöhte Tendenz zur Apoptose auf. Überdies nehmen CD70-defiziente Makrophagen weniger oxidierte Lipoproteine auf und zeigen ein verringertes Potential Lipide auszuschleusen. Die reduzierte Kapazität Lipide aus der Gefäßwand zu entfernen kann zur erhöhten Atherogenese beitragen. Tatsächlich weisen CD70-defiziente Knochenmarkschimären und junge, CD70-defiziente Mäuse größere und fortgeschrittene atherosklerotische Plaques auf. Dies geht mit vermehrter Bildung eines nekrotischen Kerns einher, welcher eine erhebliche Reduktion der Zelldichte aufweist. Das Fortschreiten der atherosklerotischen Läsion in CD70-defizienten Mäusen scheint durch eine vermehrte Lipidablagerung verursacht zu sein und nicht durch einen erhöhten Kollagengehalt, welcher unverändert bleibt.

Mäuse, denen CD70-defizientes Knochenmark transplantiert wurde, weisen nur eine geringfügige systemische Reduktion der Tregs auf. Von den CD70-exprimierenden Zellen im Thymus tötet die Bestrahlung zwar dendritische Zellen ab, jedoch überleben bestrahlungs-resistente medulläre Epithelzellen. Diese können so nach wie vor ein CD70 Signal zur Verfügung stellen, wodurch, trotz CD70 Gendefizienz in hämatopoetischen Zellen, über CD27-CD70 Interaktionen wichtige Überlebenssignale an die sich entwickelnden Tregs vermittelt werden. Daher ist die verstärkte Atheroprogression in globalen CD70-defizienten Mäusen – neben den beschriebenen Effekten auf Makrophagen - auch einer Beeinträchtigung der Treg Entwicklung zuzuschreiben, welche sich in einer systemischen Reduktion dieser Zellen niederschlägt. Überdies führt die globale Defizienz an CD70 zu einer erhöhten Konzentration oxidierter *low-density lipoprotein* Partikel-reaktiver Antikörper im Plasma, welche als pro-atherogen gelten. Fortgeschrittene Stadien der Atherosklerose scheinen weder durch CD27- noch durch CD70-Defizienz beeinflusst zu sein.

Zusammenfassend weisen CD27 und CD70 atheroprotektive Mechanismen auf, die besonders in der frühen Phase der Atherosklerose von Bedeutung sind. In späteren

Phasen scheinen andere Mechanismen zu greifen und die Rolle von CD27 und CD70 rückt in den Hintergrund.

7 REFERENCES

1. Lozano R, Naghavi M, Foreman K*, et al.* Global and regional mortality from 235 causes of death for 20 age groups in 1990 and 2010: A systematic analysis for the global burden of disease study 2010. *Lancet*. 2012;380:2095-2128
2. Weber C, Noels H. Atherosclerosis: Current pathogenesis and therapeutic options. *Nat Med*. 2011;17:1410-1422
3. Kume N, Cybulsky MI, Gimbrone MA, Jr. Lysophosphatidylcholine, a component of atherogenic lipoproteins, induces mononuclear leukocyte adhesion molecules in cultured human and rabbit arterial endothelial cells. *J Clin Invest*. 1992;90:1138-1144
4. Eriksson EE, Xie X, Werr J*, et al.* Importance of primary capture and l-selectin-dependent secondary capture in leukocyte accumulation in inflammation and atherosclerosis in vivo. *J Exp Med*. 2001;194:205-218
5. Galkina E, Ley K. Immune and inflammatory mechanisms of atherosclerosis (*). *Annu Rev Immunol*. 2009;27:165-197
6. Panousis CG, Zuckerman SH. Interferon-gamma induces downregulation of tangier disease gene (atp-binding-cassette transporter 1) in macrophage-derived foam cells. *Arterioscler Thromb Vasc Biol*. 2000;20:1565-1571
7. Khovidhunkit W, Moser AH, Shigenaga JK*, et al.* Endotoxin down-regulates abcg5 and abcg8 in mouse liver and abca1 and abcg1 in j774 murine macrophages: Differential role of lxr. *J Lipid Res*. 2003;44:1728-1736
8. Legein B, Temmerman L, Biessen EA*, et al.* Inflammation and immune system interactions in atherosclerosis. *Cell Mol Life Sci*. 2013;70:3847-3869
9. Weber C, Zernecke A, Libby P. The multifaceted contributions of leukocyte subsets to atherosclerosis: Lessons from mouse models. *Nat Rev Immunol*. 2008;8:802-815
10. Steffel J, Luscher TF, Tanner FC. Tissue factor in cardiovascular diseases: Molecular mechanisms and clinical implications. *Circulation*. 2006;113:722-731
11. Tse K, Tse H, Sidney J*, et al.* T cells in atherosclerosis. *Int Immunol*. 2013;25:615-622
12. Daugherty A, Pure E, Delfel-Butteiger D*, et al.* The effects of total lymphocyte deficiency on the extent of atherosclerosis in apolipoprotein e-/- mice. *J Clin Invest*. 1997;100:1575-1580
13. Dansky HM, Charlton SA, Harper MM*, et al.* T and b lymphocytes play a minor role in atherosclerotic plaque formation in the apolipoprotein e-deficient mouse. *Proc Natl Acad Sci U S A*. 1997;94:4642-4646
14. Roselaar SE, Kakkanathu PX, Daugherty A. Lymphocyte populations in atherosclerotic lesions of apoe -/- and ldl receptor -/- mice. Decreasing density with disease progression. *Arterioscler Thromb Vasc Biol*. 1996;16:1013-1018
15. Zhou X, Robertson AK, Hjerpe C*, et al.* Adoptive transfer of cd4+ t cells reactive to modified low-density lipoprotein aggravates atherosclerosis. *Arterioscler Thromb Vasc Biol*. 2006;26:864-870
16. Elhage R, Gourdy P, Brouchet L*, et al.* Deleting tcr alpha beta+ or cd4+ t lymphocytes leads to opposite effects on site-specific atherosclerosis in female apolipoprotein e-deficient mice. *Am J Pathol*. 2004;165:2013-2018
17. Cochain C, Koch M, Chaudhari SM*, et al.* Cd8+ t cells regulate monopoiesis and circulating ly6c-high monocyte levels in atherosclerosis in mice. *Circ Res*. 2015;117:244-253
18. Kyaw T, Winship A, Tay C*, et al.* Cytotoxic and proinflammatory cd8+ t lymphocytes promote development of vulnerable atherosclerotic plaques in apoe-deficient mice. *Circulation*. 2013;127:1028-1039

19. Zhou J, Dimayuga PC, Zhao X, *et al.* Cd8(+)cd25(+) t cells reduce atherosclerosis in apoe(-/-) mice. *Biochem Biophys Res Commun*. 2014;443:864-870
20. Khallou-Laschet J, Caligiuri G, Groyer E, *et al.* The proatherogenic role of t cells requires cell division and is dependent on the stage of the disease. *Arterioscler Thromb Vasc Biol*. 2006;26:353-358
21. Paulsson G, Zhou X, Tornquist E, *et al.* Oligoclonal t cell expansions in atherosclerotic lesions of apolipoprotein e-deficient mice. *Arterioscler Thromb Vasc Biol*. 2000;20:10-17
22. Jonasson L, Holm J, Skalli O, *et al.* Expression of class ii transplantation antigen on vascular smooth muscle cells in human atherosclerosis. *J Clin Invest*. 1985;76:125-131
23. Tse K, Gonen A, Sidney J, *et al.* Atheroprotective vaccination with mhc-ii restricted peptides from apob-100. *Front Immunol*. 2013;4:493
24. Miller YI, Choi SH, Wiesner P, *et al.* Oxidation-specific epitopes are danger-associated molecular patterns recognized by pattern recognition receptors of innate immunity. *Circ Res*. 2011;108:235-248
25. Li J, McArdle S, Gholami A, *et al.* Ccr5+t-bet+foxp3+ effector cd4 t cells drive atherosclerosis. *Circ Res*. 2016;118:1540-1552
26. Butcher M, McGary C, Galkina E. The pro-atherosclerotic milieu promotes the conversion of murine t regulatory cells to a spectrum of foxp3+ifnγ+ t cell phenotypes. *J Immunol*. 2014;vol.192 (1 Supplement) 190.9
27. Szabo SJ, Kim ST, Costa GL, *et al.* A novel transcription factor, t-bet, directs th1 lineage commitment. *Cell*. 2000;100:655-669
28. Buono C, Binder CJ, Stavrakis G, *et al.* T-bet deficiency reduces atherosclerosis and alters plaque antigen-specific immune responses. *Proc Natl Acad Sci U S A*. 2005;102:1596-1601
29. Gupta S, Pablo AM, Jiang X, *et al.* Ifn-gamma potentiates atherosclerosis in apoe knock-out mice. *J Clin Invest*. 1997;99:2752-2761
30. Whitman SC, Ravisankar P, Daugherty A. Ifn-gamma deficiency exerts gender-specific effects on atherogenesis in apolipoprotein e-/- mice. *J Interferon Cytokine Res*. 2002;22:661-670
31. McLaren JE, Ramji DP. Interferon gamma: A master regulator of atherosclerosis. *Cytokine Growth Factor Rev*. 2009;20:125-135
32. Tedgui A, Mallat Z. Cytokines in atherosclerosis: Pathogenic and regulatory pathways. *Physiol Rev*. 2006;86:515-581
33. Davenport P, Tipping PG. The role of interleukin-4 and interleukin-12 in the progression of atherosclerosis in apolipoprotein e-deficient mice. *Am J Pathol*. 2003;163:1117-1125
34. Gerdes N, Sukhova GK, Libby P, *et al.* Expression of interleukin (il)-18 and functional il-18 receptor on human vascular endothelial cells, smooth muscle cells, and macrophages: Implications for atherogenesis. *J Exp Med*. 2002;195:245-257
35. Okamura H, Tsutsui H, Kashiwamura S, *et al.* Interleukin-18: A novel cytokine that augments both innate and acquired immunity. *Adv Immunol*. 1998;70:281-312
36. Puren AJ, Fantuzzi G, Gu Y, *et al.* Interleukin-18 (ifngamma-inducing factor) induces il-8 and il-1beta via tnfalpha production from non-cd14+ human blood mononuclear cells. *J Clin Invest*. 1998;101:711-721
37. King VL, Szilvassy SJ, Daugherty A. Interleukin-4 deficiency decreases atherosclerotic lesion formation in a site-specific manner in female ldl receptor-/- mice. *Arterioscler Thromb Vasc Biol*. 2002;22:456-461
38. Binder CJ, Hartvigsen K, Chang MK, *et al.* Il-5 links adaptive and natural immunity specific for epitopes of oxidized ldl and protects from atherosclerosis. *J Clin Invest*. 2004;114:427-437

39. Cardilo-Reis L, Gruber S, Schreier SM*, et al.* Interleukin-13 protects from atherosclerosis and modulates plaque composition by skewing the macrophage phenotype. *EMBO Mol Med*. 2012;4:1072-1086
40. Robertson AK, Hansson GK. T cells in atherogenesis: For better or for worse? *Arterioscler Thromb Vasc Biol*. 2006;26:2421-2432
41. Ait-Oufella H, Taleb S, Mallat Z*, et al.* Recent advances on the role of cytokines in atherosclerosis. *Arterioscler Thromb Vasc Biol*. 2011;31:969-979
42. Zhao XN, Li YN, Wang YT. Interleukin-4 regulates macrophage polarization via the mapk signaling pathway to protect against atherosclerosis. *Genet Mol Res*. 2016;15
43. Zhou X, Paulsson G, Stemme S*, et al.* Hypercholesterolemia is associated with a t helper (th) 1/th2 switch of the autoimmune response in atherosclerotic apo e-knockout mice. *J Clin Invest*. 1998;101:1717-1725
44. Schulte S, Sukhova GK, Libby P. Genetically programmed biases in th1 and th2 immune responses modulate atherogenesis. *Am J Pathol*. 2008;172:1500-1508
45. Stockinger B, Veldhoen M. Differentiation and function of th17 t cells. *Curr Opin Immunol*. 2007;19:281-286
46. Weaver CT, Hatton RD, Mangan PR*, et al.* Il-17 family cytokines and the expanding diversity of effector t cell lineages. *Annu Rev Immunol*. 2007;25:821-852
47. Ouyang W, Kolls JK, Zheng Y. The biological functions of t helper 17 cell effector cytokines in inflammation. *Immunity*. 2008;28:454-467
48. Dong C. Diversification of t-helper-cell lineages: Finding the family root of il-17-producing cells. *Nat Rev Immunol*. 2006;6:329-333
49. Taleb S, Tedgui A, Mallat Z. Il-17 and th17 cells in atherosclerosis: Subtle and contextual roles. *Arterioscler Thromb Vasc Biol*. 2015;35:258-264
50. Korn T, Bettelli E, Oukka M*, et al.* Il-17 and th17 cells. *Annu Rev Immunol*. 2009;27:485-517
51. Eid RE, Rao DA, Zhou J*, et al.* Interleukin-17 and interferon-gamma are produced concomitantly by human coronary artery-infiltrating t cells and act synergistically on vascular smooth muscle cells. *Circulation*. 2009;119:1424-1432
52. Erbel C, Chen L, Bea F*, et al.* Inhibition of il-17a attenuates atherosclerotic lesion development in apoe-deficient mice. *J Immunol*. 2009;183:8167-8175
53. Smith E, Prasad KM, Butcher M*, et al.* Blockade of interleukin-17a results in reduced atherosclerosis in apolipoprotein e-deficient mice. *Circulation*. 2010;121:1746-1755
54. Taleb S, Romain M, Ramkhelawon B*, et al.* Loss of socs3 expression in t cells reveals a regulatory role for interleukin-17 in atherosclerosis. *J Exp Med*. 2009;206:2067-2077
55. Gistera A, Robertson AK, Andersson J*, et al.* Transforming growth factor-beta signaling in t cells promotes stabilization of atherosclerotic plaques through an interleukin-17-dependent pathway. *Sci Transl Med*. 2013;5:196ra100
56. Josefowicz SZ, Lu LF, Rudensky AY. Regulatory t cells: Mechanisms of differentiation and function. *Annu Rev Immunol*. 2012;30:531-564
57. Klein L, Jovanovic K. Regulatory t cell lineage commitment in the thymus. *Semin Immunol*. 2011;23:401-409
58. Klein L, Kyewski B, Allen PM*, et al.* Positive and negative selection of the t cell repertoire: What thymocytes see (and don't see). *Nat Rev Immunol*. 2014;14:377-391
59. Weiss JM, Bilate AM, Gobert M*, et al.* Neuropilin 1 is expressed on thymus-derived natural regulatory t cells, but not mucosa-generated induced foxp3+ t reg cells. *J Exp Med*. 2012;209:1723-1742, S1721
60. Gottschalk RA, Corse E, Allison JP. Expression of helios in peripherally induced foxp3+ regulatory t cells. *J Immunol*. 2012;188:976-980

61. Milpied P, Renand A, Bruneau J, *et al.* Neuropilin-1 is not a marker of human foxp3+ treg. *Eur J Immunol*. 2009;39:1466-1471
62. Spitz C, Winkels H, Burger C, *et al.* Regulatory t cells in atherosclerosis: Critical immune regulatory function and therapeutic potential. *Cell Mol Life Sci*. 2016;73:901-922
63. Paust S, Lu L, McCarty N, *et al.* Engagement of b7 on effector t cells by regulatory t cells prevents autoimmune disease. *Proc Natl Acad Sci U S A*. 2004;101:10398-10403
64. Qureshi OS, Zheng Y, Nakamura K, *et al.* Trans-endocytosis of cd80 and cd86: A molecular basis for the cell-extrinsic function of ctla-4. *Science*. 2011;332:600-603
65. Cao X, Cai SF, Fehniger TA, *et al.* Granzyme b and perforin are important for regulatory t cell-mediated suppression of tumor clearance. *Immunity*. 2007;27:635-646
66. Sakaguchi S, Yamaguchi T, Nomura T, *et al.* Regulatory t cells and immune tolerance. *Cell*. 2008;133:775-787
67. Ait-Oufella H, Salomon BL, Potteaux S, *et al.* Natural regulatory t cells control the development of atherosclerosis in mice. *Nat Med*. 2006;12:178-180
68. Buono C, Pang H, Uchida Y, *et al.* B7-1/b7-2 costimulation regulates plaque antigen-specific t-cell responses and atherogenesis in low-density lipoprotein receptor-deficient mice. *Circulation*. 2004;109:2009-2015
69. Driesen J, Popov A, Schultze JL. Cd25 as an immune regulatory molecule expressed on myeloid dendritic cells. *Immunobiology*. 2008;213:849-858
70. Mor A, Planer D, Luboshits G, *et al.* Role of naturally occurring cd4+ cd25+ regulatory t cells in experimental atherosclerosis. *Arterioscler Thromb Vasc Biol*. 2007;27:893-900
71. Klingenberg R, Gerdes N, Badeau RM, *et al.* Depletion of foxp3+ regulatory t cells promotes hypercholesterolemia and atherosclerosis. *J Clin Invest*. 2013;123:1323-1334
72. Lutgens E, Gijbels M, Smook M, *et al.* Transforming growth factor-beta mediates balance between inflammation and fibrosis during plaque progression. *Arterioscler Thromb Vasc Biol*. 2002;22:975-982
73. Mallat Z, Gojova A, Marchiol-Fournigault C, *et al.* Inhibition of transforming growth factor-beta signaling accelerates atherosclerosis and induces an unstable plaque phenotype in mice. *Circ Res*. 2001;89:930-934
74. Robertson AK, Rudling M, Zhou X, *et al.* Disruption of tgf-beta signaling in t cells accelerates atherosclerosis. *J Clin Invest*. 2003;112:1342-1350
75. Lievens D, Habets KL, Robertson AK, *et al.* Abrogated transforming growth factor beta receptor ii (tgfbetarii) signalling in dendritic cells promotes immune reactivity of t cells resulting in enhanced atherosclerosis. *Eur Heart J*. 2013;34:3717-3727
76. Caligiuri G, Rudling M, Ollivier V, *et al.* Interleukin-10 deficiency increases atherosclerosis, thrombosis, and low-density lipoproteins in apolipoprotein e knockout mice. *Mol Med*. 2003;9:10-17
77. Mallat Z, Besnard S, Duriez M, *et al.* Protective role of interleukin-10 in atherosclerosis. *Circ Res*. 1999;85:e17-24
78. Pinderski LJ, Fischbein MP, Subbanagounder G, *et al.* Overexpression of interleukin-10 by activated t lymphocytes inhibits atherosclerosis in ldl receptor-deficient mice by altering lymphocyte and macrophage phenotypes. *Circ Res*. 2002;90:1064-1071
79. Potekhina AV, Pylaeva E, Provatorov S, *et al.* Treg/th17 balance in stable cad patients with different stages of coronary atherosclerosis. *Atherosclerosis*. 2015;238:17-21
80. Maganto-Garcia E, Tarrio ML, Grabie N, *et al.* Dynamic changes in regulatory t cells are linked to levels of diet-induced hypercholesterolemia. *Circulation*. 2011;124:185-195

81. Peled M, Fisher EA. Dynamic aspects of macrophage polarization during atherosclerosis progression and regression. *Front Immunol*. 2014;5:579
82. Tacke F, Alvarez D, Kaplan TJ*, et al.* Monocyte subsets differentially employ ccr2, ccr5, and cx3cr1 to accumulate within atherosclerotic plaques. *J Clin Invest*. 2007;117:185-194
83. Robbins CS, Hilgendorf I, Weber GF*, et al.* Local proliferation dominates lesional macrophage accumulation in atherosclerosis. *Nat Med*. 2013;19:1166-1172
84. Lutgens E, Daemen M, Kockx M*, et al.* Atherosclerosis in apoe*3-leiden transgenic mice: From proliferative to atheromatous stage. *Circulation*. 1999;99:276-283
85. Moore KJ, Freeman MW. Scavenger receptors in atherosclerosis: Beyond lipid uptake. *Arterioscler Thromb Vasc Biol*. 2006;26:1702-1711
86. Kzhyshkowska J, Neyen C, Gordon S. Role of macrophage scavenger receptors in atherosclerosis. *Immunobiology*. 2012;217:492-502
87. Manning-Tobin JJ, Moore KJ, Seimon TA*, et al.* Loss of sr-a and cd36 activity reduces atherosclerotic lesion complexity without abrogating foam cell formation in hyperlipidemic mice. *Arterioscler Thromb Vasc Biol*. 2009;29:19-26
88. Maxfield FR, Tabas I. Role of cholesterol and lipid organization in disease. *Nature*. 2005;438:612-621
89. Kunjathoor VV, Febbraio M, Podrez EA*, et al.* Scavenger receptors class a-i/ii and cd36 are the principal receptors responsible for the uptake of modified low density lipoprotein leading to lipid loading in macrophages. *J Biol Chem*. 2002;277:49982-49988
90. Chavez-Sanchez L, Garza-Reyes MG, Espinosa-Luna JE*, et al.* The role of tlr2, tlr4 and cd36 in macrophage activation and foam cell formation in response to oxldl in humans. *Hum Immunol*. 2014;75:322-329
91. Curtiss LK, Tobias PS. Emerging role of toll-like receptors in atherosclerosis. *J Lipid Res*. 2009;50 Suppl:S340-345
92. Yvan-Charvet L, Wang N, Tall AR. Role of hdl, abca1, and abcg1 transporters in cholesterol efflux and immune responses. *Arterioscler Thromb Vasc Biol*. 2010;30:139-143
93. Yvan-Charvet L, Welch C, Pagler TA*, et al.* Increased inflammatory gene expression in abc transporter-deficient macrophages: Free cholesterol accumulation, increased signaling via toll-like receptors, and neutrophil infiltration of atherosclerotic lesions. *Circulation*. 2008;118:1837-1847
94. Zhu X, Owen JS, Wilson MD*, et al.* Macrophage abca1 reduces myd88-dependent toll-like receptor trafficking to lipid rafts by reduction of lipid raft cholesterol. *J Lipid Res*. 2010;51:3196-3206
95. Feng B, Yao PM, Li Y*, et al.* The endoplasmic reticulum is the site of cholesterol-induced cytotoxicity in macrophages. *Nat Cell Biol*. 2003;5:781-792
96. Tabas I. Consequences and therapeutic implications of macrophage apoptosis in atherosclerosis: The importance of lesion stage and phagocytic efficiency. *Arterioscler Thromb Vasc Biol*. 2005;25:2255-2264
97. Duewell P, Kono H, Rayner KJ*, et al.* Nlrp3 inflammasomes are required for atherogenesis and activated by cholesterol crystals. *Nature*. 2010;464:1357-1361
98. Kirii H, Niwa T, Yamada Y*, et al.* Lack of interleukin-1beta decreases the severity of atherosclerosis in apoe-deficient mice. *Arterioscler Thromb Vasc Biol*. 2003;23:656-660
99. Martinez FO, Gordon S. The m1 and m2 paradigm of macrophage activation: Time for reassessment. *F1000Prime Rep*. 2014;6:13
100. Van den Bossche J, Baardman J, de Winther MP. Metabolic characterization of polarized m1 and m2 bone marrow-derived macrophages using real-time extracellular flux analysis. *J Vis Exp*. 2015

101. Hanna RN, Shaked I, Hubbeling HG*, et al.* Nr4a1 (nur77) deletion polarizes macrophages toward an inflammatory phenotype and increases atherosclerosis. *Circ Res*. 2012;110:416-427
102. Maitra U, Parks JS, Li L. An innate immunity signaling process suppresses macrophage abca1 expression through irak-1-mediated downregulation of retinoic acid receptor alpha and nfatc2. *Mol Cell Biol*. 2009;29:5989-5997
103. Tiemessen MM, Jagger AL, Evans HG*, et al.* Cd4+cd25+foxp3+ regulatory t cells induce alternative activation of human monocytes/macrophages. *Proc Natl Acad Sci U S A*. 2007;104:19446-19451
104. Gong D, Shi W, Yi SJ*, et al.* Tgfbeta signaling plays a critical role in promoting alternative macrophage activation. *BMC Immunol*. 2012;13:31
105. Feig JE, Parathath S, Rong JX*, et al.* Reversal of hyperlipidemia with a genetic switch favorably affects the content and inflammatory state of macrophages in atherosclerotic plaques. *Circulation*. 2011;123:989-998
106. Stoger JL, Gijbels MJ, van der Velden S*, et al.* Distribution of macrophage polarization markers in human atherosclerosis. *Atherosclerosis*. 2012;225:461-468
107. Khallou-Laschet J, Varthaman A, Fornasa G*, et al.* Macrophage plasticity in experimental atherosclerosis. *PLoS One*. 2010;5:e8852
108. Galkina E, Kadl A, Sanders J*, et al.* Lymphocyte recruitment into the aortic wall before and during development of atherosclerosis is partially l-selectin dependent. *J Exp Med*. 2006;203:1273-1282
109. Mohanta SK, Yin C, Peng L*, et al.* Artery tertiary lymphoid organs contribute to innate and adaptive immune responses in advanced mouse atherosclerosis. *Circ Res*. 2014;114:1772-1787
110. Yla-Herttuala S, Palinski W, Butler SW*, et al.* Rabbit and human atherosclerotic lesions contain igg that recognizes epitopes of oxidized ldl. *Arterioscler Thromb*. 1994;14:32-40
111. Caligiuri G, Nicoletti A, Poirier B*, et al.* Protective immunity against atherosclerosis carried by b cells of hypercholesterolemic mice. *J Clin Invest*. 2002;109:745-753
112. Major AS, Fazio S, Linton MF. B-lymphocyte deficiency increases atherosclerosis in ldl receptor-null mice. *Arterioscler Thromb Vasc Biol*. 2002;22:1892-1898
113. Ait-Oufella H, Herbin O, Bouaziz JD*, et al.* B cell depletion reduces the development of atherosclerosis in mice. *J Exp Med*. 2010;207:1579-1587
114. Kyaw T, Tay C, Khan A*, et al.* Conventional b2 b cell depletion ameliorates whereas its adoptive transfer aggravates atherosclerosis. *J Immunol*. 2010;185:4410-4419
115. Baumgarth N. The double life of a b-1 cell: Self-reactivity selects for protective effector functions. *Nat Rev Immunol*. 2011;11:34-46
116. Montecino-Rodriguez E, Dorshkind K. New perspectives in b-1 b cell development and function. *Trends Immunol*. 2006;27:428-433
117. Tsiantoulas D, Diehl CJ, Witztum JL*, et al.* B cells and humoral immunity in atherosclerosis. *Circ Res*. 2014;114:1743-1756
118. Sage AP, Nus M, Baker LL*, et al.* Regulatory b cell-specific interleukin-10 is dispensable for atherosclerosis development in mice. *Arterioscler Thromb Vasc Biol*. 2015;35:1770-1773
119. Hilgendorf I, Theurl I, Gerhardt LM*, et al.* Innate response activator b cells aggravate atherosclerosis by stimulating t helper-1 adaptive immunity. *Circulation*. 2014;129:1677-1687
120. Karvonen J, Paivansalo M, Kesaniemi YA*, et al.* Immunoglobulin m type of autoantibodies to oxidized low-density lipoprotein has an inverse relation to carotid artery atherosclerosis. *Circulation*. 2003;108:2107-2112

121. Tsimikas S, Brilakis ES, Lennon RJ*, et al.* Relationship of igg and igm autoantibodies to oxidized low density lipoprotein with coronary artery disease and cardiovascular events. *J Lipid Res*. 2007;48:425-433
122. Ehrenstein MR, Notley CA. The importance of natural igm: Scavenger, protector and regulator. *Nat Rev Immunol*. 2010;10:778-786
123. Kyaw T, Tay C, Krishnamurthi S*, et al.* B1a b lymphocytes are atheroprotective by secreting natural igm that increases igm deposits and reduces necrotic cores in atherosclerotic lesions. *Circ Res*. 2011;109:830-840
124. Boullier A, Gillotte KL, Horkko S*, et al.* The binding of oxidized low density lipoprotein to mouse cd36 is mediated in part by oxidized phospholipids that are associated with both the lipid and protein moieties of the lipoprotein. *J Biol Chem*. 2000;275:9163-9169
125. Nimmerjahn F, Ravetch JV. Fcgamma receptors as regulators of immune responses. *Nat Rev Immunol*. 2008;8:34-47
126. Frank MM, Miletic VD, Jiang H. Immunoglobulin in the control of complement action. *Immunol Res*. 2000;22:137-146
127. Lichtman AH, Binder CJ, Tsimikas S*, et al.* Adaptive immunity in atherogenesis: New insights and therapeutic approaches. *J Clin Invest*. 2013;123:27-36
128. Afek A, George J, Gilburd B*, et al.* Immunization of low-density lipoprotein receptor deficient (ldl-rd) mice with heat shock protein 65 (hsp-65) promotes early atherosclerosis. *J Autoimmun*. 2000;14:115-121
129. Schett G, Xu Q, Amberger A*, et al.* Autoantibodies against heat shock protein 60 mediate endothelial cytotoxicity. *J Clin Invest*. 1995;96:2569-2577
130. Zhou X, Caligiuri G, Hamsten A*, et al.* Ldl immunization induces t-cell-dependent antibody formation and protection against atherosclerosis. *Arterioscler Thromb Vasc Biol*. 2001;21:108-114
131. Freigang S, Horkko S, Miller E*, et al.* Immunization of ldl receptor-deficient mice with homologous malondialdehyde-modified and native ldl reduces progression of atherosclerosis by mechanisms other than induction of high titers of antibodies to oxidative neoepitopes. *Arterioscler Thromb Vasc Biol*. 1998;18:1972-1982
132. Schiopu A, Bengtsson J, Soderberg I*, et al.* Recombinant human antibodies against aldehyde-modified apolipoprotein b-100 peptide sequences inhibit atherosclerosis. *Circulation*. 2004;110:2047-2052
133. Tsimikas S, Miyanohara A, Hartvigsen K*, et al.* Human oxidation-specific antibodies reduce foam cell formation and atherosclerosis progression. *J Am Coll Cardiol*. 2011;58:1715-1727
134. Wang J, Cheng X, Xiang MX*, et al.* Ige stimulates human and mouse arterial cell apoptosis and cytokine expression and promotes atherogenesis in apoe-/- mice. *J Clin Invest*. 2011;121:3564-3577
135. Muscari A, Bozzoli C, Gerratana C*, et al.* Association of serum iga and c4 with severe atherosclerosis. *Atherosclerosis*. 1988;74:179-186
136. Muscari A, Bozzoli C, Puddu GM*, et al.* Increased serum iga levels in subjects with previous myocardial infarction or other major ischemic events. *Cardiology*. 1993;83:383-389
137. Tesselaar K, Gravestein LA, van Schijndel GM*, et al.* Characterization of murine cd70, the ligand of the tnf receptor family member cd27. *J Immunol*. 1997;159:4959-4965
138. Gravestein LA, Blom B, Nolten LA*, et al.* Cloning and expression of murine cd27: Comparison with 4-1bb, another lymphocyte-specific member of the nerve growth factor receptor family. *Eur J Immunol*. 1993;23:943-950
139. Borst J, Hendriks J, Xiao Y. Cd27 and cd70 in t cell and b cell activation. *Curr Opin Immunol*. 2005;17:275-281
140. Hendriks J, Xiao Y, Rossen JW*, et al.* During viral infection of the respiratory tract, cd27, 4-1bb, and ox40 collectively determine formation of cd8+ memory t

cells and their capacity for secondary expansion. *J Immunol*. 2005;175:1665-1676
141. Tesselaar K, Xiao Y, Arens R*, et al.* Expression of the murine cd27 ligand cd70 in vitro and in vivo. *J Immunol*. 2003;170:33-40
142. Laouar A, Haridas V, Vargas D*, et al.* Cd70+ antigen-presenting cells control the proliferation and differentiation of t cells in the intestinal mucosa. *Nat Immunol*. 2005;6:698-706
143. Kashii Y, Giorda R, Herberman RB*, et al.* Constitutive expression and role of the tnf family ligands in apoptotic killing of tumor cells by human nk cells. *J Immunol*. 1999;163:5358-5366
144. Sanchez PJ, McWilliams JA, Haluszczak C*, et al.* Combined tlr/cd40 stimulation mediates potent cellular immunity by regulating dendritic cell expression of cd70 in vivo. *J Immunol*. 2007;178:1564-1572
145. Wherry EJ, Teichgraber V, Becker TC*, et al.* Lineage relationship and protective immunity of memory cd8 t cell subsets. *Nat Immunol*. 2003;4:225-234
146. Loenen WA, De Vries E, Gravestein LA*, et al.* The cd27 membrane receptor, a lymphocyte-specific member of the nerve growth factor receptor family, gives rise to a soluble form by protein processing that does not involve receptor endocytosis. *Eur J Immunol*. 1992;22:447-455
147. Kato K, Chu P, Takahashi S*, et al.* Metalloprotease inhibitors block release of soluble cd27 and enhance the immune stimulatory activity of chronic lymphocytic leukemia cells. *Exp Hematol*. 2007;35:434-442
148. Ramakrishnan P, Wang W, Wallach D. Receptor-specific signaling for both the alternative and the canonical nf-kappab activation pathways by nf-kappab-inducing kinase. *Immunity*. 2004;21:477-489
149. Nakano H, Sakon S, Koseki H*, et al.* Targeted disruption of traf5 gene causes defects in cd40- and cd27-mediated lymphocyte activation. *Proc Natl Acad Sci U S A*. 1999;96:9803-9808
150. Gravestein LA, Amsen D, Boes M*, et al.* The tnf receptor family member cd27 signals to jun n-terminal kinase via traf-2. *Eur J Immunol*. 1998;28:2208-2216
151. Prasad KV, Ao Z, Yoon Y*, et al.* Cd27, a member of the tumor necrosis factor receptor family, induces apoptosis and binds to siva, a proapoptotic protein. *Proc Natl Acad Sci U S A*. 1997;94:6346-6351
152. Py B, Slomianny C, Auberger P*, et al.* Siva-1 and an alternative splice form lacking the death domain, siva-2, similarly induce apoptosis in t lymphocytes via a caspase-dependent mitochondrial pathway. *J Immunol*. 2004;172:4008-4017
153. Arens R, Nolte MA, Tesselaar K*, et al.* Signaling through cd70 regulates b cell activation and igg production. *J Immunol*. 2004;173:3901-3908
154. Huang J, Jochems C, Anderson AM*, et al.* Soluble cd27-pool in humans may contribute to t cell activation and tumor immunity. *J Immunol*. 2013;190:6250-6258
155. Hendriks J, Gravestein LA, Tesselaar K*, et al.* Cd27 is required for generation and long-term maintenance of t cell immunity. *Nat Immunol*. 2000;1:433-440
156. Coquet JM, Ribot JC, Babala N*, et al.* Epithelial and dendritic cells in the thymic medulla promote cd4+foxp3+ regulatory t cell development via the cd27-cd70 pathway. *J Exp Med*. 2013;210:715-728
157. van Oosterwijk MF, Juwana H, Arens R*, et al.* Cd27-cd70 interactions sensitise naive cd4+ t cells for il-12-induced th1 cell development. *Int Immunol*. 2007;19:713-718
158. Hintzen RQ, Lens SM, Lammers K*, et al.* Engagement of cd27 with its ligand cd70 provides a second signal for t cell activation. *J Immunol*. 1995;154:2612-2623
159. Stuhler G, Zobywalski A, Grunebach F*, et al.* Immune regulatory loops determine productive interactions within human t lymphocyte-dendritic cell clusters. *Proc Natl Acad Sci U S A*. 1999;96:1532-1535

160. Peperzak V, Xiao Y, Veraar EA, *et al.* Cd27 sustains survival of ctls in virus-infected nonlymphoid tissue in mice by inducing autocrine il-2 production. *J Clin Invest*. 2010;120:168-178
161. Peperzak V, Veraar EA, Xiao Y, *et al.* Cd8+ t cells produce the chemokine cxcl10 in response to cd27/cd70 costimulation to promote generation of the cd8+ effector t cell pool. *J Immunol*. 2013;191:3025-3036
162. Arens R, Tesselaar K, Baars PA, *et al.* Constitutive cd27/cd70 interaction induces expansion of effector-type t cells and results in ifngamma-mediated b cell depletion. *Immunity*. 2001;15:801-812
163. Tesselaar K, Arens R, van Schijndel GM, *et al.* Lethal t cell immunodeficiency induced by chronic costimulation via cd27-cd70 interactions. *Nat Immunol*. 2003;4:49-54
164. Lens SM, Drillenburg P, den Drijver BF, *et al.* Aberrant expression and reverse signalling of cd70 on malignant b cells. *Br J Haematol*. 1999;106:491-503
165. Nolte MA, van Olffen RW, van Gisbergen KP, *et al.* Timing and tuning of cd27-cd70 interactions: The impact of signal strength in setting the balance between adaptive responses and immunopathology. *Immunol Rev*. 2009;229:216-231
166. Kobata T, Jacquot S, Kozlowski S, *et al.* Cd27-cd70 interactions regulate b-cell activation by t cells. *Proc Natl Acad Sci U S A*. 1995;92:11249-11253
167. Xiao Y, Hendriks J, Langerak P, *et al.* Cd27 is acquired by primed b cells at the centroblast stage and promotes germinal center formation. *J Immunol*. 2004;172:7432-7441
168. Jacquot S, Kobata T, Iwata S, *et al.* Cd154/cd40 and cd70/cd27 interactions have different and sequential functions in t cell-dependent b cell responses: Enhancement of plasma cell differentiation by cd27 signaling. *J Immunol*. 1997;159:2652-2657
169. Agematsu K, Kobata T, Yang FC, *et al.* Cd27/cd70 interaction directly drives b cell igg and igm synthesis. *Eur J Immunol*. 1995;25:2825-2829
170. Agematsu K, Nagumo H, Oguchi Y, *et al.* Generation of plasma cells from peripheral blood memory b cells: Synergistic effect of interleukin-10 and cd27/cd70 interaction. *Blood*. 1998;91:173-180
171. van Montfrans JM, Hoepelman AI, Otto S, *et al.* Cd27 deficiency is associated with combined immunodeficiency and persistent symptomatic ebv viremia. *J Allergy Clin Immunol*. 2012;129:787-793 e786
172. Salzer E, Daschkey S, Choo S, *et al.* Combined immunodeficiency with life-threatening ebv-associated lymphoproliferative disorder in patients lacking functional cd27. *Haematologica*. 2013;98:473-478
173. Alkhairy OK, Perez-Becker R, Driessen GJ, *et al.* Novel mutations in tnfrsf7/cd27: Clinical, immunologic, and genetic characterization of human cd27 deficiency. *J Allergy Clin Immunol*. 2015;136:703-712 e710
174. Dang LV, Nilsson A, Ingelman-Sundberg H, *et al.* Soluble cd27 induces igg production through activation of antigen-primed b cells. *J Intern Med*. 2012;271:282-293
175. Matter M, Odermatt B, Yagita H, *et al.* Elimination of chronic viral infection by blocking cd27 signaling. *J Exp Med*. 2006;203:2145-2155
176. Jacobi AM, Odendahl M, Reiter K, *et al.* Correlation between circulating cd27high plasma cells and disease activity in patients with systemic lupus erythematosus. *Arthritis Rheum*. 2003;48:1332-1342
177. Font J, Pallares L, Martorell J, *et al.* Elevated soluble cd27 levels in serum of patients with systemic lupus erythematosus. *Clin Immunol Immunopathol*. 1996;81:239-243
178. Han BK, White AM, Dao KH, *et al.* Increased prevalence of activated cd70+cd4+ t cells in the periphery of patients with systemic lupus erythematosus. *Lupus*. 2005;14:598-606

179. Oelke K, Lu Q, Richardson D*, et al.* Overexpression of cd70 and overstimulation of igg synthesis by lupus t cells and t cells treated with DNA methylation inhibitors. *Arthritis Rheum*. 2004;50:1850-1860
180. Zhao M, Sun Y, Gao F*, et al.* Epigenetics and sle: Rfx1 downregulation causes cd11a and cd70 overexpression by altering epigenetic modifications in lupus cd4+ t cells. *J Autoimmun*. 2010;35:58-69
181. Han BK, Olsen NJ, Bottaro A. The cd27-cd70 pathway and pathogenesis of autoimmune disease. *Semin Arthritis Rheum*. 2016;45:496-501
182. Sawalha AH, Jeffries M. Defective DNA methylation and cd70 overexpression in cd4+ t cells in mrl/lpr lupus-prone mice. *Eur J Immunol*. 2007;37:1407-1413
183. Park JK, Han BK, Park JA*, et al.* Cd70-expressing cd4 t cells produce ifn-gamma and il-17 in rheumatoid arthritis. *Rheumatology (Oxford)*. 2014;53:1896-1900
184. Lee WW, Yang ZZ, Li G*, et al.* Unchecked cd70 expression on t cells lowers threshold for t cell activation in rheumatoid arthritis. *J Immunol*. 2007;179:2609-2615
185. Oflazoglu E, Boursalian TE, Zeng W*, et al.* Blocking of cd27-cd70 pathway by anti-cd70 antibody ameliorates joint disease in murine collagen-induced arthritis. *J Immunol*. 2009;183:3770-3777
186. Atarashi K, Nishimura J, Shima T*, et al.* Atp drives lamina propria t(h)17 cell differentiation. *Nature*. 2008;455:808-812
187. Manocha M, Rietdijk S, Laouar A*, et al.* Blocking cd27-cd70 costimulatory pathway suppresses experimental colitis. *J Immunol*. 2009;183:270-276
188. Komori M, Blake A, Greenwood M*, et al.* Cerebrospinal fluid markers reveal intrathecal inflammation in progressive multiple sclerosis. *Ann Neurol*. 2015;78:3-20
189. Francosalinas G, Cantaert T, Nolte MA*, et al.* Enhanced costimulation by cd70+ b cells aggravates experimental autoimmune encephalomyelitis in autoimmune mice. *J Neuroimmunol*. 2013;255:8-17
190. Coquet JM, Middendorp S, van der Horst G*, et al.* The cd27 and cd70 costimulatory pathway inhibits effector function of t helper 17 cells and attenuates associated autoimmunity. *Immunity*. 2013;38:53-65
191. Diegmann J, Junker K, Gerstmayer B*, et al.* Identification of cd70 as a diagnostic biomarker for clear cell renal cell carcinoma by gene expression profiling, real-time rt-pcr and immunohistochemistry. *Eur J Cancer*. 2005;41:1794-1801
192. Junker K, Hindermann W, von Eggeling F*, et al.* Cd70: A new tumor specific biomarker for renal cell carcinoma. *J Urol*. 2005;173:2150-2153
193. Ryan MC, Kostner H, Gordon KA*, et al.* Targeting pancreatic and ovarian carcinomas using the auristatin-based anti-cd70 antibody-drug conjugate sgn-75. *Br J Cancer*. 2010;103:676-684
194. Wischhusen J, Jung G, Radovanovic I*, et al.* Identification of cd70-mediated apoptosis of immune effector cells as a novel immune escape pathway of human glioblastoma. *Cancer Res*. 2002;62:2592-2599
195. Trebing J, El-Mesery M, Schafer V*, et al.* Cd70-restricted specific activation of trailr1 or trailr2 using scfv-targeted trail mutants. *Cell Death Dis*. 2014;5:e1035
196. Claus C, Riether C, Schurch C*, et al.* Cd27 signaling increases the frequency of regulatory t cells and promotes tumor growth. *Cancer Res*. 2012;72:3664-3676
197. Gajewski TF, Schreiber H, Fu YX. Innate and adaptive immune cells in the tumor microenvironment. *Nat Immunol*. 2013;14:1014-1022
198. Zou W. Regulatory t cells, tumour immunity and immunotherapy. *Nat Rev Immunol*. 2006;6:295-307
199. van de Ven K, Borst J. Targeting the t-cell co-stimulatory cd27/cd70 pathway in cancer immunotherapy: Rationale and potential. *Immunotherapy*. 2015;7:655-667

200. Yang ZZ, Grote DM, Xiu B*, et al.* Tgf-beta upregulates cd70 expression and induces exhaustion of effector memory t cells in b-cell non-hodgkin's lymphoma. *Leukemia*. 2014;28:1872-1884
201. Grewal IS. Cd70 as a therapeutic target in human malignancies. *Expert Opin Ther Targets*. 2008;12:341-351
202. *https://clinicaltrials.gov/ct2/results?term=cd70+tumor&Search=Search*.
203. He LZ, Prostak N, Thomas LJ*, et al.* Agonist anti-human cd27 monoclonal antibody induces t cell activation and tumor immunity in human cd27-transgenic mice. *J Immunol*. 2013;191:4174-4183
204. *https://clinicaltrials.gov/ct2/results?term=varlilumab&Search=Search*.
205. Vitale LA, He LZ, Thomas LJ*, et al.* Development of a human monoclonal antibody for potential therapy of cd27-expressing lymphoma and leukemia. *Clin Cancer Res*. 2012;18:3812-3821
206. van Olffen RW, de Bruin AM, Vos M*, et al.* Cd70-driven chronic immune activation is protective against atherosclerosis. *J Innate Immun*. 2010;2:344-352
207. Hoeksema MA, Gijbels MJ, Van den Bossche J*, et al.* Targeting macrophage histone deacetylase 3 stabilizes atherosclerotic lesions. *EMBO Mol Med*. 2014;6:1124-1132
208. Virmani R, Kolodgie FD, Burke AP*, et al.* Lessons from sudden coronary death: A comprehensive morphological classification scheme for atherosclerotic lesions. *Arterioscler Thromb Vasc Biol*. 2000;20:1262-1275
209. Koltsova EK, Garcia Z, Chodaczek G*, et al.* Dynamic t cell-apc interactions sustain chronic inflammation in atherosclerosis. *J Clin Invest*. 2012;122:3114-3126
210. Livak KJ, Schmittgen TD. Analysis of relative gene expression data using real-time quantitative pcr and the 2(-delta delta c(t)) method. *Methods*. 2001;25:402-408
211. Nolte MA, Arens R, van Os R*, et al.* Immune activation modulates hematopoiesis through interactions between cd27 and cd70. *Nat Immunol*. 2005;6:412-418
212. Murphy AJ, Akhtari M, Tolani S*, et al.* Apoe regulates hematopoietic stem cell proliferation, monocytosis, and monocyte accumulation in atherosclerotic lesions in mice. *J Clin Invest*. 2011;121:4138-4149
213. Sage AP, Mallat Z. Multiple potential roles for b cells in atherosclerosis. *Ann Med*. 2014;46:297-303
214. Beishuizen CR, Kragten NA, Boon L*, et al.* Chronic cd70-driven costimulation impairs igg responses by instructing t cells to inhibit germinal center b cell formation through fasl-fas interactions. *J Immunol*. 2009;183:6442-6451
215. Foks AC, Lichtman AH, Kuiper J. Treating atherosclerosis with regulatory t cells. *Arterioscler Thromb Vasc Biol*. 2015;35:280-287
216. Potteaux S, Esposito B, van Oostrom O*, et al.* Leukocyte-derived interleukin 10 is required for protection against atherosclerosis in low-density lipoprotein receptor knockout mice. *Arterioscler Thromb Vasc Biol*. 2004;24:1474-1478
217. Stritesky GL, Yeh N, Kaplan MH. Il-23 promotes maintenance but not commitment to the th17 lineage. *J Immunol*. 2008;181:5948-5955
218. Maloy KJ, Powrie F. Fueling regulation: Il-2 keeps cd4+ treg cells fit. *Nat Immunol*. 2005;6:1071-1072
219. Barron L, Dooms H, Hoyer KK*, et al.* Cutting edge: Mechanisms of il-2-dependent maintenance of functional regulatory t cells. *J Immunol*. 2010;185:6426-6430
220. Pen JJ, De Keersmaecker B, Maenhout SK*, et al.* Modulation of regulatory t cell function by monocyte-derived dendritic cells matured through electroporation with mrna encoding cd40 ligand, constitutively active tlr4, and cd70. *J Immunol*. 2013;191:1976-1983

221. Zhang WC, Wang J, Shu YW*, et al.* Impaired thymic export and increased apoptosis account for regulatory t cell defects in patients with non-st segment elevation acute coronary syndrome. *J Biol Chem*. 2012;287:34157-34166
222. Thiault N, Darrigues J, Adoue V*, et al.* Peripheral regulatory t lymphocytes recirculating to the thymus suppress the development of their precursors. *Nat Immunol*. 2015;16:628-634
223. Covarrubias A, Byles V, Horng T. Ros sets the stage for macrophage differentiation. *Cell Res*. 2013;23:984-985
224. O'Neill LA, Hardie DG. Metabolism of inflammation limited by ampk and pseudo-starvation. *Nature*. 2013;493:346-355
225. Freemerman AJ, Johnson AR, Sacks GN*, et al.* Metabolic reprogramming of macrophages: Glucose transporter 1 (glut1)-mediated glucose metabolism drives a proinflammatory phenotype. *J Biol Chem*. 2014;289:7884-7896
226. Tannahill GM, Curtis AM, Adamik J*, et al.* Succinate is an inflammatory signal that induces il-1beta through hif-1alpha. *Nature*. 2013;496:238-242
227. Huang SC, Everts B, Ivanova Y*, et al.* Cell-intrinsic lysosomal lipolysis is essential for alternative activation of macrophages. *Nat Immunol*. 2014;15:846-855
228. Out R, Hoekstra M, Meurs I*, et al.* Total body abcg1 expression protects against early atherosclerotic lesion development in mice. *Arterioscler Thromb Vasc Biol*. 2007;27:594-599
229. Lammers B, Out R, Hildebrand RB*, et al.* Independent protective roles for macrophage abcg1 and apoe in the atherosclerotic lesion development. *Atherosclerosis*. 2009;205:420-426
230. Meurs I, Lammers B, Zhao Y*, et al.* The effect of abcg1 deficiency on atherosclerotic lesion development in ldl receptor knockout mice depends on the stage of atherogenesis. *Atherosclerosis*. 2012;221:41-47
231. Tarling EJ, Bojanic DD, Tangirala RK*, et al.* Impaired development of atherosclerosis in abcg1-/- apoe-/- mice: Identification of specific oxysterols that both accumulate in abcg1-/- apoe-/- tissues and induce apoptosis. *Arterioscler Thromb Vasc Biol*. 2010;30:1174-1180
232. Ranalletta M, Wang N, Han S*, et al.* Decreased atherosclerosis in low-density lipoprotein receptor knockout mice transplanted with abcg1-/- bone marrow. *Arterioscler Thromb Vasc Biol*. 2006;26:2308-2315
233. Moore KJ, Sheedy FJ, Fisher EA. Macrophages in atherosclerosis: A dynamic balance. *Nat Rev Immunol*. 2013;13:709-721
234. Martin RM, Brady JL, Lew AM. The need for igg2c specific antiserum when isotyping antibodies from c57bl/6 and nod mice. *J Immunol Methods*. 1998;212:187-192
235. Lewis MJ, Malik TH, Ehrenstein MR*, et al.* Immunoglobulin m is required for protection against atherosclerosis in low-density lipoprotein receptor-deficient mice. *Circulation*. 2009;120:417-426
236. Tse K, Gonen A, Sidney J*, et al.* Atheroprotective vaccination with mhc-ii restricted peptides from apob-100. *Frontiers in Immunology*. 2013;4:493
237. Hermansson A, Ketelhuth DF, Strodthoff D*, et al.* Inhibition of t cell response to native low-density lipoprotein reduces atherosclerosis. *J Exp Med*. 2010;207:1081-1093
238. Silence K, Dreier T, Moshir M*, et al.* Argx-110, a highly potent antibody targeting cd70, eliminates tumors via both enhanced adcc and immune checkpoint blockade. *MAbs*. 2014;6:523-532

8 ACKNOWLEDGEMENTS

Kaum zu glauben, aber endlich ist es soweit und meine Promotion geht dem Ende entgegen. Ich habe viel gelernt während dieser Zeit, die sehr viele gute aber manchmal auch schwierige Momente mit sich brachte. Wie Einstein schon sagte: „Zwei Dinge sind zu unserer Arbeit nötig: Unermüdliche Ausdauer und die Bereitschaft, etwas, in das man viel Zeit und Arbeit gesteckt hat, wieder wegzuwerfen“. Gerade in diesen Phasen ist man froh und dankbar, wenn man Unterstützung in seinem Umfeld erfährt. An dieser Stelle möchte ich mich allen Personen danken, die mich während der letzten 5 Jahre und darüber hinaus begleitet und mir geholfen haben.

Zunächst möchte ich mich bei Prof. Dr. Christian Weber bedanken, dass ich die Möglichkeit hatte am IPEK zu promovieren, darin inbegriffen seine fortwährende finanzielle aber auch persönliche Unterstützung in meinem Werdegang. Durch deine, Norberts und Esthers Fürsprache habe ich eine tolle Postdoktorandenstelle gefunden und freue mich sehr auf das was jetzt kommt. Ich habe eine großartige Zeit hier am Institut gehabt, nicht nur während der Arbeit, aber auch während der Betriebsausflüge und Oktoberfestbesuche, welche ich größtenteils mit organisieren durfte.

Ein großes Dankeschön geht an meinen Doktorvater Prof. Dr. Alexander Faussner für die Betreuung und wissenschaftliche Zusammenarbeit während meiner Promotion. Lieber Sascha, vielen Dank für die Unterstützung und die guten Gespräche. Auf den letzten Metern hast du mir sehr geholfen diese Arbeit zu Ende zu bringen.

Lieber Norbert, liebster und einziger Zimmergenosse auf Konferenzen (was wohl auch an unserer Fähigkeit zur nächtlichen Geräuschkulisse liegt), Stammtischmitglied, Stangentanzlehrer, und Motivationskünstler, vielen Dank für all die Jahre (schon seit Aachen), die ich nun schon mit dir zusammenarbeiten darf. Ich habe viel von dir gelernt, nicht nur in wissenschaftlicher, aber auch in menschlicher Hinsicht. Wo ich an vielen Stellen etwas zu pessimistisch war hast du es mit deiner positiven Art ausgeglichen. Dies war vor allem bei diversen Auswertungen und Hiobsbotschaften vom Zoll nötig, wenn aus Versehen ganze Studien bei Raumtemperatur in der Asservatenkammer vergessen wurden. Vielen Dank für all die großartigen Unterhaltungen über alle möglichen Themen, die von wissenschaftlich bis zensiert reichten. Manchmal haben unsere wissenschaftlichen Diskussionen Überlänge gehabt und uns war nicht ganz klar wie wir vom ursprünglichen Thema abgedriftet sind. Dennoch habe ich dadurch extrem viel gelernt. Danke, dass du meine

wissenschaftliche Selbstständigkeit stets gefordert und gefördert hast. Trotz all der Arbeit kam der Spaß niemals zu kurz. Manchmal jagte ein Spruch den nächsten. Besonders gefährlich wurde es an Tagen, wenn einer von uns durstig „wie eine Natter unter dem heißen Stein“ war. Ich hoffe, dass wir eines Tages das EFJ zusammen gründen werden. Werbung dafür haben wir schon zu genüge auf der Gordon Konferenz in Maine betrieben ;-). Neben all der Arbeitszeit habe ich auch gerne Freizeit mit dir verbracht und würde dich nun mehr als Freund denn als Vorgesetzten sehen. Dennoch bist du mir bis jetzt eins schuldig geblieben, ich warte immer noch auf deinen Karaoke Auftritt.

Liefde Esther, hartelijk bedankt voor alles.
Dear Esther, since my Dutch is rather rudimentary I'll switch to English now. Thank you very much for all the support in financial but also personal aspects. Through all the years you constantly supported me and you and Norbert arranged that I could spend part of my PhD at your lab in Amsterdam. This was a unique setting and I feel very privileged that I was given the opportunity experiencing this. Through all the years I really appreciated your positivity and directness (yes, indeed, my beard length is correlating with the duration of my thesis ☺). Although you claimed being a bad chef, I still remember that the Jamie Oliver style risotto back in Maastricht was absolutely great and tasty. Haha, and as chef is translatable with boss in German, I can disagree twice with your statement.
Norbert, Esther, without your support I would have never been able to pursue a research internship during my thesis in the US which definitely broadened my horizon. Furthermore, you always supported me to participate in conferences. Thank you very much for given me the opportunity and support. It was a great pleasure to work with both of you.

Liebe/r Tobi, Geli, Sigrid, Chrissy, Maiwand, Sandra, Svenja und Charlotte. Vielen Dank für all die gemeinsamen Jahre. Vielen Dank für eure großartige Hilfe und Unterstützung nicht nur bei (überdimensionierten) Experimenten, welche wir ohne Fließbandaufteilung manchmal nicht an einem Tag bewältigt hätten. Überdies möchte ich mich bei euch für die tolle Atmosphäre während der Arbeitszeit aber auch bei der Bewältigung des Laboralltags, manchmal auch beim Feierabendbier, bedanken. Wir haben viel zusammengelernt, unter anderem, dass Mäuse scheinbar zu Rammstein weniger gut narkotisierbar sind (komisch, hat einige wenige von uns bei langen Experimenten immer sehr entspannt). Ich habe mich jedes Mal über die diversen Themen, besonderes das Philosophieren über die Bundesligaspiele oder das übliche

Niveaulimbo beim Mittagessen, gefreut, auch wenn es mal für den/die eine/n etwas eintönig oder peinlich wurde An dieser Stelle ein Dankeschön an den HSV, der in den letzten Jahren sehr häufig hier für Gesprächsstoff gesorgt hat (und das nicht unbedingt immer positiv, ganz zu meinem Leidwesen). Liebe Sigrid, vielen Dank für deine immerwährende Unterstützung, den vielen Kaffee, und natürlich den freitäglichen Sekt in den letzten Jahren. Häufig hast du Aufgaben für mich übernommen, wenn ich diese mal nicht geschafft oder (sehr selten natürlich ;-)) vergessen habe. Ein großes Dankeschön an Geli und dich für die unfassbare Geduld unzählige Herzen zu schneiden. Lieber Tobi, liebe Geli, ich bin immer noch froh nach unserem Ski-Ausflug ohne Tobi nach Hause gegangen zu sein ☺. Die Zeit mit euch beiden war großartig, weil wir mehr oder weniger zur selben Zeit hier losgelegt haben und zusammen „erwachsen“ geworden sind. Danke euch beiden für alles. Im Speziellen hier auch nochmal ein großes Dankeschön an Svenja, mit der ich viele Projekte, lustige Momente, großartige Konversationen und auch Leidenszeiten in München und Amsterdam geteilt habe. Ich bin froh, dass du zu der CD27/CD70/GITR Truppe gestoßen bist. Ein großes Dankeschön natürlich auch für das Korrekturlesen dieser Arbeit.

Next, I would like to thank all the current and past members of Esther’s group in Amsterdam and in Maastricht (especially Linda, Tom, Esther S., Anett, Myrthe, and Erwin) and Jan from Menno’s group. Without you this work would not have been fully accomplishable. Thank you for working with me on all these long-lasting projects. Linda, you have been a great help through all these years. Thank you so much, especially trying to rescue those flattened arches ☺. Erwin, it has been sometime that you introduced flow cytometry to me in a 2-week intense course. During this period, I think my head was on fire and my liver on heavy duty. By now, I can’t even tell how many hours of my life I spent in front of our Canto.

Dear Dirk, lustiger Holzhackerbub, the time I spend working with you was absolutely fantastic. It all started in Aachen with a memorable first impression in your fancy sweater and red chinos. Only a few years later, you are dressed in leather chaps “performing” Mr. Boombastic. Who could tell would have happened without my backup? Too bad you left too early for a “serious” job. I will never forget our skiing trip where pure confidence met ignorance (“Move b****”). We had absolutely fantastic times at our Stammtisch and especially in the football stadium a couple of years ago. Some of the most used expressions and idioms at our Abendbrotzeit stem from you (Plataten, Bonobonen; Aaaaabahhh, This is so bad, you can’t even clean a window with it; Life is

a…). Thank you for all the support, friendship, extensive nights on the roof terrace, and the good memories through all the years.

This brings me to the next person I would like to mention. Dear Remco, thank you very much for all the support and friendship in the past years. Although we only recently shared projects, we always had great moments of nonsense conversations and laughter together. Thank you for teaching me a lot of Dutch expressions and idioms I never heard of, starting by the monkey and the sleeve, 3 kilo klopfend paars…☺. I will truly miss the outstanding conversations with you, Norbert, Martin and Dirk spanning private life and future, but also including the more inappropriate and censored topics. Certainly, I am grateful that I could learn a lot about microscopy techniques and technical background regarding our equipment. Furthermore, you helped Mr. Mullet for a comeback not only by founding the mullets on tour competition but also proudly wearing the wig at a lot of occasions. But this passion about mullets is not very surprising since you are originating from New Kids land, Junge. And one of the biggest achievements, of course besides our Karoake performance, is seeing you being a bigger Christian Steiffen Fan than Martin, Norbert and I am by now.

Lieber David, alten Schalker, dir möchte ich auch einen kleinen Abschnitt widmen. Vielen Dank für die großartige Zeit, die wir im und nach dem Labor verbracht haben. Mit dir hatte ich ein paar intensive Laborwochen, gekrönt von einem der intensivsten Oktoberfestbesuche. Wer hätte gedacht, dass der Besitzer des Slayermobils gleichzeitig alle Heino Songs auswendig kennen würde? Ich habe es immer noch in meinem Hinterkopf als du in Aachen mal sagtest: „Egal was du tust, nimm bloß nicht das CD27/CD70 Projekt oder GITR, die sind verflucht!!!!“ Haha, daran habe ich öfters während der letzten 5 Jahre denken müssen, obwohl ich als Wissenschaftler NATÜRLICH nicht an Flüche glaube. Dennoch bin ich sehr froh über die Entscheidung an den drei Projekten gearbeitet zu haben und: Ende gut, Alles gut!. Auch wenn wir uns über die Jahre immer nur kurz und manchmal unbewusst gesehen haben (wie z.B. bei Rock am Ring) werde ich die Zeit nicht vergessen.

Lieber Schmitti, nach dem ich jetzt schon die ganze Bande erwähnt habe, darfst du natürlich nicht fehlen. Seit 6 Jahren bist du nun vorwiegend Freund und dann Kollege. Ich weiß gar nicht, wo ich all die tollen Momente aufzählen soll, die wir erlebt haben. Ich fang trotzdem mal an. Neben dem besten Büro aller Zeiten in Aachen haben wir uns auch außerhalb vom Labor ordentlich rumgetrieben. Karneval, der Chiemsee rockt, Boschek ist verliebt (in Hamburg, und zwar nicht nur ins Dosenbier), die

Scherbenpolka, diverse Oktober/Herbst/Frühjahrs/Starkbierfestbesuche, Grillen bei euch daheim, Dropkick Murphys… Eine der größten Herausforderungen, die wir zusammen gemeistert haben, war die Gordon Konferenz 2015. Selten war eine Konferenz anspruchsvoller für Gehirn und Leber. Das anschließende Wochenende in Boston werde ich auch nicht vergessen, vor allem stillose Menschen im Beacon Hill Pub. Ich weiß nicht, wo ich mich nur bei dir und Yvonne bedanken soll für alles, was ihr für mich getan habt, innerhalb und außerhalb des Labors. Vielen Dank für eure Freundschaft.

Liebe Helene, dein Weggehen nach Amsterdam hat schon eine große Lücke hier zurückgelassen. Wir haben viel erlebt in der Zeit in Aachen und München, nicht nur während der Arbeit, aber überwiegend auch danach. Ich bin froh um jede einzelne Geschichte, die ich mit dir erleben durfte (Junggesellenabschied der Engländer fällt mir da spontan ein). Umso schöner fand ich es, dass ich dich regelmäßig in Amsterdam besuchen konnte und immer einen Schlafplatz auf deiner Couch hatte. Danke für alles, deine Unterstützung und Hilfe, aber vor allem für deine Freundschaft, die mir wirklich viel bedeutet. Und natürlich hier auch lieben Dank für das Korrekturlesen!

An dieser Stelle möchte ich mich bei allen anderen Kollegen und Kolleginnen am Institut bedanken, welche meinen Alltag und Erfahrungsschatz bereichert haben und für eine angenehme Arbeitsatmosphäre gesorgt haben. Ich habe sowohl wissenschaftlich als auch persönlich viel von euch gelernt. Bitte seht es mir nach, wenn ich euch nicht alle persönlich erwähne (stellvertretend seien hier genannt: die ganze AG Söhnlein, AG Döring….). Ein besonderes Dankeschön an alle Gartenhäusler (Verena, Sabine, He, Julian, Veit, Kathrin, Mariam, Yuanfang, Zhe, Markus, Sarajo, Chanyung) und speziell an Nada, Ann, Johan, Mariaelvy, Philipp, Janina, Carlos N., Carlos SR., Quinte, Petteri, Michael, Donato, Martina, Patti, Yvonne J., Larisa, Virginia, Mariam, Tanja, Michael und Zhen. Einige von euch kenne ich noch aus Aachener Zeiten, Amsterdam oder von den ersten Tagen in München. Ihr alle habt definitiv meinen Alltag hier bereichert und ich bin dankbar für alles, was ich mit euch während der Arbeit und auch außerhalb erleben durfte. Auch hier seien mal wieder diverse Oktoberfest- und Starkbierfestausflüge erwähnt. Vielen Dank, Michael, für die vielen Stunden mit mir am Sorter.

Liebe Manu, ich muss immer wieder an die Illertaler Inzester, Kool Savas und die anfängliche Kellerzeit zurückdenken, als Jürgen und Klaus noch neben uns saßen. Klaus, Danke für deine Weisheit/en (wie versprochen☺), they made my day. Du warst

hier in München neben Helene eine Konstante und diverse Wochenenden/Wochentage musste die Feierwut kuriert werden. Passend dazu fällt mir gerade der Tag ein, an dem ich in 2011 meinen Vertrag hier unterschieben habe.

Liebe Janina, ich hoffe du findest demnächst auch ohne mich die richtigen Tastenkombinationen (und mal einen anderen Klingelton☺). Vielen Dank für all die Gespräche mit dir und deine positive Ausstrahlung, ich habe oft herzhaft gelacht.

Lieber Xavier, mittlerweile kannst du so gut Deutsch, da brauche ich den Abschnitt gar nicht zu übersetzen. Vielen Dank für die vielen Serien und die vielen großartigen Unterhaltungen über politische, alltägliche, zensierte aber auch wissenschaftliche Themen. Du hast ein großartiges biochemisches Wissen und bist immer hilfsbereit. Man kennt dich auch als wandelndes Inventar des Gartenhauses und ohne dich wäre wohl nicht nur ich manchmal Stunden damit beschäftigt gewesen, diverse Chemikalien zu suchen. Vielen lieben Dank für das Durcharbeiten meiner Doktorarbeit und das auch noch unter etwas Zeitdruck. Du magst genauso wie ich etwas härtere Gitarrenmusik, wobei ein Großteil deiner Lieblingsmusik bzw. Albumcover mir eher etwas Angst einflößen ☺.

Weiterhin möchte ich bei unserem Sekretariat (Frau Bretzke, Frau Stöger und Frau Herrle) für die Unterstützung bei der Bewältigung der Bürokratie bedanken. Ein herzliches Dankeschön an das Personal der zentralen Versuchstierhaltung, welche einen wichtigen Beitrag zu dem tierexperimentellen Teilen dieser Arbeit beigetragen haben.

Ein großes Dankeschön geht an Thomas Brocker, Ludger Klein und allen anderen Mitgliedern des SFB1054, welcher mich und meine Arbeit finanziell unterstützt hat und es mir ermöglichte an diversen Kongressen teilzunehmen. Als Mitglied des SFB1054, der implementierten IRTG und als deren Sprecher war es mir möglich an vielen Retreats, Vorlesungen, Symposia und Seminaren teilzunehmen. Weiterhin habe ich dadurch sehr viele Wissenschaftler mit unterschiedlichsten Forschungsfeldern aus der ganzen Welt kennenlernen dürfen, wodurch sich mein berufliches aber auch privates Umfeld vergrößert hat.

An dieser Stelle vielen Dank an alle aktiven und ehemaligen Mitglieder der IRTG, besonders aber an dreimal Julia (Winnewisser, von Rohrscheidt, Maul), Christopher, Tobi, Maria, Valentin, Fabi, Domi, Isabel und Torben.

Im Speziellen bin ich aber dankbar Markus, Julia, Steffi und Andrea kennengelernt zu haben und zu meinen Freunden zählen zu dürfen. Ohne euch wäre mein Leben in München eindeutig langweiliger and farbloser gewesen. Danke, dass ich durch euch die Leute der Steinheil-WG und alle assoziierten „Mitbewohner“ (Holger, Vroni, Steffi, Domi, Joost, Andi, und so viele mehr) kennengelernt habe. Die Partys bei euch waren legendär. Ich glaub, daher war ich auch immer einer der letzten der gegangen ist/gehen musste ☺. Aber neben euren Partys zur vorgerückten Stunde in Oldschool HipHop Sessions hosted by Andi und Holger geendet sind gab es noch so viele tolle und unvergessliche gemeinsame Abende, Oktoberfestbesuche und natürlich Klangtherapiestunden. Vroni, ich hoffe du kannst auch ohne mich/Keile die Band weiterführen ☺.

Markus, ich bin mehr als froh, dass du mich mal zur Bergkichweih mitgenommen hast. Gut, dass wir zur Erinnerung ein Video dort gedreht haben, welches schon internationalen Bekanntheitsgrad hat.

Andrea, you old, Italian Viking. Rockavaria (YEAH \m/) with you was awesome and I am looking forward to the Boss and Highfield with you. The time I spent with you, Markus (and of course everyone else of the Steinis) was absolutely fantastic, particularly the boys out nights.

Ich werde euch und das Drumherum sehr vermissen.

I am deeply grateful to Prof. Ulrich von Andrian and his group in Boston for the outstanding lab exchange. Dear Uli, Mario, Aude, Carmen Ira, Scott, David, Susi, Lauren, and Guiying, thank you so much for the great experience I had staying in your lab. I learned so much from and working with you in this extraordinary environment. It definitely broadened my horizon. Furthermore, I am absolutely thankful for getting to know other members of the immunology department, especially Pete and Jennifer, Amy, Jernej, Virkam, Dimitry, Jon, and Dan, which absolutely contributed to my wonderful experience in Boston. I am still accounting 2nd place for the best costume at my first Halloween party at the immunology department’s beer hour a major achievement. It was great having some of you visiting me in Munich. Hope to see you guys soon again. I would also like to thank Gunilla, Jimmy, Flavio, Mike and the German bunch of Bostonians (Nadja, Ryan, Thomas, Lary, Christian and Juhee). I really appreciated living with you, Gunilla and Jimmy, in the most unusual and anti-posh/establishment household in Brookline. I can’t even remember how many funny conversations I witnessed and participated in and how often Jimmy had to cool his jets. It was absolutely fantastic.

Thank you, Flavio and Mike for all the time we spend together not only in Boston, but also in Munich. It was absolutely great having you here and I am blessed having you as friends. Thank you all so much for everything, these were memorable and for me unforgettable times.

Lieben Dank für die großartige Zeit, Lisa und Loll, nicht nur auf dem Chiemsee Festival. Ohne euch hätte ich Tobi, Katja und Tanja nie kennengelernt, keinen Donnerstags-Stammtisch gehabt und das IPEK wäre wohl um eine unvergessliche Weihnachtsfeier in Tobis Küche ärmer.

Liebe/r Timo, Thomas, Pati, Elke und Anette, ich bin sehr froh euch kennengelernt zu haben. Auch wenn wir uns während all der Jahre immer wieder nur sporadisch getroffen haben und das durch die halbe Welt verstreut, war es jedes Mal großartig. Ich hoffe sehr, dass wir das beibehalten.

Liebe Henny, vielen Dank für alles, was du für mich getan hast. Ich bin dankbar, dass du Teil meines Lebens bist, auch wenn die Zeiten nicht immer einfach und geradeaus waren. Ich habe viel von dir und durch dich für mein Leben und auch über mich gelernt. An dieser Stelle gilt mein Dank euch, liebe/r Ingo, Mat, Claus, Peter und Silke. Danke für die gute Zeit, die wir gemeinsam hatten.

Fast zum Schluss möchte ich all meinen Freunden aus Aachener Zeiten (unter Anderem Boschek, Calculon, Pöpe, Sunshine, Alex H., Fahri, Zutter, Eileen, Dave, Präsident, Tobi, Andrea, Eve, Aline, Jule, Marianne, Sonja, Anne) und dem Gillrather Jugendheim (Tööf, Kathrin, Pietisch, Niki, Hausi, Alyssa, Michael und Verena, Stiff, und viele, viele mehr) danken. Wir haben unfassbar viel erlebt (Zandvoort, unseren Stammtisch, den Keller des Todes, Breslau, Karneval in Köln, Karnevalsumzüge mit eigenem Wagen, Oktoberfest, Hochzeiten, Geburten, Rock am Ring, Rocco del Schlacco, Mainacht, die Vorbereitungen zur Mainacht, Tööf Rock, 30ste Geburtstage, Jaya the Cat Konzerte, WM, EM, Alemannia-Spiele in der ersten Liga, Biopartys, Fussballauswärtsspiele, Mayonnaise im Haar, …) alles hier aufzuführen würde sicherlich den Rahmen sprengen und ein eigenes Buch füllen. Leider muss ich euch etwas enttäuschen, ich habe nie an einem Zombie-Killer-Virus geforscht. Der Rasenmäher kann noch im Schuppen bleiben.
Danke, dass ihr all die Jahre für mich da wart. Kurzum, ich bin euch für jeden einzelnen Moment dankbar und ich bin froh solche Freunde wie euch in meinem Leben zu haben.

Die letzten Zeilen möchte ich meinem Bruder Torsten und meinen Eltern, Heinz-Josef und Annette, widmen. Diesen Abschnitt zu schreiben ist mir besonders schwer gefallen, weil ich nicht weiß, wo ich überhaupt anfangen soll. Ihr habt mich immer bedingungslos unterstützt und aufbauende, aufmunternde Worte gefunden, wenn es gerade bei der Doktorarbeit oder auch so mal nicht lief. Wenn nötig habt ihr den langen Weg auf euch genommen und seid mir zur Hilfe nach München geeilt. Viel schöner aber war es euch hier einfach so zu Besuch zu haben. Ohne euch, eure Fürsorge und Unterstützung wäre mein derzeitiger und zukünftiger Werdegang nicht möglich. Bald wird ein weiteres Kapitel aufgeschlagen und das wird mich noch etwas weiter weg führen. Dennoch werde ich eins sicherlich nicht vergessen: eure Tür hat schon immer für mich immer offen gestanden und bei euch ist zu Hause. Home is where the heart is! Euch gebührt mein größter Dank!

Holger

9 APPENDIX

Table I. Distribution of immune cell subsets in 18 week old *Cd27* $^{+/+}$ *Apoe* $^{-/-}$ and *Cd27* $^{-/-}$ *Apoe* $^{-/-}$ mice.

Organ		Blood									Lymph nodes									Spleen								
Mouse strain		*Cd27* $^{+/+}$ *Apoe* $^{-/-}$				*Cd27* $^{-/-}$ *Apoe* $^{-/-}$					*Cd27* $^{+/+}$ *Apoe* $^{-/-}$				*Cd27* $^{-/-}$ *Apoe* $^{-/-}$					*Cd27* $^{+/+}$ *Apoe* $^{-/-}$				*Cd27* $^{-/-}$ *Apoe* $^{-/-}$				
Subset	Parental Gate	n	Mean		SD	n	Mean		SD	*p*	n	Mean		SD	n	Mean		SD	*p*	n	Mean		SD	n	Mean		SD	*p*
CD19^{+}	of CD45^{+}	18	52.82	±	9.72	16	51.63	±	8.21	n.s.	17	50.39	±	3.78	15	48.27	±	6.25	n.s.	18	49.77	±	6.44	16	54.43	±	5.67	n.s.
CD11b^{-}CD5^{+}	of CD19^{+}	18	8.43	±	5.99	16	6.31	±	4.17	n.s.	15	13.03	±	7.58	15	11.08	±	7.91	n.s.	18	7.76	±	4.71	16	5.33	±	2.42	n.s.
B1a (CD11b^{+}CD5^{+})	of CD19^{+}	18	3.12	±	5.72	16	1.30	±	1.96	n.s.	13	2.16	±	1.41	16	2.16	±	1.68	n.s.	18	1.05	±	0.73	16	0.72	±	0.46	n.s.
B1b (CD11b^{+}CD5^{-})	of CD19^{+}	18	2.55	±	2.86	16	1.71	±	2.26	n.s.	15	2.10	±	1.00	16	2.03	±	1.22	n.s.	18	1.34	±	0.49	16	1.22	±	0.41	n.s.
B2 (CD11b^{-}CD5^{-})	of CD19^{+}	18	86.29	±	11.75	16	90.39	±	6.32	n.s.	15	79.13	±	9.25	16	81.44	±	13.34	n.s.	18	89.81	±	4.99	16	92.68	±	2.92	n.s.
CD11c^{hi}	of CD45^{+}	18	0.91	±	0.81	16	0.68	±	0.73	n.s.	18	0.46	±	0.17	16	0.56	±	0.26	n.s.	18	3.36	±	1.26	16	3.12	±	1.09	n.s.
CD8^{+}DC	of CD11c^{hi}	18	2.01	±	1.83	16	2.95	±	3.03	n.s.	17	20.71	±	8.75	13	21.25	±	4.69	n.s.	16	15.29	±	3.70	13	15.75	±	4.52	n.s.
CD8^{-}DC	of CD11c^{hi}	18	96.71	±	3.76	16	96.06	±	4.46	n.s.	17	78.99	±	8.56	13	78.38	±	4.50	n.s.	16	85.24	±	5.01	13	84.20	±	4.57	n.s.
pDC (Siglec-H^{+}PDCA-1^{+})	of CD3^{-}CD19^{-}	18	1.39	±	1.48	16	0.72	±	0.36	n.s.	18	3.32	±	2.62	16	4.31	±	3.13	n.s.	17	2.35	±	0.64	16	2.59	±	0.75	n.s.
Neutrophils (CD11b^{+}Ly6G^{+})	of CD3^{-}Nk1.1^{-}	16	29.76	±	13.97	16	22.94	±	14.24	n.s.	15	0.23	±	0.19	16	0.18	±	0.10	n.s.	15	5.17	±	4.21	16	2.76	±	3.32	n.s.
Monocytes (CD11b^{+}Ly6G^{-})	of CD3^{-}Nk1.1^{-}	14	13.82	±	3.47	16	13.38	±	4.97	n.s.	15	2.71	±	0.84	16	2.60	±	0.86	n.s.	15	9.48	±	2.60	16	9.38	±	1.79	n.s.
Ly6C^{hi} Monocytes	of CD11b^{+}Ly6G^{-}	14	40.36	±	13.35	16	45.74	±	17.08	n.s.	15	27.44	±	8.57	16	18.80	±	10.37	*	15	23.99	±	8.24	16	17.32	±	8.91	*
Ly6C^{lo} Monocytes	of CD11b^{+}Ly6G^{-}	14	13.52	±	4.67	16	11.27	±	4.77	n.s.	15	18.68	±	6.88	16	18.30	±	7.11	n.s.	15	11.72	±	2.42	16	10.32	±	2.07	n.s.
Ly6C^{neg} Monocytes	of CD11b^{+}Ly6G^{-}	14	45.74	±	13.42	16	42.75	±	14.22	n.s.	15	53.71	±	8.40	16	62.74	±	10.78	*	15	64.21	±	9.00	16	72.35	±	9.93	*
NK cells (CD3^{-}Nk1.1^{+})	of CD45^{+}	16	0.61	±	1.55	16	0.06	±	0.07	n.s.	17	0.65	±	0.23	16	0.08	±	0.06	****	17	2.03	±	0.93	16	0.13	±	0.15	****
CD3	of CD45^{+}	15	15.49	±	9.16	16	17.29	±	7.83	n.s.	17	40.29	±	6.69	16	42.58	±	9.92	n.s.	17	23.22	±	4.33	16	23.49	±	3.82	n.s.
CD4	of CD3^{+}	15	46.25	±	6.34	16	47.43	±	4.01	n.s.	17	51.71	±	4.16	16	51.00	±	3.89	n.s.	17	58.58	±	4.39	16	54.96	±	8.40	n.s.
activated CD4 (CD44^{+}CD62L^{-})	of CD4^{+}	15	52.60	±	11.58	16	46.28	±	12.52	n.s.	16	23.89	±	7.82	16	21.53	±	9.98	n.s.	17	39.92	±	12.57	16	34.46	±	9.79	n.s.
not activated CD4 (CD44^{+}CD62L^{+})	of CD4^{+}	15	46.68	±	11.86	16	53.04	±	13.18	n.s.	16	75.60	±	7.89	16	77.93	±	10.18	n.s.	17	59.90	±	12.56	16	65.34	±	9.81	n.s.
Treg (CD4^{+}Foxp3^{+})	of CD4	15	8.63	±	3.31	14	6.43	±	1.78	*	16	17.51	±	2.34	15	12.81	±	1.86	****	17	21.72	±	5.55	16	16.03	±	2.85	***
CD8	of CD3^{+}	14	39.71	±	6.36	16	40.18	±	4.14	n.s.	17	39.32	±	5.28	16	40.31	±	3.55	n.s.	17	28.57	±	7.25	16	28.91	±	6.18	n.s.
central memory CD8 (CD44^{+}CD62L^{+})	of CD8^{+}	14	18.54	±	3.81	16	18.29	±	5.59	n.s.	16	18.64	±	4.16	16	16.05	±	5.33	n.s.	17	19.99	±	5.05	16	19.90	±	4.31	n.s.
effector memory CD8 (CD44^{+}CD62L^{-})	of CD8^{+}	14	11.58	±	5.98	16	7.90	±	2.76	*	16	3.92	±	2.37	16	2.79	±	1.20	n.s.	17	7.28	±	4.92	16	4.12	±	1.11	*
naive CD8 (CD44^{-}CD62L^{-})	of CD8^{+}	14	51.21	±	9.52	16	54.59	±	12.76	n.s.	16	68.62	±	8.13	16	72.23	±	6.96	n.s.	17	67.15	±	10.51	16	71.71	±	4.60	*

Mean ± SD. Statistical significance was calculated for groups pairwise by 2-tailed *t* test. *$p < 0.05$, **$p < 0.01$, **$p < 0.01$, ***$p < 0.001$

Table II. Distribution of immune cell subsets in 28 week old *Cd27*$^{+/+}$ *Apoe*$^{-/-}$ and *Cd27*$^{-/-}$ *Apoe*$^{-/-}$ mice.

Organ		Blood									Lymph nodes									Spleen							
Mouse strain		*Cd27*$^{+/+}$ *Apoe*$^{-/-}$				*Cd27*$^{-/-}$ *Apoe*$^{-/-}$					*Cd27*$^{+/+}$ *Apoe*$^{-/-}$				*Cd27*$^{-/-}$ *Apoe*$^{-/-}$					*Cd27*$^{+/+}$ *Apoe*$^{-/-}$				*Cd27*$^{-/-}$ *Apoe*$^{-/-}$			
Subset	**Parental Gate**	**n**	**Mean**	**SD**	**n**	**Mean**	**SD**	***p***	**n**	**Mean**	**SD**	**n**	**Mean**	**SD**	***p***	**n**	**Mean**	**SD**	**n**	**Mean**	**SD**	***p***
CD19^{+}	of CD45^{+}	11	31.58 ±	13.53	11	42.22 ±	9.30	*	11	41.72 ±	6.42	12	44.28 ±	3.60	n.s.	11	46.13 ±	10.79	12	52.95 ±	6.22	0.07
CD11b^{-}CD5^{+}	of CD19^{+}	11	3.75 ±	4.43	11	12.94 ±	14.49	0.06	11	35.53 ±	15.97	12	29.00 ±	14.41	n.s.	11	4.02 ±	4.75	12	10.59 ±	11.77	0.10
B1a (CD11b^{+}CD5^{+})	of CD19^{+}	11	0.49 ±	0.42	11	1.64 ±	2.09	n.s.	11	1.81 ±	1.33	12	3.47 ±	2.51	0.07	11	0.83 ±	0.87	12	1.65 ±	1.22	0.08
B1b (CD11b^{+}CD5^{-})	of CD19^{+}	11	1.65 ±	0.77	11	1.70 ±	1.65	n.s.	11	1.71 ±	0.72	12	1.34 ±	0.66	n.s.	11	2.17 ±	0.49	12	2.08 ±	0.89	n.s.
B2 (CD11b^{-}CD5^{-})	of CD19^{+}	11	93.90 ±	4.29	11	83.44 ±	14.40	*	11	79.34 ±	13.46	12	62.84 ±	19.43	*	11	92.95 ±	5.41	12	85.58 ±	13.01	0.10
CD11c^{hi}	of CD45^{+}	11	0.65 ±	0.50	12	0.88 ±	1.47	n.s.	11	0.67 ±	0.43	12	0.71 ±	0.44	n.s.	11	2.61 ±	0.87	12	3.16 ±	1.53	n.s.
CD8^{+}DC	of CD11c^{hi}	11	3.34 ±	3.57	12	4.75 ±	6.85	n.s.	11	16.97 ±	4.66	12	15.78 ±	6.29	n.s.	11	16.53 ±	2.40	12	15.23 ±	4.92	n.s.
CD8^{-}DC	of CD11c^{hi}	11	96.65 ±	3.57	12	95.33 ±	6.83	n.s.	11	83.23 ±	4.63	12	84.38 ±	6.23	n.s.	11	83.47 ±	2.40	12	84.77 ±	4.91	n.s.
pDC (Siglec-H^{+}PDCA-1^{+})	of CD3^{-}CD19^{-}	11	0.73 ±	0.74	12	0.96 ±	0.84	n.s.	11	6.96 ±	2.88	12	4.88 ±	2.78	0.09	11	1.89 ±	0.75	12	2.12 ±	1.02	n.s.
Neutrophils (CD11b^{+}Ly6G^{+})	of CD3^{-}Nk1.1^{-}	7	19.14 ±	11.70	10	22.72 ±	10.62	n.s.	11	0.56 ±	1.62	12	0.10 ±	0.07	n.s.	11	2.28 ±	1.88	12	3.53 ±	2.84	n.s.
Monocytes (CD11b^{+}Ly6G^{-})	of CD3^{-}Nk1.1^{-}	11	21.45 ±	11.80	12	11.37 ±	5.85	*	11	1.39 ±	1.20	12	1.37 ±	0.76	n.s.	11	6.75 ±	1.95	12	7.22 ±	1.58	n.s.
Ly6C^{hi} Monocytes	of CD11b^{+}Ly6G^{-}	11	44.22 ±	17.83	12	52.04 ±	10.33	n.s.	11	59.21 ±	10.98	12	57.73 ±	14.87	n.s.	11	65.15 ±	6.24	12	67.69 ±	8.15	n.s.
Ly6C^{lo} Monocytes	of CD11b^{+}Ly6G^{-}	11	45.74 ±	19.37	12	36.30 ±	8.05	n.s.	11	30.66 ±	11.05	12	33.26 ±	15.52	n.s.	11	24.39 ±	5.04	12	21.24 ±	5.24	n.s.
Ly6C^{neg} Monocytes	of CD11b^{+}Ly6G^{-}	11	9.66 ±	2.41	12	11.02 ±	4.63	n.s.	11	9.25 ±	3.93	12	8.32 ±	3.18	n.s.	11	10.06 ±	3.39	12	10.78 ±	3.11	n.s.
NK cells (CD3^{-}Nk1.1^{+})	of CD45^{+}	11	0.84 ±	1.38	12	0.03 ±	0.02	0.05	11	0.75 ±	0.29	12	0.28 ±	0.25	***	11	1.70 ±	0.49	12	0.49 ±	0.76	***
CD3	of CD45^{+}	10	13.89 ±	8.60	11	12.56 ±	3.89	n.s.	10	42.63 ±	5.89	10	42.45 ±	3.98	n.s.	11	21.89 ±	3.51	12	17.59 ±	3.32	**
CD4	of CD3^{+}	10	42.62 ±	4.55	11	44.65 ±	5.85	n.s.	10	47.63 ±	3.92	10	49.00 ±	2.76	n.s.	11	54.39 ±	4.13	12	56.29 ±	2.44	n.s.
activated CD4 (CD44^{+}CD62L^{-})	of CD4^{+}	10	50.25 ±	8.93	11	53.52 ±	15.54	n.s.	10	24.13 ±	5.24	10	24.71 ±	5.90	n.s.	11	47.07 ±	9.38	12	54.18 ±	12.39	n.s.
not activated CD4 (CD44^{+}CD62L^{+})	of CD4^{+}	10	49.74 ±	8.95	11	46.51 ±	15.48	n.s.	10	76.12 ±	5.28	10	75.51 ±	5.92	n.s.	11	52.81 ±	9.40	12	45.68 ±	12.40	n.s.
Treg (CD4^{+}Foxp3^{+})	of CD4	10	12.58 ±	3.29	11	9.42 ±	4.80	0.10	10	15.65 ±	3.75	10	13.08 ±	2.44	0.09	11	20.56 ±	4.72	12	19.65 ±	4.72	n.s.
CD8	of CD3^{+}	10	45.50 ±	4.21	11	36.81 ±	9.08	*	10	42.26 ±	6.55	10	39.75 ±	4.66	n.s.	11	32.76 ±	7.39	12	25.29 ±	5.51	*
central memory CD8 (CD44^{+}CD62L^{+})	of CD8^{+}	10	22.33 ±	4.76	11	22.67 ±	7.08	n.s.	10	19.95 ±	5.02	10	19.80 ±	3.98	n.s.	11	28.88 ±	6.07	12	29.18 ±	9.61	n.s.
effector memory CD8 (CD44^{+}CD62L^{-})	of CD8^{+}	10	12.03 ±	4.28	11	11.69 ±	9.14	n.s.	10	2.38 ±	1.03	10	2.18 ±	0.99	n.s.	11	6.93 ±	2.54	12	5.68 ±	2.52	n.s.
naive CD8 (CD44^{-}CD62L^{-})	of CD8^{+}	10	47.04 ±	10.77	11	44.86 ±	14.42	n.s.	10	72.90 ±	5.27	10	71.91 ±	5.39	n.s.	11	61.18 ±	7.41	12	60.18 ±	8.67	n.s.

Mean ± SD. Statistical significance was calculated for groups pairwise by 2-tailed *t* test. *$p < 0.05$, **$p < 0.01$, **$p < 0.01$, ***$p < 0.001$

Table III. Distribution of immune cell subsets in 18 week old *Cd70*$^{+/+}$ *Apoe*$^{-/-}$ and *Cd70*$^{-/-}$ *Apoe*$^{-/-}$ mice.

Organ		Blood									Lymph nodes									Spleen								
Mouse strain		*Cd70*$^{+/+}$ *Apoe*$^{-/-}$				*Cd70*$^{-/-}$ *Apoe*$^{-/-}$					*Cd70*$^{+/+}$ *Apoe*$^{-/-}$				*Cd70*$^{-/-}$ *Apoe*$^{-/-}$					*Cd70*$^{+/+}$ *Apoe*$^{-/-}$				*Cd70*$^{-/-}$ *Apoe*$^{-/-}$				
Subset	**Parental Gate**	**n**	**Mean**		**SD**	**n**	**Mean**		**SD**	***p***	**n**	**Mean**		**SD**	**n**	**Mean**		**SD**	***p***	**n**	**Mean**		**SD**	**n**	**Mean**		**SD**	***p***
CD19^{+}	of CD45^{+}	7	49.27	±	8.76	16	46.29	±	8.99	n.s.	7	40.20	±	4.36	16	42.85	±	4.54	n.s.	7	48.37	±	5.78	16	52.53	±	5.35	n.s.
CD11b^{-}CD5^{+}	of CD19^{+}	7	11.16	±	2.78	16	14.60	±	11.16	n.s.	7	18.63	±	7.25	16	18.74	±	11.44	n.s.	7	15.75	±	8.04	16	15.88	±	10.97	n.s.
B1a (CD11b^{+}CD5^{+})	of CD19^{+}	7	4.76	±	6.83	16	5.21	±	7.55	n.s.	7	10.04	±	5.34	16	10.72	±	10.83	n.s.	7	9.07	±	6.13	16	5.51	±	5.54	n.s.
B1b (CD11b^{+}CD5^{-})	of CD19^{+}	7	2.38	±	0.45	16	3.13	±	0.82	*	7	4.52	±	1.64	16	4.18	±	1.62	n.s.	7	2.82	±	0.83	16	2.68	±	1.61	n.s.
B2 (CD11b^{-}CD5^{-})	of CD19^{+}	7	81.73	±	7.70	16	77.06	±	13.36	n.s.	7	66.83	±	6.63	16	66.36	±	14.54	n.s.	7	72.39	±	10.57	16	75.95	±	11.72	n.s.
CD11c^{hi}	of CD45^{+}	7	0.87	±	1.01	17	0.76	±	1.04	n.s.	7	0.86	±	1.46	17	0.57	±	0.86	n.s.	7	2.98	±	0.81	17	2.22	±	1.04	n.s.
CD8^{+}DC	of CD11c^{hi}	5	15.38	±	9.28	14	7.32	±	8.44	0.09	7	23.21	±	8.23	17	15.91	±	6.02	*	7	24.53	±	3.91	17	19.74	±	7.27	n.s.
CD8^{-}DC	of CD11c^{hi}	5	83.06	±	10.33	14	92.68	±	8.42	0.05	7	76.54	±	8.36	17	84.01	±	6.05	*	7	75.40	±	3.90	17	80.22	±	7.28	n.s.
pDC (Siglec-H^{+}PDCA-1^{+})	of CD3^{-}CD19^{-}	7	1.34	±	0.97	17	2.67	±	4.02	n.s.	7	7.34	±	3.71	17	7.46	±	5.44	n.s.	7	2.72	±	1.24	17	2.43	±	1.45	n.s.
Neutrophils (CD11b^{+}Ly6G^{+})	of CD3^{-}Nk1.1^{-}	7	20.83	±	9.10	4	18.98	±	4.51	n.s.	7	1.06	±	1.50	7	1.03	±	0.94	n.s.	5	3.94	±	1.19	5	4.97	±	3.02	n.s.
Monocytes (CD11b^{+}Ly6G^{-})	of CD3^{-}Nk1.1^{-}	7	16.11	±	4.70	7	19.42	±	12.55	n.s.	7	9.04	±	13.47	7	14.35	±	11.74	n.s.	8	15.42	±	10.79	8	19.35	±	11.61	n.s.
Ly6C^{hi} Monocytes	of CD11b^{+}Ly6G^{-}	7	37.30	±	8.27	7	45.80	±	11.41	n.s.	7	62.20	±	8.95	7	56.61	±	12.18	n.s.	8	54.65	±	14.65	8	53.74	±	14.34	n.s.
Ly6C^{lo} Monocytes	of CD11b^{+}Ly6G^{-}	7	49.14	±	9.16	7	37.10	±	13.07	0.07	7	21.91	±	8.81	7	28.87	±	10.06	n.s.	8	32.50	±	14.23	8	33.11	±	13.12	n.s.
Ly6C^{neg} Monocytes	of CD11b^{+}Ly6G^{-}	7	13.46	±	3.19	7	17.03	±	4.94	n.s.	7	12.19	±	3.25	7	13.13	±	3.96	n.s.	8	13.01	±	3.73	8	13.13	±	3.25	n.s.
NK cells (CD3^{-}Nk1.1^{+})	of CD45^{+}	7	5.92	±	2.26	7	5.94	±	3.93	n.s.	7	1.77	±	1.04	7	3.07	±	1.55	0.09	8	4.36	±	2.46	8	6.24	±	5.40	n.s.
CD3	of CD45^{+}	7	16.49	±	5.20	17	16.21	±	4.47	n.s.	5	45.70	±	6.82	17	48.61	±	5.56	n.s.	7	23.33	±	4.91	17	19.22	±	4.52	0.06
CD4	of CD3^{+}	7	45.24	±	9.76	17	48.34	±	5.58	n.s.	5	52.16	±	2.87	17	49.44	±	5.23	n.s.	7	57.84	±	4.64	17	57.30	±	4.79	n.s.
activated CD4 (CD44^{+}CD62L^{-})	of CD4^{+}	7	35.09	±	15.50	17	43.75	±	19.88	n.s.	5	20.18	±	4.37	17	22.35	±	5.81	n.s.	7	35.56	±	12.57	17	34.43	±	11.00	n.s.
not activated CD4 (CD44^{+}CD62L^{+})	of CD4^{+}	7	64.74	±	15.43	17	56.23	±	19.89	n.s.	5	79.40	±	4.62	17	77.53	±	5.81	n.s.	7	64.31	±	12.59	17	65.43	±	11.05	n.s.
Treg (CD4^{+}Foxp3^{+})	of CD4	10	7.78	±	1.93	10	6.27	±	1.20	0.05	10	14.51	±	1.65	10	11.86	±	2.01	**	10	13.97	±	1.56	10	12.15	±	1.83	*
CD8	of CD3^{+}	7	46.50	±	8.52	17	43.30	±	5.64	n.s.	5	42.14	±	2.86	17	41.09	±	4.44	n.s.	7	35.74	±	4.05	17	33.12	±	6.21	n.s.
central memory CD8 (CD44^{+}CD62L^{+})	of CD8^{+}	7	25.34	±	7.54	17	22.16	±	4.87	n.s.	5	18.30	±	6.87	17	20.07	±	6.32	n.s.	7	23.39	±	5.65	17	23.91	±	6.92	n.s.
effector memory CD8 (CD44^{+}CD62L^{-})	of CD8^{+}	7	8.86	±	5.34	17	8.66	±	4.86	n.s.	5	5.95	±	3.03	17	2.78	±	0.92	***	7	5.46	±	2.28	17	4.64	±	3.77	n.s.
naive CD8 (CD44^{-}CD62L^{-})	of CD8^{+}	7	58.64	±	14.67	17	57.73	±	12.27	n.s.	5	61.28	±	15.19	17	66.41	±	7.65	n.s.	7	66.56	±	6.26	17	66.01	±	10.30	n.s.

Mean ± SD. Statistical significance was calculated for groups pairwise by 2-tailed *t* test. *$p < 0.05$, **$p < 0.01$, **$p < 0.01$, ***$p < 0.001$

Table IV. Distribution of immune cell subsets in 28 week old *Cd70* $^{+/+}$ *Apoe* $^{-/-}$ and *Cd70* $^{-/-}$ *Apoe* $^{-/-}$ mice.

Organ		Blood									Lymph nodes									Spleen								
Mouse strain		*Cd70* $^{+/+}$ *Apoe* $^{-/-}$				*Cd70* $^{-/-}$ *Apoe* $^{-/-}$					*Cd70* $^{+/+}$ *Apoe* $^{-/-}$				*Cd70* $^{-/-}$ *Apoe* $^{-/-}$					*Cd70* $^{+/+}$ *Apoe* $^{-/-}$				*Cd70* $^{-/-}$ *Apoe* $^{-/-}$				
Subset	**Parental Gate**	**n**	**Mean**		**SD**	**n**	**Mean**		**SD**	***p***	**n**	**Mean**		**SD**	**n**	**Mean**		**SD**	***p***	**n**	**Mean**		**SD**	**n**	**Mean**		**SD**	***p***
CD19^{+}	of CD45^{+}	11	51.25	±	9.72	13	51.96	±	13.54	n.s.	11	48.55	±	3.73	13	45.70	±	7.86	n.s.	11	51.56	±	5.43	13	54.01	±	8.64	n.s.
CD11b^{-}CD5^{+}	of CD19^{+}	11	14.42	±	10.59	13	6.99	±	6.58	*	11	26.02	±	14.44	13	17.75	±	10.28	n.s.	11	21.72	±	15.31	13	12.32	±	9.05	0.08
B1a (CD11b^{+}CD5^{+})	of CD19^{+}	11	2.23	±	2.88	13	0.74	±	0.53	n.s.	11	2.57	±	1.08	13	2.24	±	1.96	n.s.	11	1.63	±	0.72	13	1.29	±	0.75	n.s.
B1b (CD11b^{+}CD5^{-})	of CD19^{+}	11	1.99	±	1.64	13	1.31	±	0.55	0.08	11	1.03	±	0.43	13	1.04	±	0.40	n.s.	11	1.10	±	0.38	13	1.45	±	0.62	0.08
B2 (CD11b^{-}CD5^{-})	of CD19^{+}	11	81.37	±	12.03	13	90.98	±	6.68	*	11	70.35	±	14.84	13	78.98	±	11.64	n.s.	11	75.56	±	15.39	13	84.95	±	9.34	n.s.
CD11c^{hi}	of CD45^{+}	11	7.00	±	9.07	13	5.11	±	3.95	n.s.	11	0.51	±	0.20	13	0.81	±	0.39	n.s.	11	2.51	±	0.83	13	2.99	±	2.11	n.s.
CD8^{+}DC	of CD11c^{hi}	11	0.68	±	0.26	13	1.14	±	1.09	n.s.	11	26.51	±	6.54	13	27.08	±	9.88	n.s.	11	14.02	±	3.79	13	19.52	±	6.83	*
CD8^{-}DC	of CD11c^{hi}	11	99.20	±	0.37	13	98.55	±	1.86	n.s.	11	73.34	±	6.62	13	72.68	±	10.32	n.s.	11	85.95	±	3.83	13	80.39	±	6.85	*
pDC (Siglec-H^{+}PDCA-1^{+})	of CD3^{-}CD19^{-}	11	0.20	±	0.22	13	0.34	±	0.38	n.s.	11	6.05	±	3.20	13	6.65	±	4.81	n.s.	11	2.14	±	0.56	13	2.68	±	2.36	n.s.
Neutrophils (CD11b^{+}Ly6G^{+})	of CD3^{-}Nk1.1^{-}	11	2.76	±	4.79	13	7.37	±	11.02	n.s.	11	0.17	±	0.07	13	0.24	±	0.19	n.s.	11	3.73	±	1.18	13	3.91	±	4.75	n.s.
Monocytes (CD11b^{+}Ly6G^{-})	of CD3^{-}Nk1.1^{-}	11	15.47	±	6.03	13	12.42	±	5.85	n.s.	11	1.40	±	0.49	13	2.00	±	1.68	n.s.	11	8.97	±	2.51	13	7.68	±	2.58	n.s.
Ly6C^{hi} Monocytes	of CD11b^{+}Ly6G^{-}	11	69.34	±	11.80	13	67.32	±	11.07	n.s.	11	69.34	±	11.80	13	67.32	±	11.07	n.s.	11	59.97	±	8.75	13	63.72	±	10.71	n.s.
Ly6C^{lo} Monocytes	of CD11b^{+}Ly6G^{-}	11	19.21	±	13.36	13	26.85	±	22.89	n.s.	11	17.73	±	8.98	13	21.39	±	11.61	n.s.	11	28.41	±	6.04	13	23.08	±	9.01	n.s.
Ly6C^{neg} Monocytes	of CD11b^{+}Ly6G^{-}	11	16.32	±	5.03	13	11.80	±	4.79	*	11	13.19	±	7.43	13	11.29	±	4.99	n.s.	11	11.29	±	4.31	13	13.11	±	6.05	n.s.
NK cells (CD3^{-}Nk1.1^{+})	of CD45^{+}	9	7.15	±	4.09	12	4.19	±	2.09	*	11	0.79	±	0.14	13	0.86	±	0.27	n.s.	11	1.90	±	0.40	13	2.01	±	0.65	n.s.
CD3	of CD45^{+}	11	12.59	±	2.99	13	12.46	±	3.99	n.s.	11	40.90	±	5.03	13	42.80	±	9.90	n.s.	11	19.47	±	4.31	13	18.48	±	4.77	n.s.
CD4	of CD3^{+}	11	43.40	±	3.65	13	45.02	±	6.68	n.s.	11	51.27	±	2.34	13	49.46	±	4.55	n.s.	11	59.19	±	3.85	13	59.82	±	7.18	n.s.
activated CD4 (CD44^{+}CD62L^{-})	of CD4^{+}	11	64.52	±	14.41	13	54.29	±	16.90	n.s.	11	33.35	±	9.72	13	35.00	±	18.01	n.s.	11	55.25	±	6.33	13	54.56	±	11.51	n.s.
not activated CD4 (CD44^{+}CD62L^{+})	of CD4^{+}	11	35.34	±	14.44	13	45.58	±	16.85	n.s.	11	66.51	±	9.82	13	64.82	±	18.01	n.s.	11	44.75	±	6.33	13	45.43	±	11.51	n.s.
Treg (CD4^{+}Foxp3^{+})	of CD4	11	12.15	±	2.26	13	8.15	±	2.58	***	11	20.25	±	2.16	13	14.74	±	2.14	****	11	23.49	±	2.71	13	19.92	±	2.44	**
CD8	of CD3^{+}	11	48.52	±	3.58	13	47.17	±	5.89	n.s.	11	38.25	±	4.35	13	41.26	±	5.24	n.s.	11	29.12	±	4.87	13	30.48	±	9.01	n.s.
central memory CD8 (CD44^{+}CD62L^{+})	of CD8^{+}	11	33.18	±	6.48	13	28.01	±	9.31	n.s.	11	25.61	±	3.38	13	25.10	±	6.35	n.s.	11	35.73	±	7.11	13	32.76	±	7.51	n.s.
effector memory CD8 (CD44^{+}CD62L^{-})	of CD8^{+}	11	12.20	±	3.97	13	10.97	±	5.68	n.s.	11	4.49	±	1.67	13	4.04	±	3.15	n.s.	11	8.61	±	3.68	13	7.27	±	3.29	n.s.
naive CD8 (CD44^{-}CD62L^{-})	of CD8^{+}	11	35.88	±	9.68	13	42.01	±	13.81	n.s.	11	56.78	±	8.34	13	54.77	±	12.60	n.s.	11	49.55	±	6.91	13	52.92	±	7.57	n.s.

Mean ± SD. Statistical significance was calculated for groups pairwise by 2-tailed *t* test. *$p < 0.05$, **$p < 0.01$, **$p < 0.01$, ***$p < 0.001$

Table V. Distribution of circulating immune cells marrow chimeric mice.

Bone marrow transplanted into *Apoe*$^{-/-}$ recipient		*Apoe*$^{-/-}$				*Cd27*$^{-/-}$ *Apoe*$^{-/-}$					*Cd70*$^{-/-}$ *Apoe*$^{-/-}$				
Subset	**Parental Gate**	**n**	**mean**		**SD**	**n**	**mean**		**SD**	***p***	**n**	**mean**		**SD**	***p***
CD3	of CD45^{+}	8	21.54	±	8.79	8	19.99	±	7.812	n.s.	8	19.15	±	4.406	n.s.
B220^{+}	of CD45^{+}	8	49.86	±	17.63	8	55.54	±	11.1	n.s.	8	56.9	±	5.426	n.s.
Neutrophils (CD11b^{+}Ly6G^{+})	of CD3^{-}B220^{-}	8	51.76	±	11.79	8	45.69	±	10.01	n.s.	8	46.44	±	5.862	n.s.
Monocytes (CD11b^{+}Ly6G^{-})	of CD3^{-}B220^{-}	8	34.71	±	7.534	8	41.58	±	8.889	n.s.	8	41.86	±	4.108	n.s.
GR1^{+} Monocytes	of Ly6G^{-}CD11b^{+}	8	54.15	±	12.74	8	57.79	±	6.338	n.s.	8	57.6	±	5.355	n.s.
GR1^{-} Monocytes	of Ly6G^{-}CD11b^{+}	8	44.65	±	12.91	8	40.83	±	6.171	n.s.	8	40.86	±	5.291	n.s.

Mean ± SD. Statistical significance was calculated by applying One-Way ANOVA followed by Dunnett's multiple comparison test . *$p < 0.05$

Table VI. Distribution of immune cells in lymph nodes of bone marrow chimeric mice.

Bone marrow transplanted into Apoe$^{-/-}$recipient		*Apoe* $^{-/-}$				*Cd27* $^{-/-}$ *Apoe* $^{-/-}$					*Cd70* $^{-/-}$ *Apoe* $^{-/-}$				
Subset	**Parental Gate**	**n**	**mean**		**SD**	**n**	**mean**		**SD**	***p***	**n**	**mean**		**SD**	***p***
CD3	of CD45^{+}	8	52.20	±	10.00	8	48.08	±	8.95	n.s.	8	47.06	±	4.06	n.s.
B220^{+}	of CD45^{+}	8	41.23	±	9.52	8	45.25	±	9.76	n.s.	8	45.65	±	3.38	n.s.
Neutrophils (CD11b^{+}Ly6G^{+})	of CD3^{-}B220^{-}	8	2.65	±	3.84	8	0.99	±	0.98	n.s.	8	1.81	±	2.42	n.s.
Monocytes (CD11b^{+}Ly6G^{-})	of CD3^{-}B220^{-}	8	44.61	±	8.60	8	44.10	±	8.68	n.s.	8	38.35	±	8.52	n.s.
GR1^{+} Monocytes	of Ly6G^{-}CD11b^{+}	8	24.60	±	11.36	7	25.64	±	12.99	n.s.	8	18.69	±	8.44	n.s.
GR1^{-} Monocytes	of Ly6G^{-}CD11b^{+}	8	73.99	±	11.21	7	72.59	±	13.50	n.s.	8	79.68	±	8.16	n.s.
resident DC (CD11c^{hi}MHCII^{+})	of CD45^{+}	8	0.89	±	0.20	8	0.92	±	0.24	n.s.	8	0.89	±	0.17	n.s.
CD11b^{+}DC	of resident DC	8	80.39	±	5.29	8	79.61	±	6.61	n.s.	8	80.19	±	3.41	n.s.
CD11b^{-}DC	of resident DC	8	18.36	±	5.50	8	19.28	±	6.95	n.s.	8	18.99	±	3.28	n.s.
CD3	of CD45^{+}	8	49.65	±	10.11	8	44.88	±	7.43	n.s.	8	38.66	±	8.95	*
CD4	of CD3^{+}	8	57.71	±	2.63	8	54.08	±	2.93	*	8	54.44	±	2.27	*
activated CD4 (CD44^{+}CD62L^{-})	of CD4^{+}	8	27.60	±	3.16	8	27.01	±	3.66	n.s.	8	29.94	±	3.19	n.s.
not activated CD4 (CD44^{+}CD62L^{+})	of CD4^{+}	8	64.91	±	4.99	8	63.74	±	5.10	n.s.	8	60.93	±	4.73	n.s.
CD8	of CD3^{+}	8	33.93	±	3.01	8	35.65	±	2.53	n.s.	8	33.99	±	3.10	n.s.
central memory CD8 (CD44^{+}CD62L^{+})	of CD8^{+}	8	25.24	±	5.76	8	19.35	±	3.56	*	8	23.58	±	4.70	n.s.
effector memory CD8 (CD44^{+}CD62L^{-})	of CD8^{+}	8	16.65	±	4.38	8	14.36	±	6.07	n.s.	8	15.75	±	2.44	n.s.
naive CD8 (CD44^{-}CD62L^{-})	of CD8^{+}	8	45.20	±	7.27	8	49.86	±	7.23	n.s.	8	45.15	±	3.63	n.s.

Mean ± SD. Statistical significance was calculated by applying One-Way ANOVA followed by Dunnett's multiple comparison test . *$p < 0.05$

Table VII. Distribution of splenic immune cells of bone marrow chimeric mice.

Bone marrow transplanted into *Apoe*$^{-/-}$ recipient		*Apoe*$^{-/-}$					*Cd27*$^{-/-}$ *Apoe*$^{-/-}$						*Cd70*$^{-/-}$ *Apoe*$^{-/-}$				
Subset	**Parental Gate**	**n**	**mean**		**SD**		**n**	**mean**		**SD**	***p***		**n**	**mean**		**SD**	***p***
CD3	of CD45^{+}	8	30.83	±	7.01		8	26.59	±	6.32	n.s.		8	26.41	±	4.07	n.s.
B220^{+}	of CD45^{+}	8	52.21	±	8.38		8	56.09	±	7.85	n.s.		8	57.01	±	4.94	n.s.
Neutrophils (CD11b^{+}Ly6G^{+})	of CD3^{-}B220^{-}	8	16.15	±	6.83		8	13.23	±	4.46	n.s.		8	11.67	±	2.83	n.s.
Monocytes (CD11b^{+}Ly6G^{-})	of CD3^{-}B220^{-}	8	34.15	±	4.08		8	37.85	±	5.87	n.s.		8	34.45	±	2.81	n.s.
GR1^{+} Monocytes	of Ly6G^{-}CD11b^{+}	8	37.28	±	8.97		8	33.78	±	6.64	n.s.		8	32.13	±	5.73	n.s.
GR1^{-} Monocytes	of Ly6G^{-}CD11b^{+}	8	61.58	±	9.08		8	64.83	±	6.80	n.s.		8	66.68	±	5.76	n.s.
resident DC (CD11c^{hi}MHCII^{+})	of CD45^{+}	8	1.74	±	0.57		8	2.22	±	0.47	n.s.		8	1.72	±	0.36	n.s.
CD11b^{+}DC	of resident DC	8	69.96	±	3.89		8	76.01	±	4.03	*		8	73.60	±	4.42	n.s.
CD11b^{-}DC	of resident DC	8	30.03	±	3.91		8	23.86	±	3.96	*		8	26.19	±	4.33	n.s.
CD3	of CD45^{+}	8	27.61	±	5.22		8	23.55	±	3.52	n.s.		8	24.55	±	3.38	n.s.
CD4	of CD3^{+}	8	62.16	±	3.08		8	62.13	±	2.15	n.s.		8	59.84	±	4.51	n.s.
activated CD4 (CD44^{+}CD62L^{-})	of CD4^{+}	8	39.61	±	4.52		8	34.39	±	5.22	*		8	38.30	±	3.00	n.s.
not activated CD4 (CD44^{+}CD62L^{+})	of CD4^{+}	8	55.45	±	5.16		8	59.19	±	5.60	n.s.		8	55.85	±	4.22	n.s.
CD8	of CD3^{+}	8	27.40	±	2.05		8	27.89	±	1.54	n.s.		8	27.48	±	1.68	n.s.
central memory CD8 (CD44^{+}CD62L^{+})	of CD8^{+}	8	32.43	±	5.68		8	22.75	±	5.90	**		8	28.84	±	5.15	n.s.
effector memory CD8 (CD44^{+}CD62L^{-})	of CD8^{+}	8	12.89	±	3.88		8	7.88	±	2.88	**		8	8.48	±	2.26	*
naive CD8 (CD44^{-}CD62L^{-})	of CD8^{+}	8	49.88	±	9.09		8	62.56	±	8.18	*		8	57.13	±	7.71	n.s.

Mean ± SD. Statistical significance was calculated by applying One-Way ANOVA followed by Dunnett's multiple comparison test . *$p < 0.05$, **$p < 0.01$

Table VIII. Probability values for comparision of differences in aortic mRNA expression levels between irradiated Apoe mice transplanted with $Cd27^{+/+}Apoe^{-/-}$ or $CD27^{-/-}Apoe^{-/-}$ bone marrow.

Gene	Crude *p* -value	*q* -value (after FDR)	Significant after FDR correction?
IL-1β	0.000384	0.00806	Yes
ICAM-1	0.012121	0.09116	Yes
Gata3	0.017488	0.09116	Yes
IL-6	0.021977	0.09116	Yes
VCAM-1	0.024242	0.09116	Yes
CCL1	0.028082	0.09116	Yes
IL-12p35	0.030386	0.09116	Yes
STAT6	0.072727	0.17422	No
CCL5	0.085292	0.17422	No
Rorγt	0.089706	0.17422	No
MCP1	0.091258	0.17422	No
IL-12p40	0.164589	0.27152	No
IL-23p19	0.168084	0.27152	No
IRF4	0.211237	0.31686	No
CXCL10	0.315152	0.44121	No
IL-2	0.388658	0.51011	No
Foxp3	0.481922	0.58278	No
T-Bet	0.499696	0.58278	No
STAT3	0.527273	0.58278	No
IL-17α	0.794483	0.83421	No
IFNγ	0.885197	0.92735	No